PB82-239278

Evaluation of Four Urban-Scale Photochemical Air Quality Simulation Models

(U.S.) Environmental Sciences Research Lab.
Research Triangle Park, NC

Apr 82

U.S. Department of Commerce
National Technical Information Service
NTIS

TECHNICAL REPORT DATA
(Please read Instructions on the reverse before completing)

1. REPORT NO. EPA-600/3-82-043	2. ORD Report	3. RECIPIENT'S ACCESSION NO. PB 82-239278
4. TITLE AND SUBTITLE EVALUATION OF FOUR URBAN-SCALE PHOTOCHEMICAL AIR QUALITY SIMULATION MODELS		5. REPORT DATE April 1982
		6. PERFORMING ORGANIZATION CODE
7. AUTHOR(S) Jack H. Shreffler and Kenneth L. Schere		8. PERFORMING ORGANIZATION REPORT NO.
9. PERFORMING ORGANIZATION NAME AND ADDRESS (same as 12)		10. PROGRAM ELEMENT NO. CDWA1A/01-1332 (FY-82)
		11. CONTRACT/GRANT NO.
12. SPONSORING AGENCY NAME AND ADDRESS Environmental Sciences Research Laboratory - RTP, NC Office of Research and Development U.S. Environmental Protection Agency Research Triangle Park, NC 27711		13. TYPE OF REPORT AND PERIOD COVERED In-house
		14. SPONSORING AGENCY CODE EPA/600/09
15. SUPPLEMENTARY NOTES		

16. ABSTRACT

The purpose of this research was to determine the accuracy of four photochemical air quality simulation models using data from the Regional Air Pollution Study in St. Louis.

The models evaluated in this report are: The Photochemical Box Model (PBM) built in-house by EPA, The Lagrangian Photochemical Model (LPM) built by Environmental Research and Technology, Inc., The Urban Airshed Model (UAM) built by Systems Applications, Inc., and The Livermore Regional Air Quality Model (LIRAQ) built by Lawrence Livermore Laboratory.

Emphasis in this report is directed at the ability of the models to reproduce the maximum 1-hour ozone concentrations observed on 10 days selected from nearly two years of data. The PBM, LPM, and UAM have been successfully tested and show potential as air quality management tools. LIRAQ does not show potential as a model for general use, irrespective of its accuracy (which was impossible to judge at this time).

The standard deviation of the differences between observed ozone maxima and predicted concentrations at the same place and time tend to be large, ranging 0.04-0.1 ppm for maxima of 0.19-0.26 ppm. Although some problems exist whose resolution could improve model performance, this high variability should be recognized by decision-makers.

17. KEY WORDS AND DOCUMENT ANALYSIS

a. DESCRIPTORS	b. IDENTIFIERS/OPEN ENDED TERMS	c. COSATI Field/Group

18. DISTRIBUTION STATEMENT RELEASE TO PUBLIC	19. SECURITY CLASS *(This Report)* UNCLASSIFIED	21. NO. OF PAGES 179
	20. SECURITY CLASS *(This page)* UNCLASSIFIED	22. PRICE

EPA Form 2220-1 (9-73)

PB82-239278

EPA-600/3-82-043
April 1982

EVALUATION OF FOUR URBAN-SCALE PHOTOCHEMICAL AIR QUALITY SIMULATION MODELS

by

Jack H. Shreffler and Kenneth L. Schere
Meteorology and Assessment Division
Environmental Sciences Research Laboratory
Research Triangle Park, North Carolina 27711

ENVIRONMENTAL SCIENCES RESEARCH LABORATORY
OFFICE OF RESEARCH AND DEVELOPMENT
U.S. ENVIRONMENTAL PROTECTION AGENCY
RESEARCH TRIANGLE PARK, NORTH CAROLINA 27711

REPRODUCED BY
NATIONAL TECHNICAL
INFORMATION SERVICE
U.S. DEPARTMENT OF COMMERCE
SPRINGFIELD, VA 22161

DISCLAIMER

This report has been reviewed by the Environmental Sciences Research Laboratory, U.S. Environmental Protection Agency, and approved for publication. Mention of trade names or commerical products does not constitute endorsement or recommendation for use.

AFFILIATION

Dr. Shreffler and Mr. Schere are on assignment to the Meteorology and Assessment Division, Environmental Sciences Research Laboratory, from the National Oceanic and Atmospheric Administration, U.S. Department of Commerce.

ABSTRACT

The purpose of this research was to determine the accuracy of four photochemical air quality simulation models using data from the Regional Air Pollution Study in St. Louis.

The models evaluated in this report are: The Photochemical Box Model (PBM) built in-house by EPA, The Lagrangian Photochemical Model (LPM) built by Environmental Research and Technology, Inc., The Urban Airshed Model (UAM) built by Systems Applications, Inc., and The Livermore Regional Air Quality Model (LIRAQ) built by Lawrence Livermore Laboratory.

Emphasis in this report is directed at the ability of the models to reproduce the maximum 1-hour ozone concentrations observed on 10 days selected from nearly two years of data. The PBM, LPM, and UAM have been successfully tested and show potential as air quality management tools. LIRAQ does not show potential as a model for general use, irrespective of its accuracy (which was impossible to judge at this time).

The standard deviation of the differences between observed ozone maxima and predicted concentrations at the same place and time tend to be large, ranging 0.04-0.1 ppm for maxima of 0.19-0.26 ppm. Although some problems exist whose resolution could improve model performance, this high variability should be recognized by decision-makers.

This report covers a period from January 1980 to March 1981 and work was completed as of July 26, 1981.

CONTENTS

Abstract iii
Figures vi
Tables xiii

1. Introduction 1
2. Conclusions and Recommendations 3
3. The Data Set 5
4. Photochemical Box Model 12
    - Overview 12
    - Method 13
    - Results 14
    - Conclusions 22
5. Lagrangian Photochemical Model 35
    - Overview 35
    - Method 35
    - Results 38
    - Additional Simulations 42
    - Conclusions 45
6. Livermore Regional Air Quality Model 58
    - Overview 58
    - Discussion of Results 58
    - Outlook for LIRAQ 60
7. Urban Airshed Model 70
    - Overview 70
    - Method 71
    - Results 73
    - Current Work 81
    - Conclusions 82

References 95

Appendices

A. PBM - Time series for remaining test days 97
B. PBM - Summary of statistical results 112
C. LPM - Time series for remaining test days 116
D. UAM - RS and RO plots for remaining test days 135
E. UAM - Summary of statistical results 157

FIGURES

Number Page

1 The St. Louis area with locations of the RAPS surface stations 8

2 Total source emissions of CO, in kilograms/10, for the RAPS area on Day 195 of 1976 at 0800 CST. Grid cells are 4 km squares; the SW corner corresponds to UTM (x,y) coordinates of Zone 15: (706, 4236) 9

3 Total source emissions of NO_x, in kilograms, for the RAPS area on Day 195 of 1976 at 0800 CST. Grid cells are 4 km squares; the SW corner corresponds to UTM (x,y) coordinates of Zone 15: (706, 4236) 10

4 Total source emissions of THC, in kilograms, for the RAPS area on Day 195 of 1976 at 0800 CST. Grid cells are 4 km squares; the SW corner corresponds to UTM (x,y) coordinates of Zone 15: (706, 4236) 11

5 Schematic drawing of the PBM domain 23

6 Map of St. Louis area depicting extent of PBM modeling domain (boxed area), city of St. Louis (shaded area), RAPS monitoring stations (circles), and radiosonde ascent site (triangle) 24

7 PBM simulation results for Day 142 of 1975. Time series of average observed (circles), range of observed (dashed lines), and model simulated (solid line) hour-average concentrations of: (a) CO 25
(b) NO_2 26
(c) O_3 26

8 PBM simulation results for Day 275 of 1976. Time series of average observed (circles), range of observed (dashed lines), and model simulated (solid line) hour-average concentrations of: (a) CO 27
(b) NO_2 28
(c) O_3 28

9 PBM simulation results for Day 251 of 1975. Time series of average observed (circles), range of observed (dashed lines), and model simulated (solid line) hour-average concentrations of: (a) CO 29
(b) NO_2 30
(c) O_3 30

10 Residual histograms from the PBM simulation results for all 10 test days for : (a) CO 31
(b) NO_2 32
(c) O_3 32

11 Residual vs. Observed plots from the PBM simulation results for all 10 test days for: (a) CO 33
(b) NO_2 34
(c) O_3 34

12 LPM simulation results for Day 231 of 1975.
(a) Parcel trajectory 46
Time series of observed and predicted Level-1 and Level-3 hourly concentrations for:
(b) O_3 47
(c) NO 47
(d) NO_2 48
(e) CO 48

13 LPM simulation results for Day 251 of 1975.
(a) Parcel trajectory 49
Time series of observed and predicted Level-1 and Level-3 hourly concentrations for:
(b) O_3 50
(c) NO 50
(d) NO_2 51
(e) CO 51

14 LPM simulation results for Day 226 of 1976.
(a) Parcel trajectory 52
Time series of observed and predicted Level-1 and Level-3 hourly concentrations for:
(b) O_3 53
(c) NO 53
(d) NO_2 54
(e) CO 54

15 LPM simulation results for Day 275 of 1976.
(a) Parcel trajectory 55
Time series of observed and predicted Level-1 and Level-3 hourly concentrations for:
(b) O_3 56
(c) NO 56
(d) NO_2 57
(e) CO 57

16 LIRAQ time series of predicted and observed pollutant concentrations at Station 109 on Day 226 of 1976. Predicted values are given for the surface (dotted line) and the layer average (solid line).
  (a) O_3 63
  (b) NO 63
  (c) NO_2 64
  (d) CO 64

17 LIRAQ scatter diagrams of predicted and observed maximum pollutant concentrations at n stations on Day 226 of 1976. The RAPS stations are 101-101+n.
  (a) O_3 65
  (b) NO 65
  (c) NO_2 66
  (d) CO 66
  (e) SO_2 67

18 LIRAQ scatter diagrams of predicted and observed maximum pollutant concentrations at n stations on Day 195 of 1976. The RAPS stations are 101-101+n.
  (a) O_3 68
  (b) NO 68
  (c) NO_2 69
  (d) CO 69

19 Schematic drawing of horizontal section of UAM domain showing locations of RAPS monitoring sites 83

20 (a) Residual histogram and (b) Residual vs. Observed plots for CO from the UAM simulation results for Day 142-75 84

21 (a) Residual histogram and (b) Residual vs. Observed plots for NO_2 from the UAM simulation results for Day 142-75 85

22 (a) Residual histogram and (b) Residual vs. Observed plots for O_3 from the UAM simulation results for Day 142-75 86

23 (a) Residual histogram and (b) Residual vs. Observed plots for CO from the UAM simulation results for Day 275-76 87

24 (a) Residual histogram and (b) Residual vs. Observed plots for NO_2 from the UAM simulation results for Day 275-76 88

25 (a) Residual histogram and (b) Residual vs. Observed plots for O_3 from the UAM simulation results for Day 275-76 89

26 (a) Residual histogram and (b) Residual vs. Observed plots for CO from the UAM simulation results for Day 195-76 90

27 (a) Residual histogram and (b) Residual vs. Observed plots for NO_2 from the UAM simulation results for Day 195-76 91

28 (a) Residual histogram and (b) Residual vs. Observed plots for O_3 from the UAM simulation results for Day 195-76 92

29 Hour-average O_3 concentrations predicted by the UAM in the lowest layer of cells from the simulation of Day 195-76 at 1400 CST 93

30 Instantaneous concentrations (arbitrary units) within the lowest layer of cells from the UAM advection-only test at (a) initial state and (b) 5 hrs. of simulation 94

A-1 PBM simulation results for Day 178 of 1975. Time series of average observed (circles), range of observed (dashed lines), and model simulated (solid line) hour-average concentrations of: (a) CO 98
(b) NO_2 99
(c) O_3 99

A-2 PBM simulation results for Day 209 of 1975. Time series of average observed (circles), range of observed (dashed lines), and model simulated (solid line) hour-average concentrations of: (a) CO 100
(b) NO_2 101
(c) O_3 101

A-3 PBM simulation results for Day 231 of 1975. Time series of average observed (circles), range of observed (dashed lines), and model simulated (solid line) hour-average concentrations of: (a) CO 102
(b) NO_2 103
(c) O_3 103

A-4 PBM simulation results for Day 159 of 1976. Time series of average observed (circles), range of observed (dashed lines), and model simulated (solid line) hour-average concentrations of: (a) CO 104
(b) NO_2 105
(c) O_3 105

A-5 PBM simulation results for Day 160 of 1976. Time series of average observed (circles), range of observed (dashed lines), and model simulated (solid line) hour-average concentrations of: (a) CO 106
(b) NO_2 107
(c) O_3 107

A-6 PBM simulation results for Day 195 of 1976. Time series of average observed (circles), range of observed (dashed lines), and model simulated (solid line) hour-average concentrations of: (a) CO 108
(b) NO_2 109
(c) O_3 109

A-7 PBM simulation results for Day 226 of 1976. Time series of average observed (circles), range of observed (dashed lines), and model simulated (solid line) hour-average concentrations of: (a) CO 110
(b) NO_2 111
(c) O_3 111

C-1 LPM simulation results for Day 142 of 1975.
(a) Parcel trajectory 117
Time series of observed and predicted Level-1 and Level-3 hourly concentrations for:
(b) O_3 118
(c) NO 118
(d) NO_2 119
(e) CO 119

C-2 LPM simulation results for Day 178 of 1975.
(a) Parcel trajectory 120
Time series of observed and predicted Level-1 and Level-3 hourly concentrations for:
(b) O_3 121
(c) NO 121
(d) NO_2 122
(e) CO 122

C-3 LPM simulation results for Day 209 of 1975.
(a) Parcel trajectory 123
Time series of observed and predicted Level-1 and Level-3 hourly concentrations for:
(b) O_3 124
(c) NO 124
(d) NO_2 125
(e) CO 125

C-4 LPM simulation results for Day 159 of 1976.
(a) Parcel trajectory 126
Time series of observed and predicted Level-1 and Level-3 hourly concentrations for:
(b) O_3 127
(c) NO 127
(d) NO_2 128
(e) CO 128

C-5 LPM simulation results for Day 160 of 1976.
(a) Parcel trajectory 129
Time series of observed and predicted Level-1 and Level-3 hourly concentrations for:
(b) O_3 130
(c) NO 130
(d) NO_2 131
(e) CO 131

C-6 LPM simulation results for Day 195 of 1976.
(a) Parcel trajectory 132
Time series of observed and predicted Level-1 and Level-3 hourly concentrations for:
(b) O_3 133
(c) NO 133
(d) NO_2 134
(e) CO 134

D-1 (a) Residual histogram and (b) Residual vs. Observed plots for CO from the UAM simulation results for Day 178-75 136

D-2 (a) Residual histogram and (b) Residual vs. Observed plots for NO_2 from the UAM simulation results for Day 178-75 137

D-3 (a) Residual histogram and (b) Residual vs. Observed plots for O_3 from the UAM simulation results for Day 178-75 138

D-4 (a) Residual histogram and (b) Residual vs. Observed plots for CO from the UAM simulation results for Day 209-75 139

D-5 (a) Residual histogram and (b) Residual vs. Observed plots for NO_2 from the UAM simulation results for Day 209-75 140

D-6 (a) Residual histogram and (b) Residual vs. Observed plots for O_3 from the UAM simulation results for Day 209-75 141

D-7 (a) Residual histogram and (b) Residual vs. Observed plots for CO from the UAM simulation results for Day 231-75 142

D-8 (a) Residual histogram and (b) Residual vs. Observed plots for NO_2 from the UAM simulation results for Day 231-75 143

D-9 (a) Residual histogram and (b) Residual vs. Observed plots for O_3 from the UAM simulation results for Day 231-75 144

D-10 (a) Residual histogram and (b) Residual vs. Observed plots for CO from the UAM simulation results for Day 251-75 145

D-11 (a) Residual histogram and (b) Residual vs. Observed plots for NO_2 from the UAM simulation results for Day 251-75 146

D-12 (a) Residual histogram and (b) Residual vs. Observed plots for O_3 from the UAM simulation results for Day 251-75 147

D-13 (a) Residual histogram and (b) Residual vs. Observed plots for CO from the UAM simulation results for Day 159-76 148

D-14 (a) Residual histogram and (b) Residual vs. Observed plots for NO_2 from the UAM simulation results for Day 159-76 149

D-15 (a) Residual histogram and (b) Residual vs. Observed plots for O_3 from the UAM simulation results for Day 159-76 150

D-16 (a) Residual histogram and (b) Residual vs. Observed plots for CO from the UAM simulation results for Day 160-76 151

D-17 (a) Residual histogram and (b) Residual vs. Observed plots for NO_2 from the UAM simulation results for Day 160-76 152

D-18 (a) Residual histogram and (b) Residual vs. Observed plots for O_3 from the UAM simulation results for Day 160-76 153

D-19 (a) Residual histogram and (b) Residual vs. Observed plots for CO from the UAM simulation results for Day 226-76 155

D-20 (a) Residual histogram and (b) Residual vs. Observed plots for NO_2 from the UAM simulation results for Day 226-76 155

D-21 (a) Residual histogram and (b) Residual vs. Observed plots for O_3 from the UAM simulation results for Day 226-76 156

TABLES

Number Page

1 Summary of Meteorological Conditions on 10 Test Days 7
2 Predicted and Observed O_3 Maxima for the PBM 20
3 Initial Pollutant Concentrations Assigned in the LPM 37
4 Predicted and Observed O_3 Maxima for the LPM 42
5 Predicted and Observed O_3 Maxima for the UAM 79
6 O_3 Regression Statistics for the UAM 80
B-1 Summary of Model Performance Statistics From the PBM 113
E-1 Summary of Mean Concentration Statistics From the UAM 159
E-2 Summary of Analysis of Trends Data From the UAM 161
E-3 Summary of Concentration Maxima Statistics From the UAM 163

SECTION 1

INTRODUCTION

The Regional Air Pollution Study (RAPS) was conducted in the St. Louis region over the period 1974-1977 (Schiermeier, 1978). RAPS was designed to provide a comprehensive data set for the testing and evaluation of numerical air quality simulation models on an urban scale. While the RAPS field measurements were in progress EPA surveyed the available, state-of-the-art, photochemical air quality simulation models, and selected three for evaluation. In addition, there was a need to look at a simple box-model approach which was not embodied in an existing model. A box model was therefore constructed by EPA.

The models evaluated by EPA in this report are:

Photochemical Box Model (PBM) - a single cell Eulerian model constructed by EPA.

Lagrangian Photochemical Model (LPM) - a multi-level parcel model developed by Environmental Research and Technology, Inc.

Livermore Air Quality Model (LIRAQ) - a single-level Eulerian grid model developed by Lawrence Livermore Laboratory.

Urban Airshed Model (UAM) - a multi-level, Eulerian grid model developed by Systems Applications, Inc.

This report describes the results of simulations for 10 days when maximum measured O_3 concentrations exceeded 0.19 ppm in St. Louis. Generally these days exhibit stagnation conditions with little cloud cover and represent situations conducive to the production of photochemical oxidant from local emissions.

The models were tested extensively and corrections of obvious errors or deficiencies were made. However, no effort was made to adjust or tune the model predictions to observed concentration values. The prevailing philosophy behind the evaluation effort was to use the models in an off-the-shelf mode, much as they would be eventually applied by a user in a regulatory situation. However, great care was taken in preparation of data sets and model executions. Although model assumptions vary, effort was made to use data in similar manners in all models. Data preparation and actual execution of the models was accomplished solely by the authors at EPA. The goal of the evaluation was to provide a fair and objective determination of the accuracy of a set of photochemical models when tested in an operational mode against a comprehensive urban data base.

Interest in the accuracy of models stems from their planned use in emissions control strategies where models may be used to predict the effect on ozone levels of an introduction of new sources or a reduction in existing sources. In this report, models are tested against the RAPS data to see how well they predict absolute levels of ozone under known conditions. However, there is no way to be certain that the model will respond accurately to changing emissions senarios, even if the absolute levels are acceptably reliable. The judgement that control strategy work is warranted with a given model is part of the decision-making process, based on the integrity of the physicochemical mechanism and evidence for reliability from tests with an accurate data base.

SECTION 2

CONCLUSIONS AND RECOMMENDATIONS

The evaluations of urban photochemical air quality simulation models presented in this report represent the first comprehensive effort to examine model performance under controlled conditions. Great care was taken in establishing the same data base and impartial running procedures for all models. Detailed numerical results and conclusions are presented for individual models in the Sections 4, 5, 6 and 7. A brief summary of the conclusions follows.

1. The PBM is a model which performs best in near-stagnation conditions.

2. The LPM needs modification of the fixed-box formulation for the air parcel. Unrealistically high ozone predictions result under certain circumstances.

3. For a variety of reasons, LIRAQ lacks potential as a model for general use and might be phased out of the evaluation program. No decision is made on use by specialized groups for specific locales.

4. The UAM tends to consistently underpredict ozone. It is possible that the effect results from spurious numerical diffusion.

5. For all models, the user should have a strong scientific background and be extremely careful in implementing air quality simulations.

6. In general the variability between specific 1-hour predicted and observed concentrations at a particular location tends to be substantial. Decision makers in regulatory agencies should be cognizant of this variability.

Using the results described in this report and the possible model problems they elucidate, a final investigation of the structure of each model should be carried out. If any further problems are identified, with workable solutions, they should be corrected. Model modifications should be based on sound scientific judgement and not solely on a desire to improve the results. In the special case of LIRAQ, a decision should be made on whether or not to pursue further development and testing. Upon conclusion of final model changes, another set of runs should be made and analyzed. Perhaps up to 10 additional days from the RAPS could be included in the final analysis.

SECTION 3

THE DATA SET

As an integral part of the RAPS a network of 25 surface stations was established in and around the St. Louis region. These stations, shown in Figure 1, comprise the Regional Air Monitoring System (RAMS). The RAMS stations continually monitored various meteorological variables as well as ambient concentrations of pollutant gases. Schiermeier (1978) provides details on the instrumentation. In addition to the RAMS, upper air balloons were released each hour from urban and rural sites to provide wind profiles for modeling purposes.

An essential element in the data set for an air quality modeling exercise is a complete source emissions inventory for all gaseous and particulate species over the domain of interest. Littman (1979) summarizes the comprehensive data gathering and archiving of the RAPS emissions inventory. The inventory is divided into point source and area source classes with points defined as sources emitting at least 0.01 percent of the total emissions of a pollutant for the whole air quality control region. Line source emissions are included in the area source class. The area source emissions data are subdivided onto a horizontal grid of 1989 cells with variable spatial resolution, dependent upon the emissions source density. Grid resolution varies from 1 km in the more dense areas to 10 km in the sparse areas. The temporal resolution of the emission inventory is one hour. Criteria pollutants included in the inventory are TSP (total suspended particles), SO_2 (sulfur dioxide), NO_x (nitrogen oxides), THC (total hydrocarbons), and CO (carbon monoxide). Furthermore, total hydrocarbons are broken down into the component classes of non-reactives, olefins, paraffins, aldehydes, and aromatics. Figures 2, 3 and 4 show the emissions distribution from all sources, both point and area, averaged over 4 km grid cells for the St. Louis region for CO, NO_x, and THC respectively. These particular emissions data represent the period 0800-0900 CST on July 13, 1976, but are also representative of a weekday summer morning rush-hour distribution. The central area of the figures encompasses the downtown and industrial sections of St. Louis where emissions are higher. The ratio of point to total emissions is generally greater for NO_x than for either CO or THC. The stacks from two large power plants are clearly seen in the NO_x distribution as unusually large emissions within a cell, one located in the northern section of the grid and one in the southern.

This report presents the results of model simulations for ten individual days chosen from the RAPS data base. These days, five each from 1975 and 1976, account for some of the higher O_3 measurements observed in the RAPS surface monitoring network. Maximum hour-average single station O_3 values all exceeded 0.19 ppm on the 10 days. Table 1 lists the basic characteristics of the days: wind speed and direction, temperature, and solar radiation computed as averages over 0700-1359 CST. Also listed are the maximum mixing heights for each day as determined from the upper air sounding data. Higher O_3 levels generally occur when a prevailing high atmospheric pressure system exists over the area with little associated cloud cover, and represent the situations conducive to production of O_3 from locally generated precursor emissions. Both the dates and Julian day numbers for the 10 days are listed in Table 1 and either form may be used throughout this report to reference a particular day. Although chosen from both 1975 and 1976, the Julian dates are unique and will be used alone in the text.

TABLE 1. A SUMMARY OF WIND SPEED (WS), WIND DIRECTION (WD), TEMPERATURE, SOLAR RADIATION (ALL WAVELENGTHS), AND MAXIMUM AFTERNOON MIXING HEIGHT (MH) FOR THE 10 DAYS EXAMINED.[a]

Date	Day (Julian)	WS (m/s)	WD (deg)	Temp (°C)	Solar (ly/min)	Max MH (m)
5/22/75	142	1.1	224	29	1.12	1504
6/27/75	178	0.4	245	29	0.96	1822
7/28/75	209	2.0	18	30	0.98	1909
8/19/75	231	1.3	168	28	0.95	1052
9/08/75	251	1.8	181	25	0.89	1797
6/07/76	159	1.0	129	25	1.06	1972
6/08/76	160	1.3	284	27	1.01	1772
7/13/76	195	2.3	145	28	1.02	1853
8/13/76	226	1.1	273	30	0.86	1427
10/01/76	275	0.6	222	22	0.78	527

[a] Meteorological variables (except MH) are network averages over the period 0700-1359 CST.

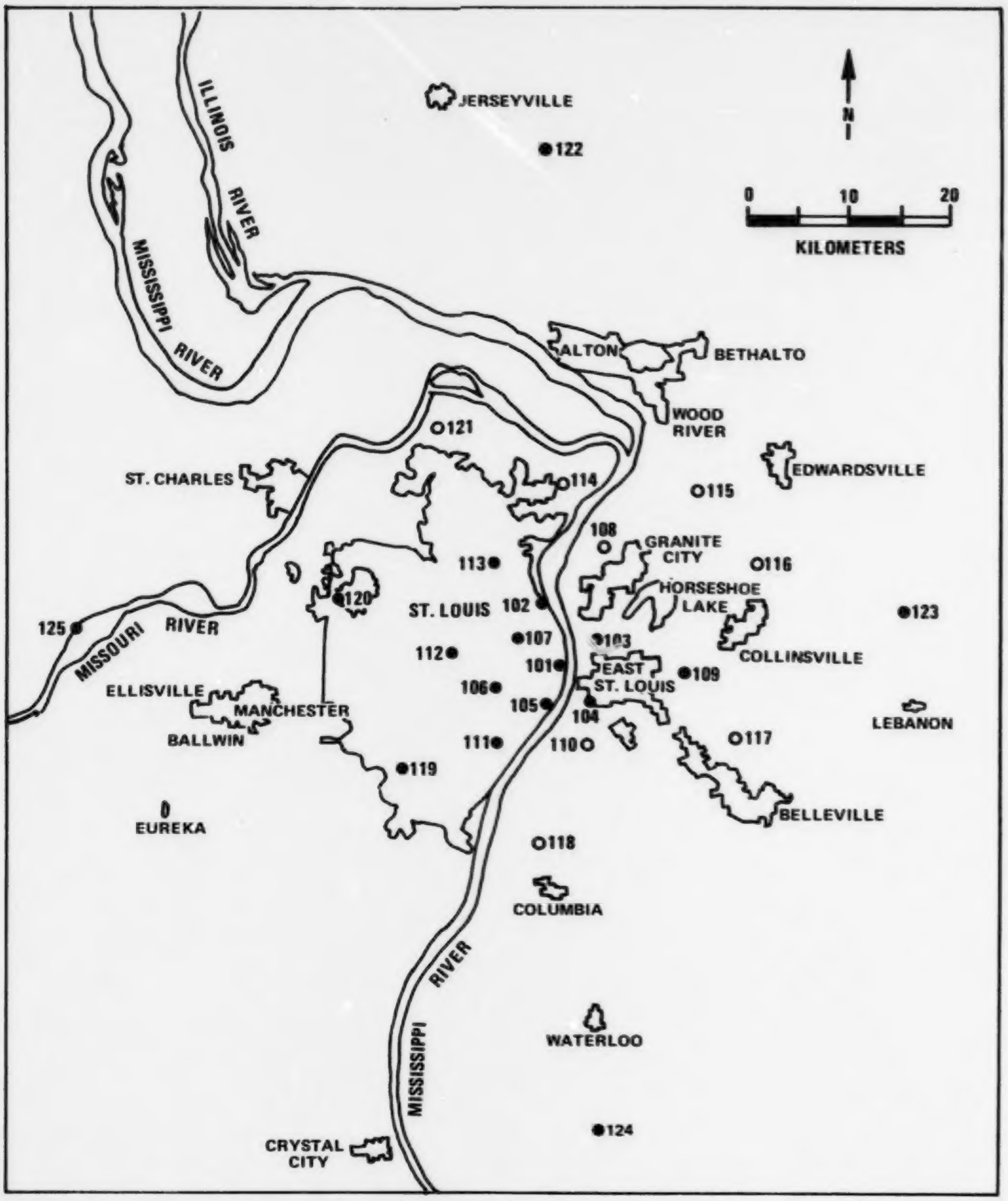
N
0
10
20
KILOMETERS
JERSEYVILLE
●122
ILLINOIS RIVER
MISSISSIPPI RIVER
ALTON
BETHALTO
WOOD RIVER
○121
EDWARDSVILLE
ST. CHARLES
○114
○115
108 ○
GRANITE CITY
○116
113●
HORSESHOE LAKE
●120
ST. LOUIS
102●
●123
125●
MISSOURI RIVER
●107
●103
COLLINSVILLE
112●
101●
EAST ST. LOUIS
●109
ELLISVILLE
MANCHESTER
106●
105●
104
LEBANON
BALLWIN
111●
110○
○117
●119
BELLEVILLE
EUREKA
○118
COLUMBIA
MISSISSIPPI RIVER
WATERLOO
●124
CRYSTAL CITY

Figure 1. The St. Louis area with locations of the RAPS surface stations.

BEGIN LAST LINE OF TEXT
BOTTOM OF IMAGE AREA, OUTSIDE DIMENSION FOR TABLES AND ILLUSTRATIONS
3/8"

PAGE NUMBER
EPA Form 2350-4 (4-80)
(PREVIOUSLY CIN. EPA FORM 287)
TYPING GUIDE SHEET

DAY:195-1976
HR:8

CO EMISSIONS

0	0	0	0	0	0	0	0	0	0	0	0	0	0	0	0	0
0	0	0	0	0	0	0	1	4	9	2	2	2	2	2	2	2
0	0	7	9	14	27	29	11	6	24	2	2	4	2	3	3	3
0	0	9	12	14	19	31	32	9	48	37	26	28	8	4	3	3
3	4	9	11	10	7	21	20	29	47	178	68	21	4	5	4	4
10	15	7	6	12	26	13	21	27	40	49	750	21	15	19	7	7
19	15	24	49	31	23	88	72	45	13	29	24	8	3	16	8	2
17	12	84	95	84	179	132	120	128	43	34	23	22	13	13	12	6
7	9	28	92	97	184	108	202	146	56	23	29	27	14	23	11	7
5	17	19	57	147	108	161	129	259	171	472	24	19	29	29	7	5
7	62	34	52	115	99	137	202	243	190	33	112	32	40	14	4	2
2	26	58	67	88	78	186	275	361	638	131	75	40	14	16	4	3
20	27	71	87	82	100	112	118	233	187	45	44	59	29	34	21	12
21	23	32	99	94	68	120	141	197	22	24	31	42	53	37	12	14
22	18	13	22	53	81	117	77	17	19	5	4	9	40	68	17	11
16	8	17	14	24	44	39	48	16	14	2	5	5	8	12	12	2
2	4	7	13	23	43	31	20	4	23	12	5	5	5	5	6	6
3	4	6	11	2	35	35	10	2	3	6	2	3	3	4	6	6
4	2	6	5	2	31	14	2	1	2	8	2	2	3	4	5	7
3	1	3	3	2	54	4	1	1	2	10	2	1	2	3	3	7
1	1	3	3	5	19	2	2	1	2	2	2	1	1	2	2	2
1	4	2	1	8	33	3	2	1	1	2	2	2	2	2	2	2

Figure 2. Total source emissions of CO, in kilograms/10, for the RAPS area on Day 195 of 1976 at 0800 CST. Grid cells are 4 km squares; the SW corner corresponds to UTM (x,y) coordinates of Zone 15: (706, 4236).

BEGIN FIRST LINE OF TEXT HERE
CENTER OF PAGE
TOP OF IMAGE AREA
DROPPED HEAD; BEGIN SECTIONS HERE
BEGIN LAST LINE OF TEXT
3/8"
BOTTOM OF IMAGE AREA; OUTSIDE DIMENSION FOR TABLES AND ILLUSTRATIONS
PAGE NUMBER
EPA Form 2350-4 (4-80)
(PREVIOUSLY CIN. EPA FORM 257)
U.S. GOVERNMENT PRINTING OFFICE 1980-
TYPING GUIDE SHEET

DAY:195-1976
HR:8

NOX EMISSIONS

0	0	0	0	0	0	0	0	0	0	0	0	0	0	0	0	0
0	0	0	0	0	0	0	2	7	13	7	5	5	5	6	5	5
0	0	4	5	6	10	7	8	10	26	7	5	7	5	7	9	9
0	0	5	7	7	9	7	8267	11	56	41	30	26	11	9	11	11
1	1	5	7	6	4	6	8	16	67	1567	302	21	8	11	11	12
3	6	6	7	7	3	9	14	15	23	22	325	115	20	25	14	16
44	28	25	142	166	35	75	79	42	10	5	31	14	8	22	17	5
30	21	98	157	173	216	175	154	147	61	49	48	36	22	21	28	14
8	11	14	131	127	200	169	192	384	66	35	34	37	24	36	25	15
5	82	37	104	135	93	151	177	351	259	475	34	28	40	32	15	11
13	322	104	89	176	91	143	237	337	1016	123	89	55	45	17	7	5
3	57	168	228	160	125	233	485	911	718	269	86	50	16	18	7	8
20	32	97	119	127	131	146	139	298	417	230	51	56	29	33	23	16
18	23	41	145	146	83	107	174	436	36	26	37	44	63	37	16	29
40	25	23	33	72	114	304	82	29	31	10	8	15	44	61	21	16
36	17	13	15	19	61	63	81	24	18	6	9	9	12	16	18	6
3	5	6	12	20	61	29	26	12	21	13	9	9	8	9	10	10
3	5	6	10	3	64	4386	10	5	4	7	4	6	7	8	10	10
4	3	7	6	3	61	19	6	4	3	9	3	4	6	8	9	13
4	1	3	4	3	184	9	3	4	4	11	3	3	5	6	7	13
1	1	4	3	10	34	3	4	4	4	3	3	2	2	3	3	5
1	4	2	2	12	37	7	6	4	2	3	3	4	3	3	3	5

Figure 3. Total source emissions of NO_x, in kilograms, for the RAPS area on Day 195 of 1976 at 0800 CST. Grid cells are 4 km squares; the SW corner corresponds to UTM (x, y) coordinates of Zone 15: (706, 4236).

BEGIN FIRST LINE OF TEXT HERE
CENTER OF PAGE
TOP OF IMAGE AREA
DROPPED HEAD: BEGIN SECTIONS HERE
BEGIN LAST LINE OF TEXT
BOTTOM OF IMAGE AREA OUTSIDE DIMENSION FOR TABLES AND ILLUSTRATIONS
PAGE NUMBER
EPA Form 2350-4 (4-80)
(PREVIOUSLY CIN. EPA FORM 232)
U.S. GOVERNMENT PRINTING OFFICE
TYPING GUIDE SHEET

DAY:195-1976
HR:8

THC EMISSIONS

0	0	0	0	0	0	0	0	0	0	0	0	0	0	0	0	0
0	0	0	0	0	0	0	2	7	32	61	21	8	6	8	5	2
0	0	21	28	41	79	96	44	24	110	20	8	12	12	15	9	8
0	0	28	37	42	55	104	108	34	200	184	118	132	48	16	10	10
9	21	28	34	34	26	71	75	107	133	210	911	247	8	14	12	11
35	84	30	23	49	93	40	98	131	130	124	370	904	33	72	20	12
53	65	100	203	41	85	402	299	171	67	112	200	17	11	108	60	33
41	31	300	296	245	940	412	402	447	172	77	87	68	45	44	42	39
15	25	82	166	329	1156	345	464	543	140	183	221	70	44	71	31	33
21	31	73	178	573	618	427	477	2251	254	476	63	38	64	134	19	20
121	111	85	154	290	345	427	580	959	782	160	150	131	146	112	10	2
4	79	270	202	264	229	566	667	897	1441	677	310	136	50	26	12	7
59	168	216	339	295	439	441	604	649	760	311	231	222	87	120	87	77
78	128	96	1655	279	574	305	308	486	101	89	112	132	243	139	56	66
95	52	30	65	141	238	409	341	72	69	12	10	27	109	240	56	24
51	22	95	46	71	152	153	153	49	33	8	14	14	25	32	24	3
4	29	29	45	84	138	112	33	12	77	36	14	14	20	23	15	15
6	42	35	27	17	97	102	31	5	16	16	6	8	16	22	15	15
16	26	33	44	24	135	50	6	6	7	17	10	6	10	15	9	35
18	2	9	8	10	114	9	8	9	8	34	14	5	5	8	4	42
1	3	7	5	16	58	7	9	9	8	5	5	2	4	6	6	2
4	24	9	7	19	98	10	5	3	3	5	5	15	13	6	6	2

Figure 4. Total source emissions of THC, in kilograms, for the RAPS area on Day 195 of 1976 at 0800 CST. Grid cells are 4 km squares; the SW corner corresponds to UTM (x, y) coordinates of Zone 15: (706, 4236).

SECTION 4

PHOTOCHEMICAL BOX MODEL

OVERVIEW

The Photochemical Box Model (PBM), a single cell Eulerian air quality simulation model, simulates the transport and chemical transformation of air pollutants in smog-prone urban atmospheres. The model's domain is set in a variable volume, well-mixed reacting cell where the physical and chemical processes responsible for the generation of O_3 by its HC and NO_x precursors are mathematically created. These processes include the transport and dispersion of pollutant species through the cell, the injection of primary precursor species by emission sources, and the chemical transformation of the reactive species into intermediate and secondary products. They are schematically illustrated in Figure 5.

In the application of the model to the St. Louis RAPS data base the horizontal length scale of the single cell was 20 km and the vertical scale was time-varying, proportional to the depth of the mixed layer. The model domain was centered on downtown St. Louis such that the 20x20 km area encompassed most of the major emissions sources on either side of the Mississippi River. Source emissions were assumed to be distributed uniformly across the surface face of the cell. All of St. Louis City (shaded area, Figure 6) except the extreme northern and southern tips was included in the model domain. Twelve of the RAMS surface monitoring stations as well as one upper air sounding location were also located within the cell's boundaries.

Model simulations were conducted using the PBM for each of the 10 test days listed in Table 1. Although a summary of results for O_3 predictions on all days is given, detailed descriptions of model results are presented for only three of these days. Emphasis is placed on the simulation results for the pollutants CO, NO_2, and O_3 for the Julian days 142, 251, and 275.

METHOD

While the data requirements for the PBM are not particularly rigorous, three data preprocessors must be executed prior to each model simulation. The first accesses the RAPS hour-average air quality and meteorological data base forming the initial concentrations of participating species, determining the hour-average wind vectors that guide transport through the model domain, and choosing the hourly updated concentrations of species at the upwind boundary of the box. The first preprocessor also forms similar spatial averages of concentrations of monitored pollutant species for comparison with model predictions.

The second preprocessor accesses the RAPS minute-average air quality and meteorological data base to determine ten-minute average values of total solar radiation from pyranometer measurements. From these values the time-varying photolytic rate constants can be determined through a series of empirical and theoretical relationships. The temporal resolution of these data for the model is greater than for most other data because of the rapid chemical reactions which are associated with these rate constants. This preprocessor also calculates the diurnal growth pattern of the mixed layer, or the depth of the model domain. To perform this calculation, the morning minimum and afternoon maximum mixed layer heights are provided by the user. These heights were determined in the RAPS application by studying the vertical structure of temperature and moisture from the radiosondes released at site 141 (solid triangle in Figure 6). Releases occurred throughout the day at six-hour intervals beginning one hour before sunrise. The model fits a piece-wise linear function between the specified minimum and maximum depths that simulates the actual mixed layer growth as observed by acoustic sounder, lidar, and radiosonde techniques. Ten-minute averages of mixed layer height are formed for the PBM; photolytic rate constants for the corrresponding time period are integrated through the mixed layer. The third preprocessor is responsible for forming hourly emissions source terms for CO, NO, NO_2, and non-methane hydrocarbons. The RAPS area and point source modelers' emission inventory archives are accessed and all source emissions, both area and point, within the model domain are summed to provide a total emission rate for each primary pollutant species at every hour of model simulation.

The PBM may be executed when the data files from the three preprocessors have been created. The only other relevant information needed at this time is the concentration of O_3 at the top boundary of the modeling domain, or that pollutant mass transported into the area by winds aloft during the night.

This value is determined from the O_3 measurements at the far upwind surface monitoring sites after the nocturnal temperature inversion has eroded and the air aloft mixes down through the atmosphere to the surface. Concentrations of other pollutants at the top of the modeling region are assumed to be negligible. Model simulation is started at 0500 CST and continues through 1700 CST.

The PBM contains a chemical kinetic mechanism with 36 reactions and 27 reactive species (Demerjian and Schere, 1980). The set of equations describing the rates of change of the concentrations of these species is numerically solved at time steps on the order of 10 minutes. From these solutions the model then determines the hour-average predicted concentrations of all modeled species.

RESULTS

Among the 10 selected days for model simulations from the RAPS data base are 3 in which the maximum observed afternoon O_3 concentration occurred within the PBM domain. These were days when extreme stagnation conditions existed with very light and variable winds. Very little of the primary emissions moved out of the modeled area. It is during this type of stagnation episode that a single cell box model would most likely be appropriate for air quality simulation since most of the pollutant mass stays within the model domain. On the other modeled days the maximum O_3 level occurred farther downwind, outside of the PBM's boundaries. Simulations were also conducted with the PBM on these days even though maximum O_3 measurements within the box area were somewhat lower than those downwind.

The PBM simulated concentrations represent spatial averages over the volume of the box. The appropriate observed concentration with which to compare predictions is the average over all 12 monitoring sites within the box. These observed average concentrations are represented by the open circles in the concentration time series described below. Another factor for consideration is the range of concentration values observed among the 12 sites within the PBM domain. The highest and lowest measurements are described by the dashed lines in the time series. A coarse measure of model performance is made by observing whether the PBM predicted concentrations (shown as solid lines), fall within the range of observed concentrations (between the dashed lines) and preferably as close as possible to the average observed concentrations (shown as circles).

The first simulation day to be focused upon is Day 142 (5/22/75). The synoptic meteorological conditions on this day showed an expansive high pressure system centered over western Virginia and a general windflow from the southwest in the mid-Mississippi Valley area. Wind speeds in St. Louis, however, were light and on the order of 1.0 m s^{-1}. Skies were completely clear. The maximum afternoon hour-average O_3 measurement occurred at noon at site 101 in downtown St. Louis. According to the convention for time referencing employed here, the 1200 hour-average refers to the average concentration from 1200 to 1300 h.

Figure 7a shows the time series for CO on Day 142. The model predictions fall within the envelope or range of observed concentrations and actually track the average observed values quite well. Carbon monoxide is included in this analysis because it reacts very slowly in the atmosphere and may be considered virtually inert for the time scales discussed here.

As such, any problems with the emissions or the advective and dispersive portions of the PBM would be reflected in the CO predictions, whereas the complex chemical interactions of a more reactive pollutant could mask problems with transport or emissions. One interesting aspect of a primary pollutant's ambient concentration is demonstrated by the sharp peaks in the upper boundary of the observed concentration envelope at 1100 and 1400 hours. A single station within the model domain at these times was most likely affected by a strong CO source, possibly a nearby roadway. These peaks also drive the average concentration toward higher values. Secondary pollutants, such as O_3, with no significant emission sources, do not exhibit such anomalous behavior. The model response, driven in part by a homogeneous emissions distribution, does not display these discontinuities.

The time series for NO_2 on the same day is shown in Figure 7b. Here the model predictions throughout the simulation are consistently greater than the average observations but generally fall within the concentration envelope. Figure 7c displays the O_3 time series. PBM predictions track the average observations through mid-morning and then diverge near noon. At that time, observed O_3 levels begin to decrease while the predictions continue to increase, peaking one hour later at 1300 CST. The model-predicted peak O_3 concentration reached 0.175 ppm compared with the average observed peak of 0.137 ppm, a 28% overprediction. The model predictions fall mostly within the concentration envelope except for the last few hours of the simulation. Background concentrations of O_3 on Day 142 were on the order of 0.06 ppm.

The indication from the reactive species time series is that the simulated chemical interactions may have been somewhat overreactive, especially in view of the opposite predictive trends for CO and NO_2. This assumption presumes no major errors in the emissions inventory as well. Other simulations on this 10 day series may help to substantiate or dispel this indication.

Day 275 (10/1/76) is considered to be the most extreme case of stagnation during the 1975-76 RAPS project. The synoptic meteorological conditions revealed a high pressure region over the Texas-Arkansas area with northwest flow aloft over St. Louis. Near the surface, however, winds were very light and variable in direction with little transport through the St. Louis area. Skies were clear all day and a subsidence inversion over the city held the mixed depth to a maximum of 500 m above ground during the afternoon. The greatest hour-average O_3 measurement occurred at site 102, just north of downtown, at 1400 CST.

Figure 8a shows the CO time series for Day 275. The overall concentration levels are substantially greater than those on Day 142. The model-predicted CO concentrations are smaller than the average observations during the morning hours when the concentrations are at high levels. The peak to mean ratio (single station peak; spatially averaged mean) for the observed CO values within the model domain is apparently very large at 0700 CST. The atmosphere was extremely stable during the early morning hours and late afternoon hours after sunset as is apparent from the precipitous concentration gradients at these times. Enhanced motor vehicle rush-hour CO emissions combine with stable atmospheric conditions to exaggerate the effect. Because a PBM simulation begins as a well-mixed cell of finite depth and not as a stably stratified volume, as the atmosphere actually exists on a morning like that of Day 275, it is difficult, if not impossible, to correctly simulate the peak observed CO concentration. This is a natural limitation of the simple box model for stable conditions.

The concentration levels of both NO_2 and O_3 as seen in Figures 8b and 8c are also substantially greater than those on Day 142. The model-predicted NO_2 concentrations follow the average observed concentrations well and show slightly smoother temporal gradients than those observed. Simulated concentrations of O_3 also display a trend similar to observed O_3. The afternoon predictions actually track the upper boundary of the concentration envelope better than they do the average observed concentrations. The model-predicted hour-average O_3 maximum is 0.228 ppm occurring at 1500 CST while the average observed peak is 0.183 ppm at 1400 CST, a 25% overprediction. Background O_3 on this day was approximately 0.06 ppm. After sunset the NO_x concentrations rose rapidly and consequently produce dramatic decreases in the observed O_3 level as the air near the surface is cut off from the rest of the atmosphere's boundary layer. This very stable situation again points to the problem of PBM simulation in such a case. The more slowly varying model predicted functions of NO_2 and O_3 do not show the same behavior after sunset as do the observations.

These discussions of model performance for Days 142 and 275 indicate the ability of the PBM to simulate urban air quality for selected pollutants in relatively stagnant conditions. For a case with a more defined advective flow through the area, the usefulness for air quality simulation of the PBM may be diminish. For example, on Day 251 a definite flow from the south came through the St. Louis area. Wind speeds were on the order of 2 m s^{-1}, and while still relatively light and of persistent direction, they are capable of carrying primary emissions from St. Louis a distance of 72 km over a 10 hour period. Indeed the maximum hour-average observed O_3 concentration occurred at site 122 at 0.255 ppm at 1400 CST, a considerable distance north of the PBM domain. Prevailing meteorological conditions indicated a nearly stationary front lying just north of St. Louis with strong high pressure areas to the north and south of this frontal zone.

The CO time series for Day 251 (9/8/75) in Figure 9a shows a substantial early morning peak in observed concentration. Model predictions did not come close to the peak although simulated results look better throughout the remainder of the day. A similar trend is noticed in the NO_2 predictions shown in Figure 9b. Because of the apparently large peak-to-mean ratios in the observed concentrations of both species and their association with motor vehicle emissions, it is highly likely that one or two RAPS monitoring sites were immediately downwind of a roadway during the morning rush hours.

Figure 9c displays the O_3 time series on Day 251. The observed concentrations were only somewhat greater than the 0.06 ppm background value on that day. The peak in the averaged observed O_3 concentration was 0.084

ppm at 1500 CST. However, the model prediction at the same hour was 0.204 ppm, an overprediction of 143% but a value actually closer to the single station maximum recorded that day north of the PBM domain. The simulated concentrations were generally overpredicted for O_3, and fall out of the range of the concentration envelope through most of the simulation. One of the problems with advection in a simple box model is the hysteresis, or 'memory retention' within the numerical approximation for transport. Venkatram (1978) discusses this issue relative to box models in general. Briefly, a box model cannot be ventilated by a transport wind as quickly as actually occurs in the atmosphere, since there is a time lag for this process to occur in the model. Thus the O_3 concentrations predicted on the given day may display the potential effects of chemical reaction and transport had the precursor species not been advected out as rapidly as they are in the real St. Louis atmosphere. The similarity between the predicted O_3 peak and that at site 122 north of the city tends to lend support to this hypothesis.

One significant aspect of photochemical transformation has been omitted from these discussions on PBM simulation in an urban atmosphere. This aspect pertains to the presence of volatile organic compounds, or hydrocarbons (HC), in the smog mixture. While the chemical kinetic mechanism in the PBM does account for the HC interactions through a five-class structural approach, discussion of the details of these interactions on O_3 predictions are beyond the scope of this paper.

Table 2 presents a summary of the predicted and PBM domain-average observed O_3 maxima and an elementary statistical analysis of the results for all 10 modeled days. The 'specific' model predictions are those that correspond to the same hour as the observed maximum and the 'global' predictions represent the peak at any hour of the simulation. The specific and global predictions may not coincide, indicating a phase lag between observed and predicted O_3 peaks. This lag often appears when the maximum observed O_3 within the model domain occurs before noon. Statistics on the residual concentration, ΔC, have been computed for both the specific and global predictions. Both the average signed residual and absolute residual, and

TABLE 2. A SUMMARY OF PREDICTED AND OBSERVED O_3 MAXIMA FOR THE PBM

Day[a]	Hour (CST)	Observed at 4-meters (ppm)	PBM Predicted	
			Specific (ppm)	Global (ppm)
142 (1975)	12	0.14	0.15	0.18
178	14	0.16	0.22	0.22
209	10	0.11	0.09	0.12
231	10	0.08	0.07	0.11
251	15	0.08	0.20	0.20
159 (1976)	13	0.13	0.21	0.21
160	14	0.16	0.18	0.19
195	15	0.15	0.15	0.15
226	15	0.14	0.17	0.17
275	14	0.18	0.22	0.23

[a] Ten days selected from 1975 and 1976.

For the data displayed above:

ΔC = Obs minus Specific

$\overline{\Delta C} = -0.033$

$\text{s.d.}(\Delta C) = 0.041$

$\overline{|\Delta C|} = 0.039$

ΔC = Obs minus Global

$\overline{\Delta C} = -0.045$

$\text{s.d.}(\Delta C) = 0.033$

$\overline{|\Delta C|} = 0.045$

standard deviation are presented for the analyses. The average residual is negative in both the specific and global cases, indicating an overprediction of O_3. The fact that the average absolute residual is either close or equal to the magnitude of the average signed residual implies that the overprediction is consistent through all modeling days. The magnitude of the standard deviation (s.d.) is on the same order as the average residual itself. The discrepancy on Day 251 accounts for a good portion of the s.d. The average value of the model's overprediction for O_3 over all ten days is 31%.

Although the analysis presented in Table 2 summarizes one aspect of model performance, it is clearly not a complete picture of the accuracy or precision of the PBM. In order to more fully appreciate the PBM performance it is instructive to view the model results from a broader statistical perspective. Figure 10 presents frequency histograms (RS) of the residual concentrations, the observed minus predicted model results, for CO, NO_2, and O_3 over all test days. An ideal distribution would be narrow with a peak at the 0.0 residual. While all three histograms show peaks near 0.0 they tend to be skewed toward the over or underprediction side. The RS for CO shows the model to be underpredicting more frequently while O_3 is seen to be overpredicted. The nitrogen dioxide RS is more symmetrical than the others but does contain a few outliers on the underpredictive side.

A plot of residual versus observed concentrations (RO) should indicate whether the bias in the predictions displays any trend with the magnitude of the measured concentrations. These plots for the same species are shown in Figure 11. For CO and NO_2, both primary pollutant species, there appears to be a trend toward greater underprediction with higher ambient concentrations. The trend is more clearly discernible with CO. Ozone however displays no particular trend with observed concentration but the PBM generally overpredicts ambient values above 0.05 ppm.

The PBM has been exercised on a variety of days taken from the RAPS data base. The prevailing meteorological conditions occurring on some of them may not have been compatible with the environment for optimum results from the model. Using this model in a regulatory capacity could be restricted to worst case stagnation conditions where the model seems to perform best. Time series for pollutant species on test days other than those presented in this discussion are displayed in Appendix A. Also, tabulated model performance statistics for mean concentration data, analysis of trends data, and concentration maxima data from the PBM are presented in Appendix B.

CONCLUSIONS

The evaluation of the PBM is a continuing effort at EPA's Meteorology Division. The analysis presented here is the first major step toward a thorough understanding of model performance. Initial evidence shows that the model is a useful tool in assessing the urban air quality for photochemically reactive pollutants, especially in stagnation conditions. The PBM is relatively simple to use and its data requirements are far less stringent than most other numerical air quality simulation models. The areas of further study that may be pursued include:

(1) The hysteresis problem during advection conditions.

(2) The relationship between the average O_3 concentration observed within the model domain and the maximum O_3 level observed at a single station.

(3) The continued testing and refinement of the chemical kinetic mechanism within the PBM.

(4) The sensitivity of the model to variations in selected parameters such as initial and boundary concentrations, initial cell depth, emissions, wind speed, and solar radiation.

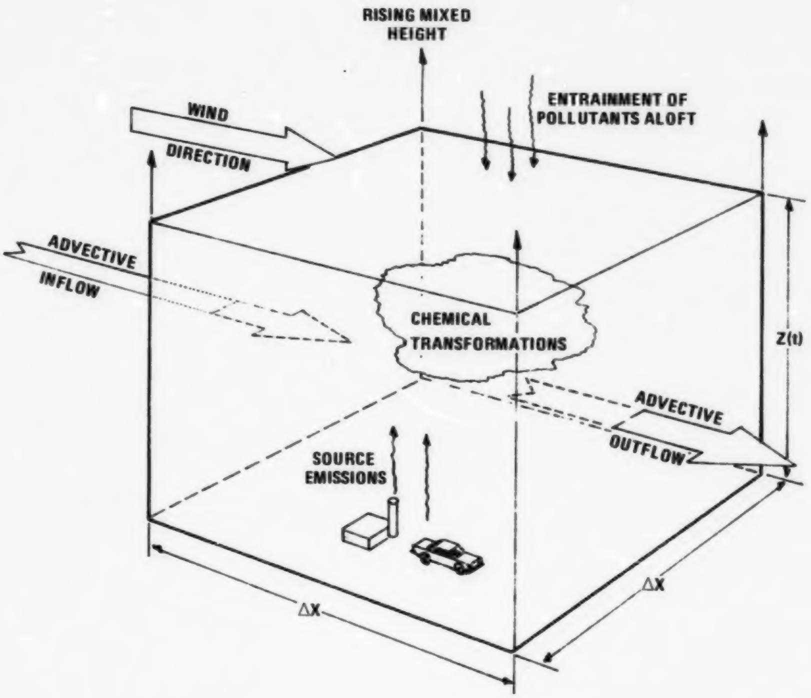
RISING MIXED HEIGHT
WIND DIRECTION
ENTRAINMENT OF POLLUTANTS ALOFT
ADVECTIVE INFLOW
CHEMICAL TRANSFORMATIONS
Z(t)
ADVECTIVE OUTFLOW
SOURCE EMISSIONS
ΔX
ΔX

Figure 5. Schematic drawing of the PBM domain.

BEGIN LAST LINE OF TEXT
3/8"
PAGE NUMBER
BOTTOM OF IMAGE AREA OUTSIDE DIMENSION FOR TABLES AND ILLUSTRATIONS
EPA Form 2350-4 (4-80)
(PREVIOUSLY CIN: EPA FORM 787)
☆ U.S. GOVERNMENT PRINTING OFFICE 1980-665/428
TYPING GUIDE SHEET

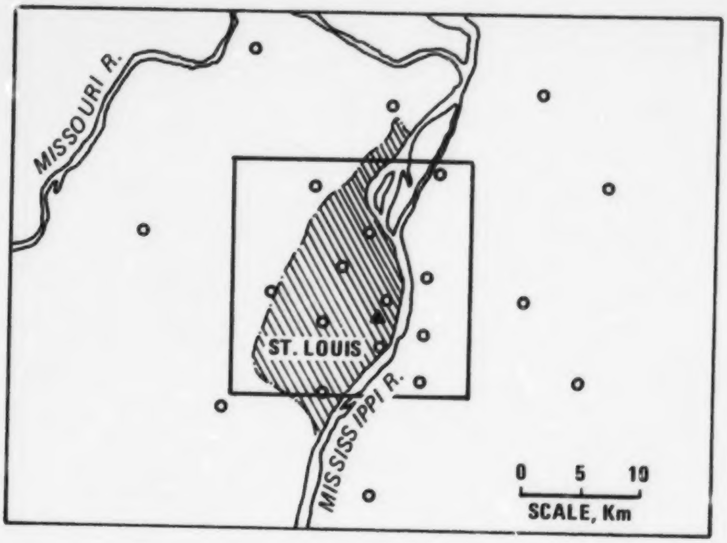
MISSOURI R.
ST. LOUIS
MISSISSIPPI R.
0
5
10
SCALE, Km

Figure 6. Map of St. Louis area depicting extent of PBM modeling domain (boxed area), city of St. Louis (shaded area), RAPS monitoring stations (circles), and radiosonde ascent site (triangle).

BEGIN LAST LINE OF TEXT
3/8"
BOTTOM OF IMAGE AREA; OUTSIDE DIMENSION FOR TABLES AND ILLUSTRATIONS

PAGE NUMBER
EPA Form 2350-4 (4-80)
(PREVIOUSLY CIN. EPA FORM 357)
U.S. GOVERNMENT PRINTING OFFICE
TYPING GUIDE SHEET

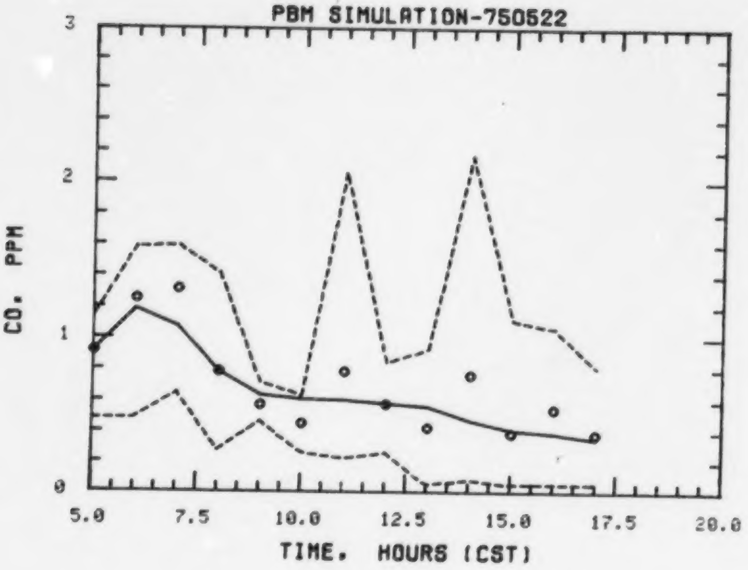

Figure 7a. PBM simulation results for Day 142 of 1975. Time series of average observed (circles), range of observed (dashed lines), and model simulated (solid line) hour-average concentrations of CO.

BEGIN LAST LINE OF TEXT
3/8"
BOTTOM OF IMAGE AREA; OUTSIDE DIMENSION FOR TABLES AND ILLUSTRATIONS

EPA Form 2350-4 (4-80)
(PREVIOUSLY EIN. EPA FORM 333)
PAGE NUMBER
U.S. GOVERNMENT PRINTING OFFICE
TYPING GUIDE SHEET

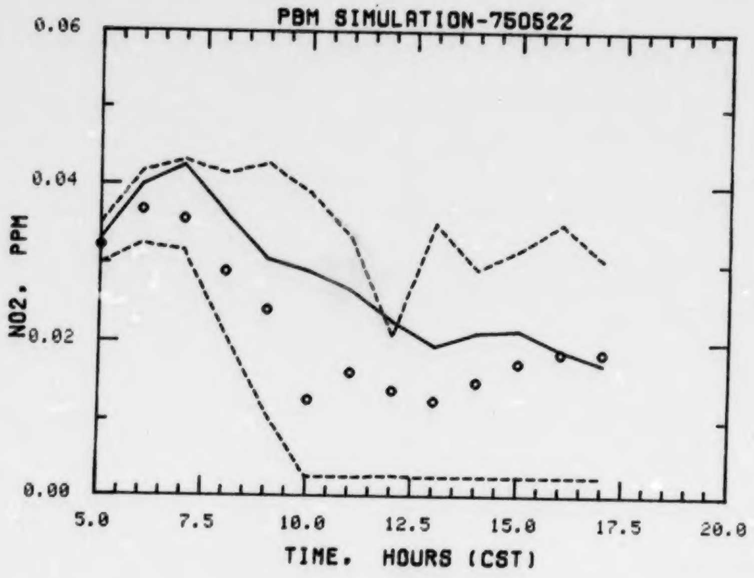

Figure 7b. PBM simulation results for NO_2 - Day 142 of 1975. Keys to figure described in 7a.

9-1/8"

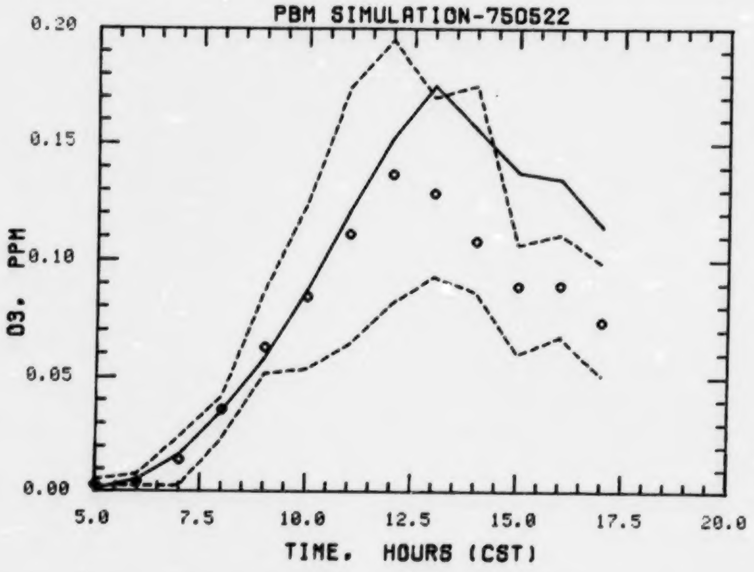

Figure 7c. PBM simulation results for O_3 - Day 142 of 1975. Keys to figure described in 7a.

BEGIN LAST LINE OF TEXT
BOTTOM OF IMAGE AREA; OUTSIDE DIMENSION FOR TABLES AND ILLUSTRATIONS
3/8"

PAGE NUMBER
EPA Form 2350-4 (4-80)
(PREVIOUSLY CIN. EPA FORM 237)
TYPING GUIDE SHEET

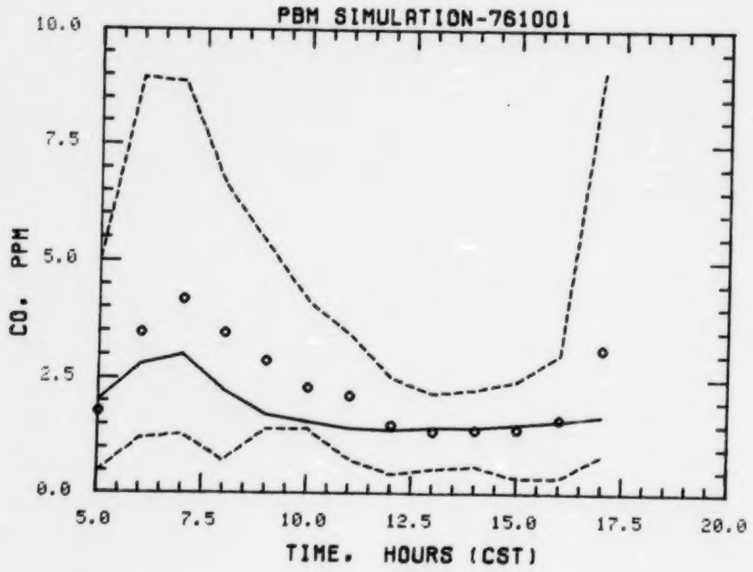

Figure 8a. PBM simulation results for Day 275 of 1976. Time series of average observed (circles), range of observed (dashed lines), and model simulated (solid line) hour-average concentrations of CO.

BEGIN LAST LINE OF TEXT
BOTTOM OF IMAGE AREA; OUTSIDE DIMENSION FOR TABLES AND ILLUSTRATIONS
3/8"

PAGE NUMBER
EPA-287 (Cin.)
(4-76)

TYPING GUIDE SHEET
BEGIN FIRST LINE OF TEXT HERE
CENTER
TOP OF IMAGE AREA
DROPPED HEAD; BEGIN SECTIONS HERE

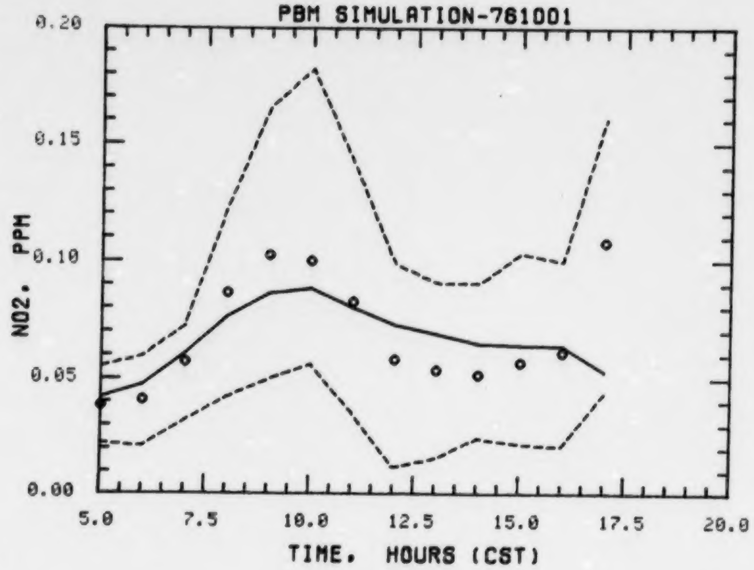

Figure 8b. PBM simulation results for NO_2 - Day 275 of 1976. Keys to figure described in 8a.

9-1/8"

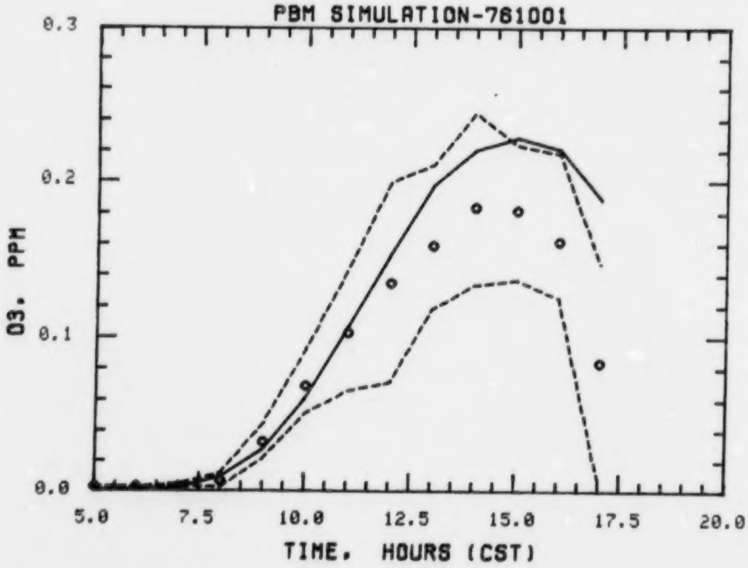

Figure 8c. PBM simulation results for O_3 - Day 275 of 1976. Keys to figure described in 8a.

BEGIN LAST LINE OF TEXT
BOTTOM OF IMAGE AREA; OUTSIDE DIMENSION FOR TABLES AND ILLUSTRATIONS
3/8"

PAGE NUMBER
EPA-287 (Cin.)
(4-76)

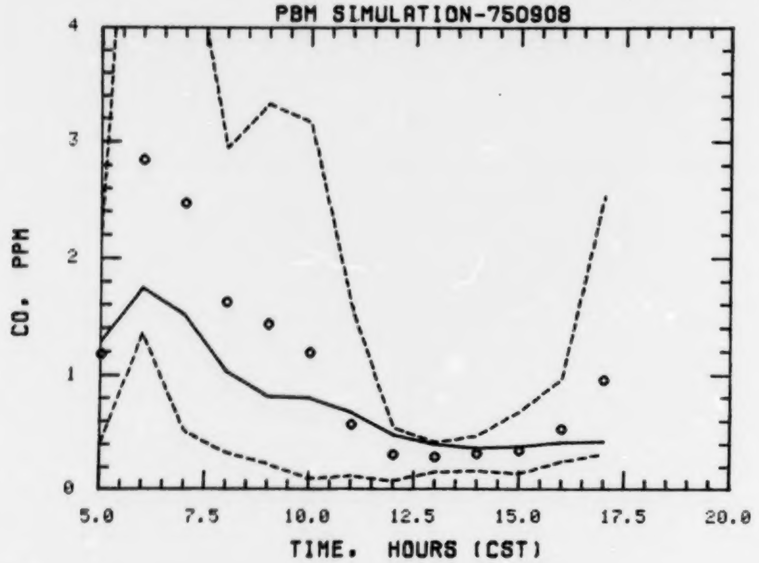

Figure 9a. PBM simulation results for Day 251 of 1975. Time series of average observed (circles), range of observed (dashed lines), and model simulated (solid line) hour-average concentrations of CO.

BEGIN LAST LINE OF TEXT
BOTTOM OF IMAGE AREA; OUTSIDE DIMENSION FOR TABLES AND ILLUSTRATIONS
3/8"

PAGE NUMBER
EPA-287 (Cin.)
(4-76)

TYPING GUIDE SHEET
BEGIN FIRST LINE OF TEXT HERE
CENTER
TOP OF IMAGE AREA
DROPPED HEAD; BEGIN SECTIONS HERE

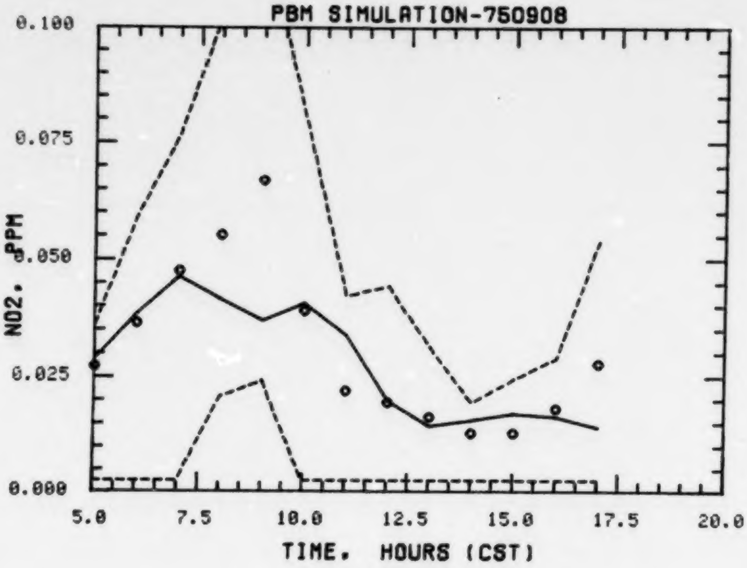

Figure 9b. PBM simulation results for NO_2 - Day 251 of 1975.
Keys to figure described in 9a.

9-1/8"

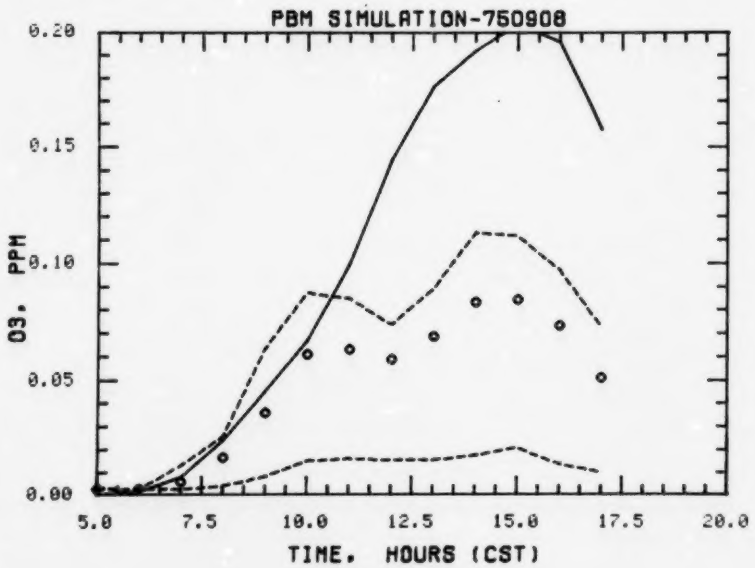

Figure 9c. PBM simulation results for O_3 - Day 251 of 1975.
Keys to figure described in 9a.

BEGIN LAST LINE OF TEXT
BOTTOM OF IMAGE AREA; OUTSIDE DIMENSION FOR TABLES AND ILLUSTRATIONS
3/8"

PAGE NUMBER
EPA-287 (Cin.)
(4-76)

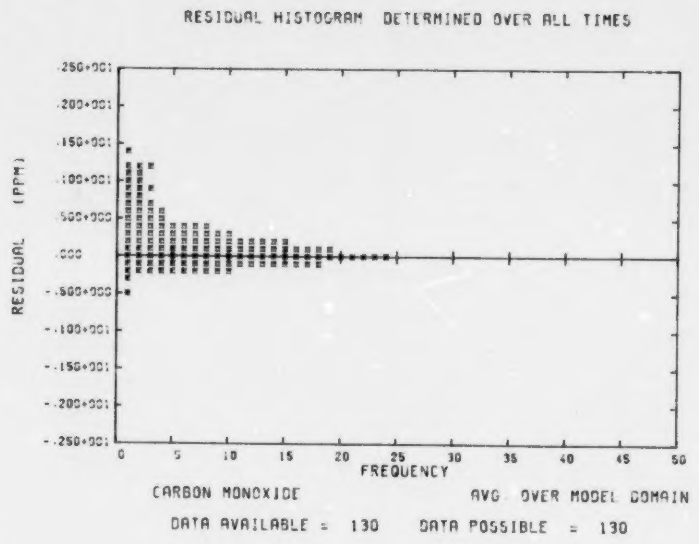

Figure 10a. Residual histogram from the PBM simulation results for all 10 test days for CO.

BEGIN LAST LINE OF TEXT
Reproduced from best available copy.
BOTTOM OF IMAGE AREA; OUTSIDE DIMENSION FOR TABLES AND ILLUSTRATIONS
3/8"

PAGE NUMBER
EPA-287 (Cin.)
(4-76)

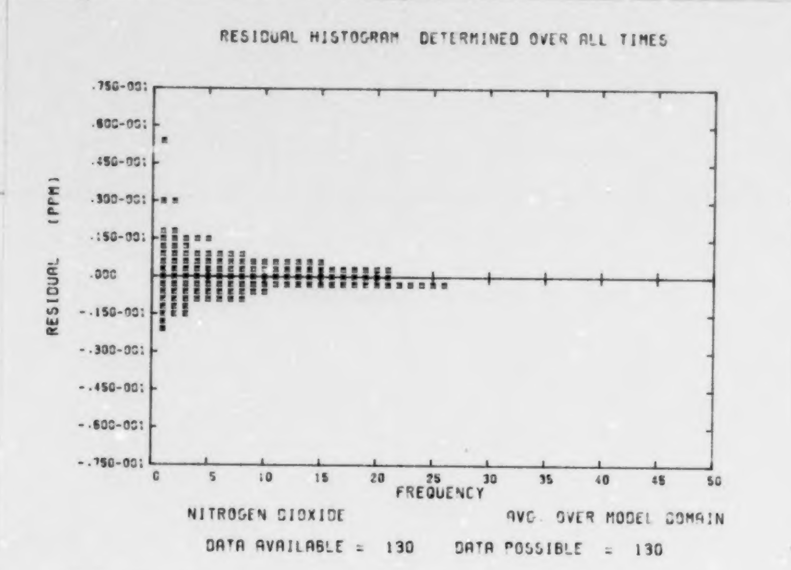

Figure 10b. Residual histogram from the PBM simulation results for all 10 test days for NO_2.

9-1/8''

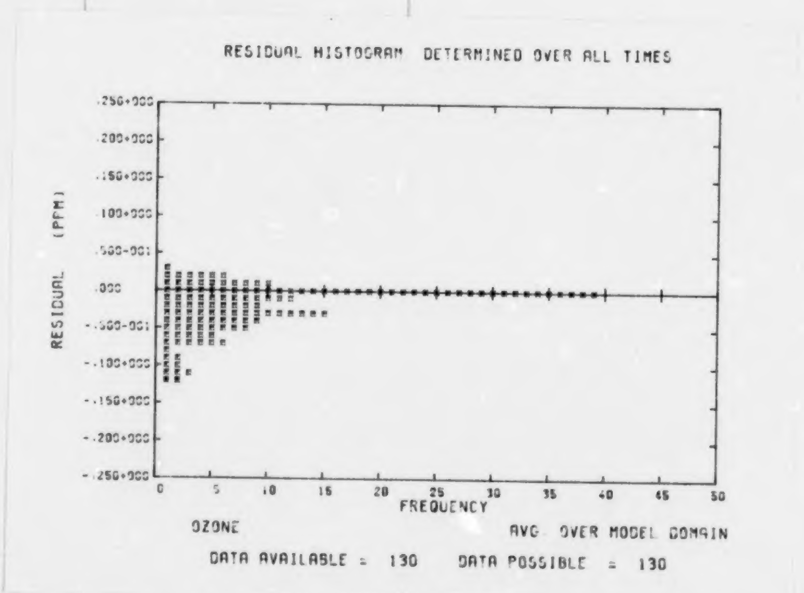

Figure 10c. Residual histogram from the PBM simulation results for all 10 test days for O_3.

BEGIN LAST LINE OF TEXT
BOTTOM OF IMAGE AREA; OUTSIDE DIMENSION FOR TABLES AND ILLUSTRATIONS
3/8''

PAGE NUMBER
EPA-287 (Cin.)
(4-76)

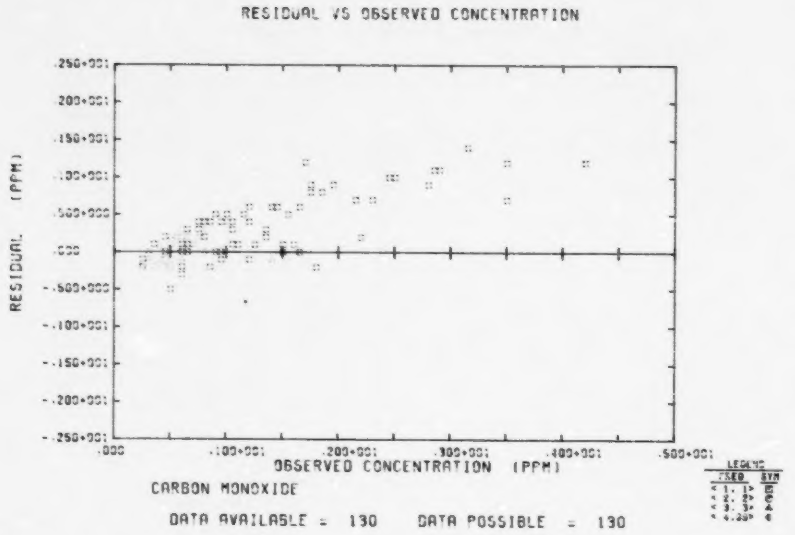

Figure 11a. Residual vs. observed plot from the PBM simulation results for all 10 test days for CO.

BEGIN LAST LINE OF TEXT
BOTTOM OF IMAGE AREA; OUTSIDE DIMENSION FOR TABLES AND ILLUSTRATIONS
3/8"

PAGE NUMBER
EPA-287 (Cin.)
(4-76)

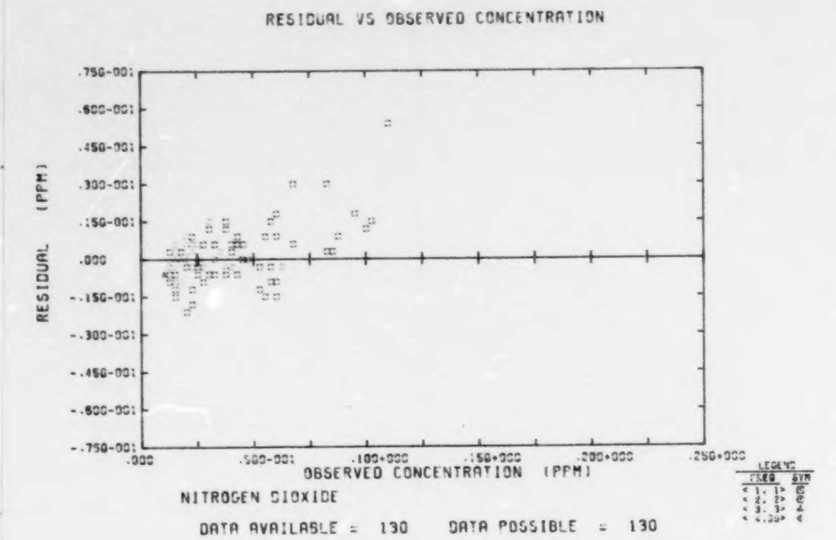

Figure 11b. Residual vs. observed plot from the PBM simulation results for all 10 test days for NO_2.

9-1/8"

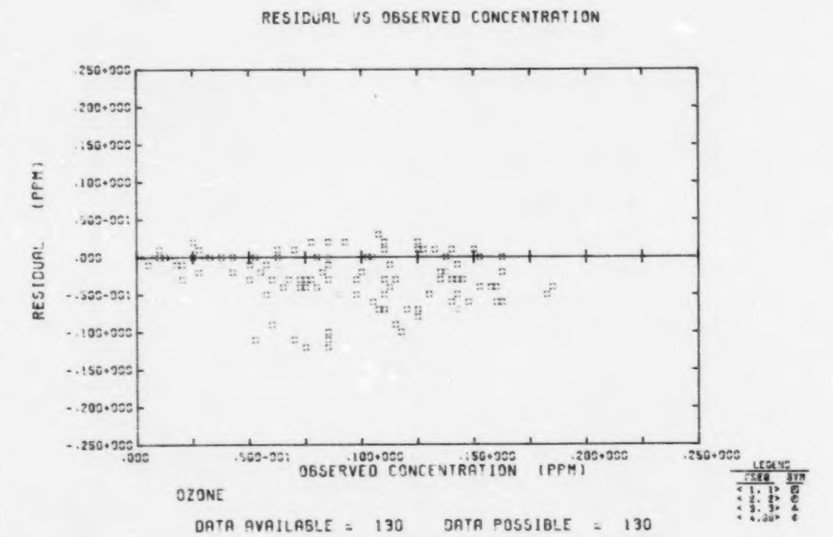

Figure 11c. Residual vs. observed plot from the PBM simulation results for all 10 test days for O_3.

BEGIN LAST LINE OF TEXT
BOTTOM OF IMAGE AREA; OUTSIDE DIMENSION FOR TABLES AND ILLUSTRATIONS
3/8"

PAGE NUMBER
EPA-287 (Cin.)
(4-76)

SECTION 5

LAGRANGIAN PHOTOCHEMICAL MODEL

OVERVIEW

The Lagrangian Photochemical Model (LPM) was developed by Environmental Research and Technology, Inc. and adapted under contract with EPA for use with the RAPS data base. (The LPM is essentially identical to the general-use model named ELSTAR). The LPM envisions a portion of the atmosphere as an identifiable parcel which can be tracked from early morning to the late afternoon. As the parcel moves over the various emissions sources, pollutants are assimilated, vertically mixed, and subjected to photochemical reactions in the presence of solar radiation. The LPM is attractive relative to grid models in that it is fairly simple to execute and uses a moderate amount of computer time. On the other hand, the LPM calculates concentrations only within a parcel and not over a complete spatial field.

Model simulations were conducted using the LPM for each of the 10 test days listed in Table 1. Special emphasis will be placed on the results of Days 231, 251, 226, and 275, but a tabulation of the observed and predicted O_3 maxima is presented for all.

METHOD

The LPM is executed using a series of program modules. They are METMOD, EMMOD, AND KEMOD, sequentially performing calculations on meteorology and air quality, emissions, and photochemistry. The input and running procedures described by Lurmann et al. (1979) have been generally followed, although some modifications were deemed necessary as more experience with the RAPS data base was acquired.

The first step in setting up a simulation is to determine the starting point of a parcel so that it will arrive at a specified point at an assigned time. A backward trajectory can be generated by the METMOD. The parcel trajectory is usually determined by $1/R^2$ weighting of winds from the closest three stations (see Figure 1). However, experience with wind data (Shreffler, 1979) suggests that even closely situated stations can show large, unexplained differences in wind vectors from time to time. Reliance on a single anomalous station, if the parcel has a close approach, can create an erratic trajectory. In one test case, the backward and subsequent forward trajectories were radically different, and no proper start point could be found. To eliminate the possibility of such vagaries, it was decided to compute a single resultant wind vector from the network and assign it to all stations for a given hour. The resultant gives a general movement of the air mass over the region but is weighted toward the city center because of the clustering of stations there.

Because of the difficulty in solving the chemistry set with minimal solar radiation, the start time of a parcel (which is on the hour) must be at least 10 minutes past local sunrise. Once the start position is set, the METMOD is run in a forward-trajectory mode until 1800 CST or the parcel leaves the region.

Mixing heights are available from radiosondes released approximately one hour before sunrise and at six hour intervals thereafter. The temperature and wind profiles are processed automatically by the model to give vertical eddy diffusivities throughout the day. The trajectory information from METMOD is stored and is available to EMMOD to enable that module to obtain the emissions that the parcel will encounter. METMOD also stores the observed pollutant concentrations along the trajectory using a $1/R^2$ weighting scheme on the closest three stations. These observations are available for setting initial conditions in the parcel and later comparisons with the model predictions. In most cases, the parcel starts in a relatively clean rural environment, and levels of hydrocarbons (HC), NO, and NO_2 are assumed to decrease with height according to an assigned formula. On the other hand, ozone is depleted near the ground at night; thus, the initial O_3 increases from the surface to a value at 400 m which is equal to the observed 1000-1200 CST surface concentration upwind of the city (Shreffler and Evans, 1981). Values of initial concentrations assigned to the parcel at the start time are given in Table 3.

The EMMOD creates a record of the emissions entering the parcel as it traverses its trajectory. These emissions are used by the KEMOD to simulate the photochemical reactions which will take place as a function of time, yielding concentrations of 39 chemical species at 30 minute intervals.

TABLE 3. INITIAL SURFACE CONCENTRATIONS ASSIGNED TO THE PARCEL FOR REACTIVE HYDROCARBON (RHC), NO, CO, O_3, AND INITIAL CONCENTRATIONS ASSIGNED FOR O_3 ALOFT.

Day	RHC (ppm)	NO (ppm)	CO (ppm)	O_3 (ppm)	O_3 Aloft (ppm)
142	0.26	0.03	0.44	0.00[a]	0.06
178	0.19	0.01	0.41	0.00	0.08
209	0.32	0.02	0.73	0.01	0.08
231	0.15	0.01	0.48	0.01	0.06
251	1.28	0.08	2.60	0.00[a]	0.06
159	0.22	0.01	0.86	0.01	0.11
160	0.05[a]	0.01	0.32	0.02	0.11
195	0.05[a]	0.00[a]	0.17	0.03	0.08
226	0.41	0.01	0.97	0.01	0.09
275	0.70	0.10	2.82	0.01	0.06

[a] Defaults: RHC=0.05, NO=0.0025, O_3=0.0025

RESULTS

The objective of this model evaluation is not only to determine how well predictions and observations agree but also to notice and comprehend any systematic deviations in the behavior between the model pollutants and those observed in the atmosphere. For the 10 days examined in this study, time series of concentrations of O_3, NO, NO_2, and CO along the trajectory have been generated as well as a statistical summary of the O_3 maxima. Time series from four selected days are presented and discussed below for both predictions and observations.

Figure 12a presents a trajectory map for Day 231. This map covers a square 100 km on a side, and only 9 of the stations are shown to avoid cluttering the figure. These stations are (compare Figure 1) 101 in downtown, 122 and 114 to the north, 109 and 123 to the east, 118 and 124 to the south, and 120 and 125 to the west. The location of the parcel each hour along the trajectory is indicated. On Day 231, the parcel starts in a rural locale south of the city. It moves over the high emissions areas at 0800-1100 CST and continues to the northwest. The O_3 maximum was recorded at 1400 CST by station 121.

In viewing the individual time series of pollutant concentrations, special attention is called to some aspects which seem to be common to a substantial number of the 10 days considered. (The reader is reminded that the time series represent the concentrations within a moving parcel and not at a single point in space). Figure 12b gives the O_3 concentrations for Day 231. The RAPS observed values are given by a solid line. The model-predicted values at Level-1 (L-1, understood to be the surface) are given by a dotted line, and the Level-3 (L-3, about 300 m in most cases) predictions are given by a dashed line. The observed O_3 is somewhat higher in the morning than the predicted O_3, but the general levels up to the time of the observed maximum agree fairly well. Continued rise in the model O_3 after 1400 CST is understandable in two respects. First, the modeled air parcel is leaving the region of the RAPS stations and the observations refer to air which is quite distant from that being simulated. This effect does not reflect adversely on model performance. A second reason for the deviation of predicted and observed values is based on the rigid-wall concept of the air parcel. Beyond station 121 the parcel is outside the region of significant emissions, and, in the atmosphere, such a parcel would tend to be diluted by horizontal diffusion. The model parcel maintains its constant dimensions, and all emissions which entered during the day remain. The modeled O_3 reaches a value at 1700 CST which is in excess of any observed during RAPS.

In Figure 12c the L-1 NO shows a pronounced build-up in the early morning as the parcel moves near the city center. The build-up at L-3 is buffered since most of the NO emissions are at the surface. The predicted and observed values are not in particularly good accord, although L-3 results seem to agree more closely in the general level of concentration than the L-1 results. (The RAPS measurements were taken with an intake manifold at 4m). In Figure 12d, the NO_2 predictions exceed the observed peak by a factor of two. The CO L-1 predictions, Figure 12e, indicate a tendency to show dramatic peaks in response to emissions, much like those seen for NO. Likewise the L-3 predictions seem to track observations more accurately. The deviation of the predicted and observed values after 1400 CST is due to the same two factors discussed previously for O_3 in Figure 12b. However, for the inert pollutant CO, the effect of no lateral diffusion in the parcel is graphically illustrated. The predictions throughout the parcel approach a constant concentration reflecting the total emissions accumulated during the day. This is clearly an unrealistic aspect of the LPM.

The trajectory for Day 251 is given in Figure 13a. The start point is near downtown St. Louis, and initial loading of the parcel with HC and NO is high. Furthermore, winds are very low during the first four hours so that the parcel accumulates large quantities of pollutants from emissions. After 1000 CST the parcel moves more rapidly and arrives at station 122 at 1400 CST. In Figure 13b, the O_3 predictions clearly outstrip the observations. The Day 251 maximum was the highest O_3 concentration observed during the RAPS program, but it was only half that predicted by LPM. The L-1 NO shows the tendency for the model to build unrealistic surface concentrations over the emission areas, and the same is true of NO_2 and CO. The approach to a constant CO is again apparent in Figure 13e.

As seen in Figure 14a, the trajectory for Day 226 moves from the west side of the city to the east, reaching station 109 at 1300 CST. It then turns and moves back into the city towards evening. Given the modeling problems previously discussed, these O_3 predictions in Figure 14b, like those for Day 231, should be deemed quite good. The L-1 accumulation of NO_x and CO is again apparent, and the L-3 values seem to track the observations more consistently.

The trajectory in Figure 15a indicates that Day 275 was a very calm day. The parcel starts out southwest of the city center and reaches station 102 at 1400 CST. It then moves south and nearly returns to its origin. Two points should be made concerning such calm conditions. First, the trajectory is subject to great uncertainty, and all that is really known is that the air mass was nearly stationary. Second, the LPM point-source module is not designed to function well when the wind speed is so low that the emissions grid (5x5 km) is not traversed in a single hour. The precise impact of this problem is unknown but may be minimal. The O_3 predictions are again encouraging as seen in Figure 15b. The rather substantial difference between L-1 and L-3 predictions of O_3 is probably caused by the presence of surface NO emissions throughout the day. The early morning increase in observed O_3, as seen also for Day 231, should be noted. The behavior of the NO_x and CO series are now familiar from the previous discussions. The initial loading of HC and NO_x is comparable on Days 251 and 275 and is far above those seen on the other eight days of the study. The fact that O_3 predictions did not get out of control on Day 275 is probably due to the parcel remaining over the emissions areas where NO tends to deplete O_3. While the problem of horizontal diffusion is just as real in such a case, it is masked because the air surrounding the parcel has comparable concentrations.

Table 4 summarizes the predicted and observed O_3 maxima and a rudimentary statistical evaluation of the results for the 10 days of the study. The prediction refers to the model prediction at the time and position of the observed O_3 maximum. The residual, ΔC, is based on the L-1 prediction since there is little difference for O_3 between this and the L-3 prediction. The average residual is fortuitously small, and the s.d. (ΔC) conveys considerable uncertainty in the model's ability to reproduce the observed maxima. About one-half the s.d. (ΔC) arises from the comparisons on Days 142 and 251. As seen previously, Day 251 predictions are substantially enhanced by the model assumption of no lateral diffusion. A careful look at Day 142 following this analysis raises questions about the reliability of the observed maximum; it may be lower. Also, the maximum O_3 on that day occurs at station 101 where local NO emissions are very high. One must consider whether the model can realistically simulate O_3 production in the presence of high local emissions. The third largest residual, that for Day 195, does not have an easily explained origin at this time.

Although Table 4 summarizes one aspect of model performance, one should resist the temptation to quote, without qualification, the "accuracy" developed here. While the s.d. (ΔC) reflects performance for a more-or-less random application in an urban setting, individual applications could be another matter. For instance, in control strategy investigations, it might be perfectly reasonable to start all parcels at the highest emissions area in the central city, much as happened by chance on Day 251. Clearly the LPM would show a totally unacceptable $\overline{\Delta C} < 0$. Moreover, other aspects of model performance must be considered (the time series) which cannot be easily quantified.

TABLE 4. A SUMMARY OF PREDICTED AND OBSERVED O_3 MAXIMA FROM THE LPM FOR 10 DAYS SELECTED FROM 1975-1976.

Day	Hour	Station	Observed 4-meters (ppm)	LPM Predicted Level-1 (ppm)	LPM Predicted Level-3 (ppm)
142 (1975)	12	101	0.20	0.05	0.09
178	14	112	0.20	0.24	0.34
209	11	118	0.21	0.16	0.16
231	14	121	0.23	0.20	0.20
251	14	122	0.26	0.53	0.54
159 (1976)	15	122	0.20	0.22	0.23
160	16	115	0.22	0.19	0.21
195	15	114	0.22	0.10	0.11
226	13	109	0.23	0.28	0.30
275	14	102	0.24	0.28	0.32

ΔC = Observed minus Level-1

$\overline{\Delta C} = -0.004$

$\text{s.d.}(\Delta C) = 0.11$

$\overline{|\Delta C|} = 0.080$

ADDITIONAL SIMULATIONS

The preceding results were based on testing the model under a normal operating mode. In addition, several simulations were designed to check the importance of initial conditions, emissions, and meteorological factors.

Initial Conditions of HC and NO

Days 251 and 275 both show a high initial loading of HC and NO and a large accumulation of emissions within the modeled parcel. In order to determine the effect of the initial conditions on the final ozone predictions, these days were simulated using lower default values for initial NO and HC conditions. For Day 251 the resulting Hour 14 prediction of O_3 was 0.15 ppm while for Day 275 the Hour 14 prediction was 0.13 ppm. These computed values are much less than those in Table 4 and show a very strong influence of initial loading on the final O_3 predictions.

The Effect of Basic Model Inputs

Additional simulations were designed to test the effects of O_3 aloft, wind speed, temperature, and solar radiation. In these tests, a basic scenario was designed using as standard inputs the values from Day 195, with the exception of wind data. The input data were taken as constant from the south at 1.67 m/s, and the parcel was started at 0500 CST at a position so as to arrive at 0800 CST in the city center (encircled by sites 101, 105, 106, and 107). The NO and HC initial conditions were only slightly above lower default values.

The 1500 CST O_3 prediction for the basic scenario was 0.23 ppm, and this is the result against which all other results are compared in the ensuing parametric analysis.

The O_3 aloft represents a considerable reservoir of ozone in the parcel, and it is reasonable to ask if the final predictions are sensitive to its specification. The model was run with assumed values of 0.02 ppm and 0.15 ppm which span the range of observations during RAPS. The predicted surface O_3 values were 0.22 ppm and 0.25 ppm, respectively. Obviously, the predicted O_3 is not significantly influenced by the initial O_3 aloft, and this finding is consistent with the empirical result of Shreffler and Evans (1981).

Day 195 was quite clear, and solar radiation was high. For two additional runs, the radiation in the basic scenario was multiplied by 0.8 and 0.6. The resulting O_3 predictions at 1500 CST were 0.17 ppm and 0.12 ppm, respectively. From the work of Shreffler and Evans, the rate of change of maximum O_3 with total radiation was 0.24 ppm/ly/min. The model response is 0.25 ppm/ly/min and, therefore, is in excellent agreement with empirical data.

The temperature of the basic scenario was changed by adding 5°C and subtracting 5°C at each hour in two runs. The resulting 1500 CST predictions were 0.240 ppm and 0.206 ppm, respectively. The model response was thus 0.0034 ppm/°C. The empirical data of Shreffler and Evans indicate a much higher response of 0.01 ppm/°C.

Wind speed was set to 1 m/s and 2.5 m/s in two additional runs. The start position of the parcel at 0500 CST was adjusted so it arrived in the city center at 0800 CST, but the initial conditions of NO and HC were retained from the basic scenario. The changes in wind speed were allowed to influence the calculated eddy diffusivities. The predicted O_3 values for 1 m/s and 2.5 m/s were 0.26 ppm and 0.19 ppm, respectively, showing a response of -0.047 ppm/m/s. The data of Shreffler and Evans indicated an empirical response of -0.027 ppm/m/s over the range 0-8 m/s, and the response could be larger at the low speeds.

In summary, the effects in the model of wind speed, O_3 aloft, and solar radiation are in good agreement with empirical data from RAPS. The modeled temperature effect on O_3 production is only about 1/3 that seen in the data.

The Day 142 O_3 Maximum

Finally, some investigations were made to determine the cause of the low O_3 prediction on Day 142. The maximum occurred at 1200, an unusually early time, and this was one factor which highlighted the day and influenced its selection for the test set. Nearby station data were examined, and there does not seem to be reason to distrust the observations. Since site 101 is in downtown St. Louis, it was possible that the model was not reacting well to high local emissions of NO. To investigate that possibility, two runs were executed with deleted emissions.

First, the area sources alone were deleted in the period 1100 - 1230 CST. The resulting O_3 predictions were very similar to those in the original Day 142 simulation. Second, the point sources alone were deleted in the period 1100 - 1230 CST. In that case, the L-1 O_3 predictions were 0.085 ppm and 0.13 ppm at 1200 and 1300 CST, respectively. The corresponding L-3 predictions were 0.14 and 0.16 ppm. Whereas local point sources do have an effect in depleting O_3, this effect is not sufficient to totally explain the model's inability to match the unusually early O_3 peak recorded on Day 142.

CONCLUSIONS

The LPM shows promise as an effective tool to understand O_3 production in an urban region. The model is relatively easy to use, inexpensive to execute, and seems immune to various execution errors which tend to arise unexpectedly in complex computations of this sort. Areas of further research will include the following:

(1) The importance of the initial conditions versus the emissions accumulated in the parcel.

(2) Reasonable methods to include horizontal diffusion.

(3) The vertical diffusivity as it relates to unrealistic build-up of pollutants at Level-1.

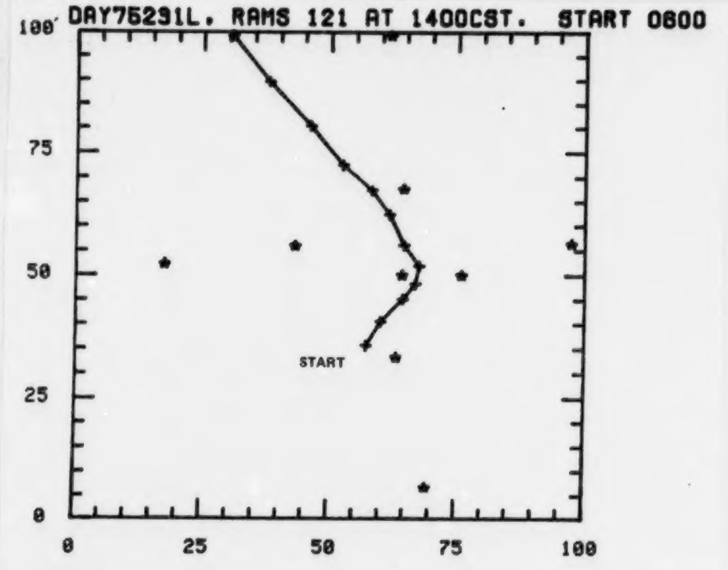

Figure 12a. LPM parcel trajectory for Day 231 of 1975.

BEGIN LAST LINE OF TEXT
3/8"
BOTTOM OF IMAGE AREA; OUTSIDE DIMENSION FOR TABLES AND ILLUSTRATIONS

PAGE NUMBER
EPA Form 2350-4 (4-80)
(PREVIOUSLY CIN. EPA FORM 287)
U.S. GOVERNMENT PRINTING OFFICE 1980-660-838
TYPING GUIDE SHEET

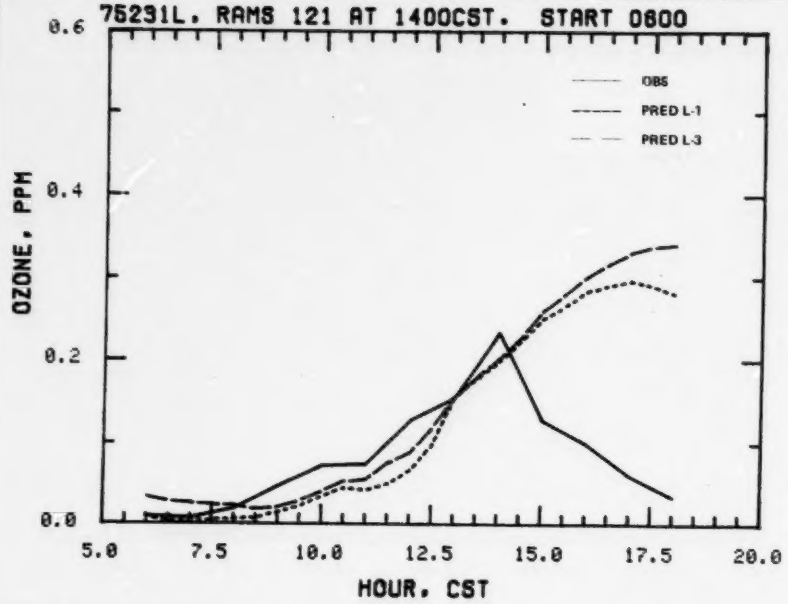

Figure 12b. LPM time series of observed and predicted O_3 hourly concentrations on Day 231 of 1975.

9-1/8"

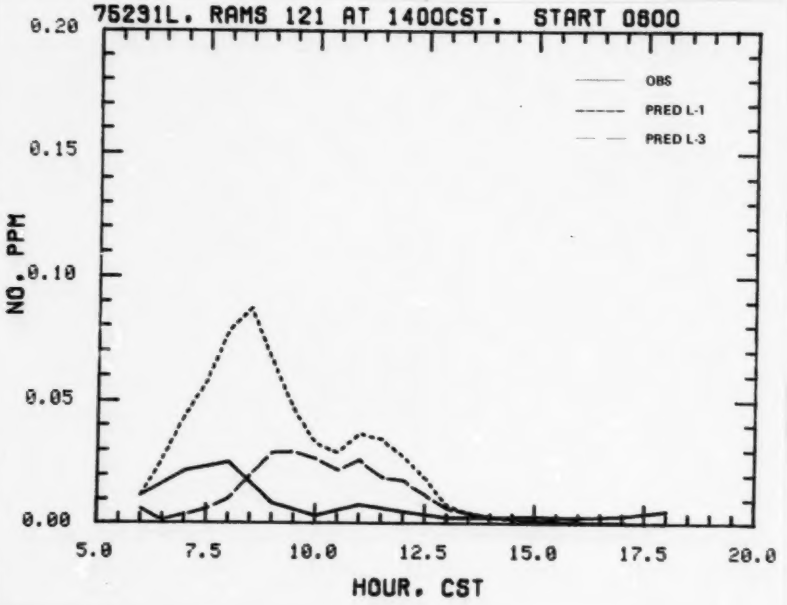

Figure 12c. LPM time series of observed and predicted NO hourly concentrations on Day 231 of 1975.

BEGIN LAST LINE OF TEXT
BOTTOM OF IMAGE AREA OUTSIDE DIMENSION FOR TABLES AND ILLUSTRATIONS
3/8"

PAGE NUMBER
EPA Form 2350-4 (4-80)
(PREVIOUSLY CIN. EPA FORM 287)
U.S. GOVERNMENT PRINTING OFFICE 1980-660-839
TYPING GUIDE SHEET

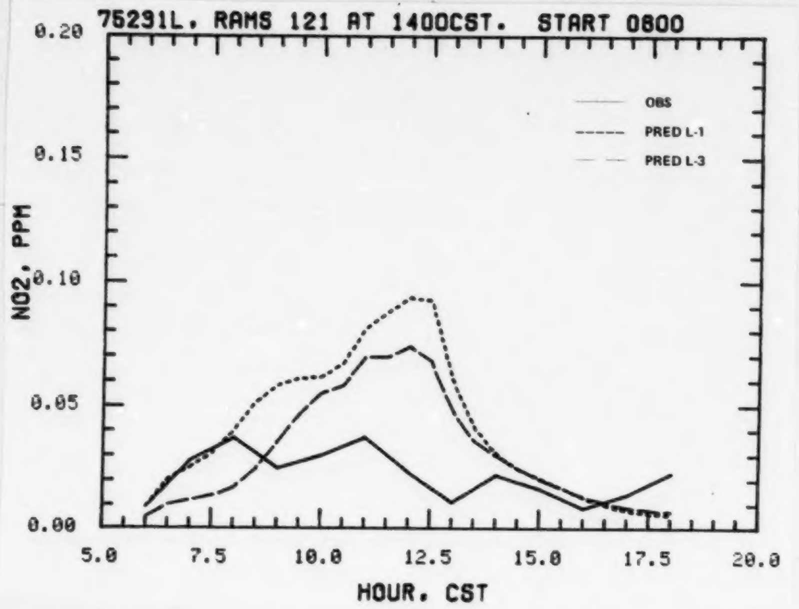

Figure 12d. LPM time series of observed and predicted NO_2 hourly concentrations on Day 231 of 1975.

9-1/8"

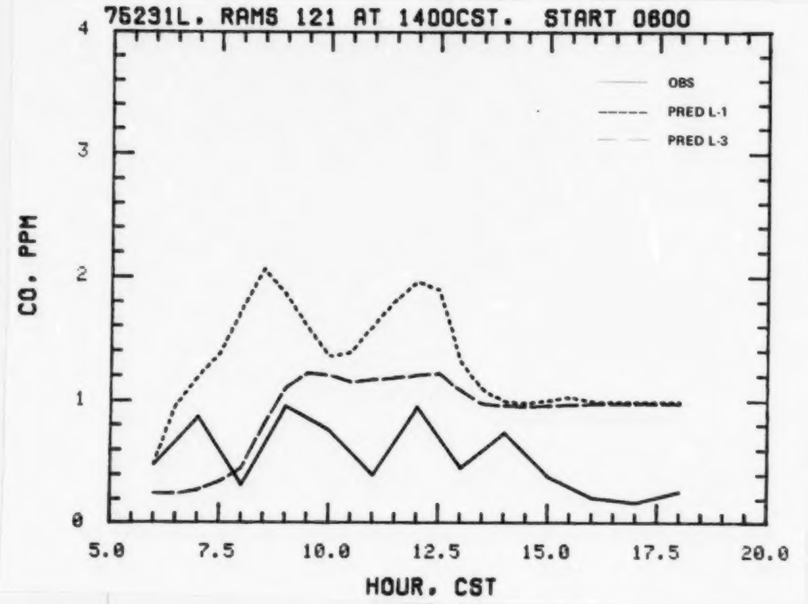

Figure 12e. LPM time series of observed and predicted CO hourly concentrations on Day 231 of 1975.

BEGIN LAST LINE OF TEXT
BOTTOM OF IMAGE AREA OUTSIDE DIMENSION FOR TABLES AND ILLUSTRATIONS
3/8"

PAGE NUMBER
EPA Form 2350-4 (4-80)
(PREVIOUSLY CIN EPA FORM 287)
U.S. GOVERNMENT PRINTING OFFICE 1980-660-809
TYPING GUIDE SHEET

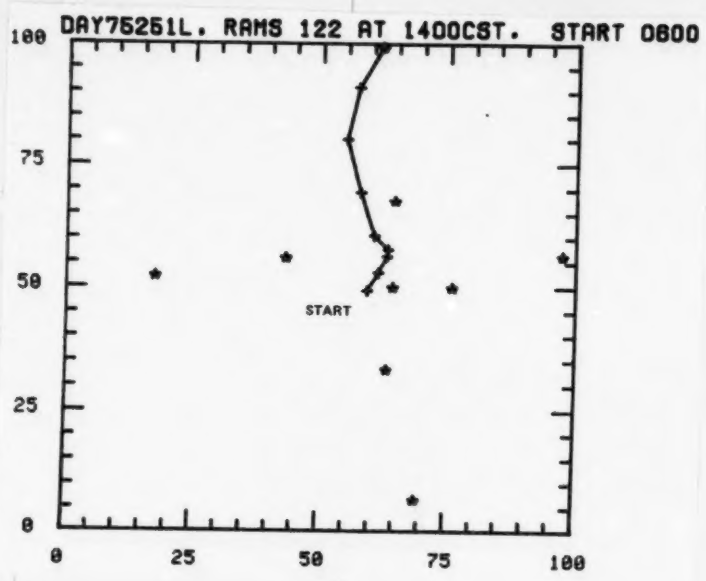

Figure 13a. LPM parcel trajectory for Day 251 of 1975.

BEGIN LAST LINE OF TEXT
3/8"
BOTTOM OF IMAGE AREA, OUTSIDE DIMENSION FOR TABLES AND ILLUSTRATIONS

PAGE NUMBER
EPA Form 2350-4 (4-80)
(PREVIOUSLY CIN. EPA FORM 251)
☆ U.S. GOVERNMENT PRINTING OFFICE 1980-660-639
TYPING GUIDE SHEET

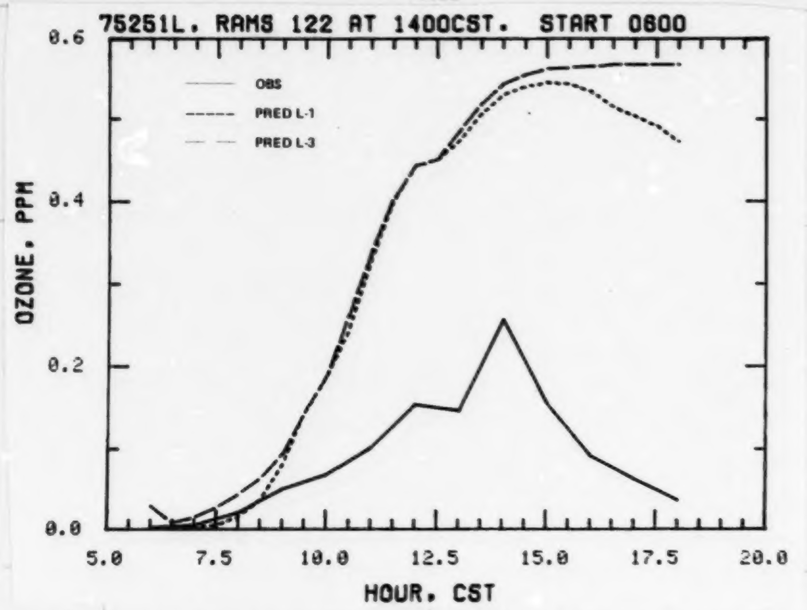

Figure 13b. LPM time series of observed and predicted O_3 hourly concentrations on Day 251 of 1975.

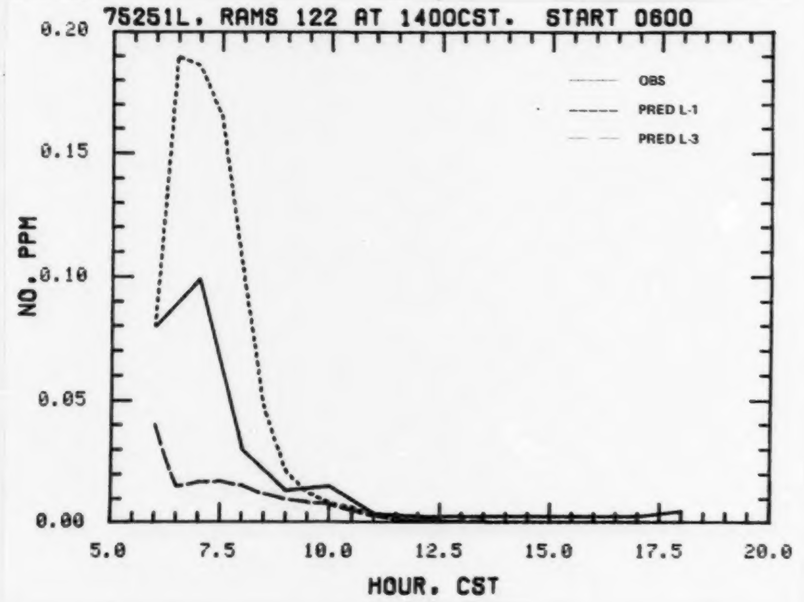

Figure 13c. LPM time series of observed and predicted NO hourly concentrations on Day 251 of 1975.

BEGIN FIRST LINE OF TEXT HERE
CENTER OF PAGE
TOP OF IMAGE AREA
DROPPED HEAD; BEGIN SECTIONS HERE
9-1/8"
BEGIN LAST LINE OF TEXT
3/8"
BOTTOM OF IMAGE AREA; OUTSIDE DIMENSION FOR TABLES AND ILLUSTRATIONS
PAGE NUMBER
EPA Form 2350-4 (4-80)
(PREVIOUSLY CIN. EPA FORM 287)
© U.S. GOVERNMENT PRINTING OFFICE 1980-660-839
TYPING GUIDE SHEET

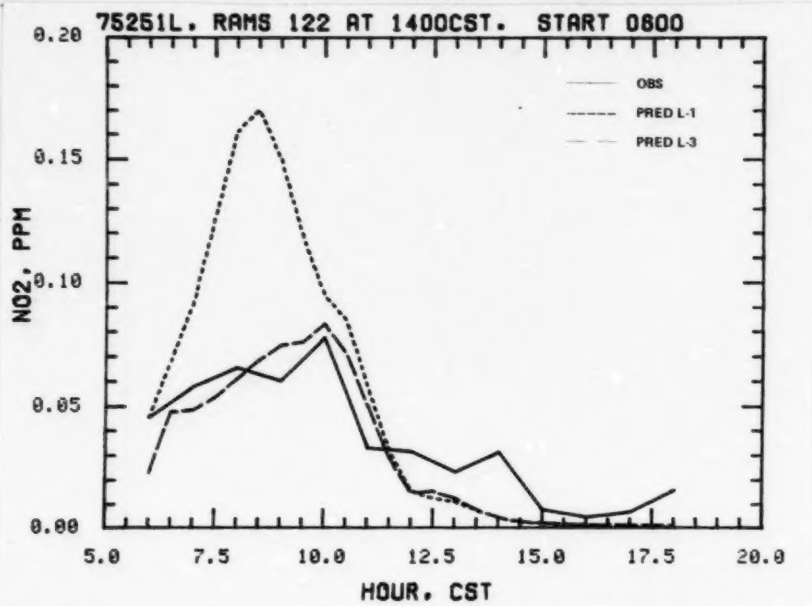

Figure 13d. LPM time series of observed and predicted NO_2 hourly concentrations on Day 251 of 1975.

9-1/8"

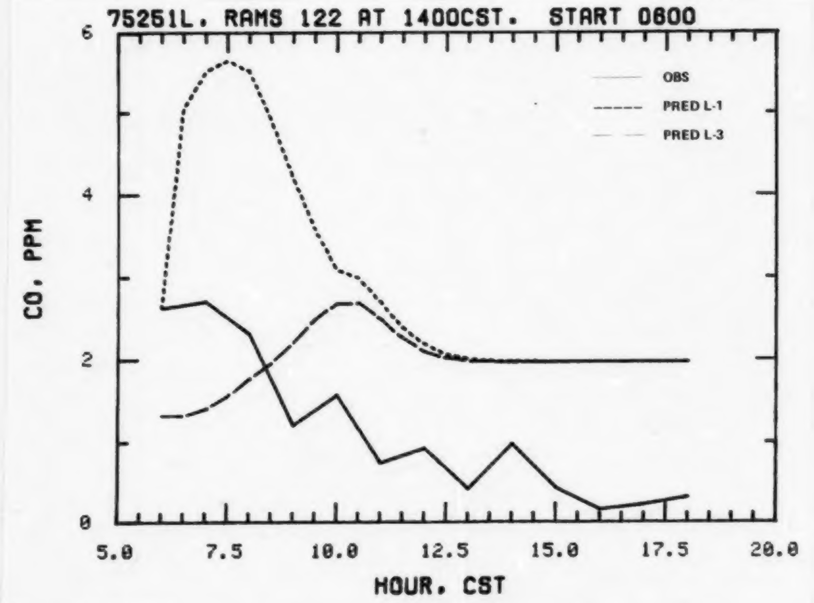

Figure 13e. LPM time series of observed and predicted CO hourly concentrations on Day 251 of 1975.

BEGIN LAST LINE OF TEXT
BOTTOM OF IMAGE AREA; OUTSIDE DIMENSION FOR TABLES AND ILLUSTRATIONS
3/8"

PAGE NUMBER
EPA Form 2350-4 (4-80)
(PREVIOUSLY CIN. EPA FORM 287)
U.S. GOVERNMENT PRINTING OFFICE 1980-660-638
TYPING GUIDE SHEET

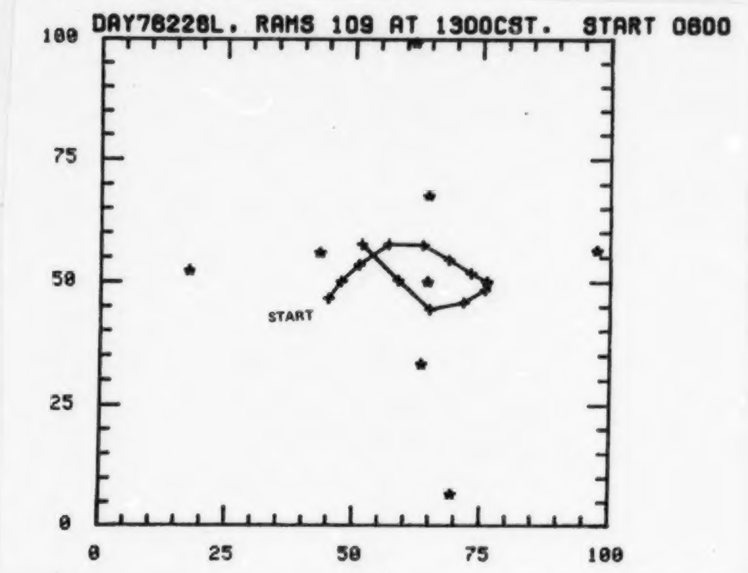

Figure 14a. LPM parcel trajectory for Day 226 of 1976.

EPA Form 2350-4 (4-80)
(PREVIOUSLY CIN. EPA FORM 287)
TYPING GUIDE SHEET

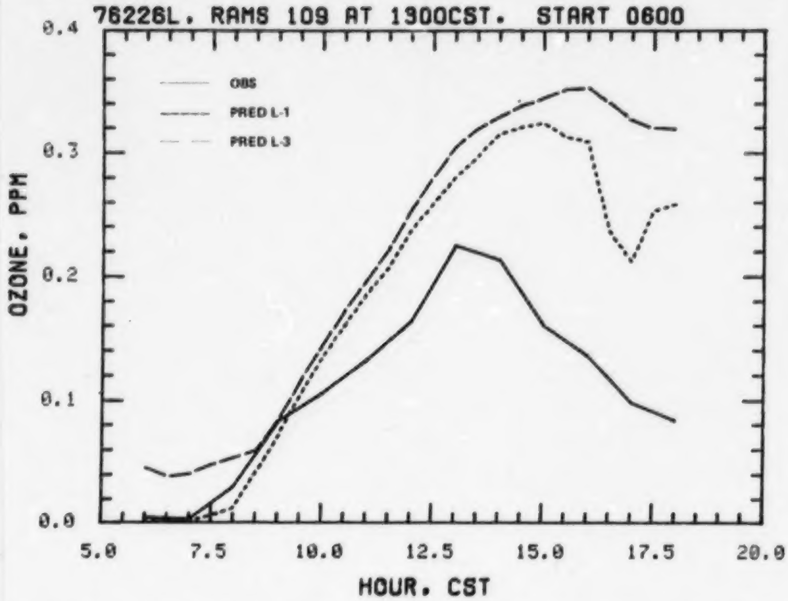

Figure 14b. LPM time series of observed and predicted O_3 hourly concentrations on Day 226 of 1976.

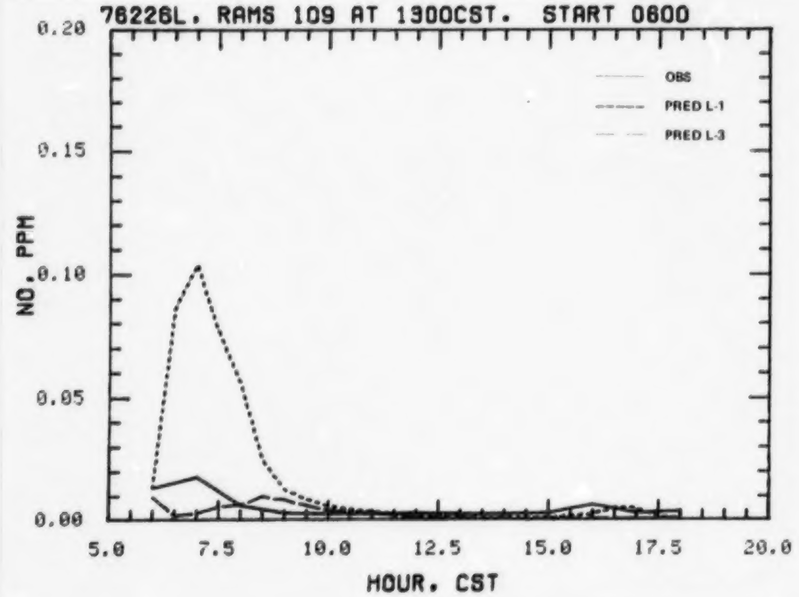

Figure 14c. LPM time series of observed and predicted NO hourly concentrations on Day 226 of 1976.

BEGIN FIRST LINE OF TEXT HERE
CENTER OF PAGE
TOP OF IMAGE AREA
DROPPED HEAD; BEGIN SECTIONS HERE
9-1/8"
BEGIN LAST LINE OF TEXT
3/8"
PAGE NUMBER
BOTTOM OF IMAGE AREA, OUTSIDE DIMENSION FOR TABLES AND ILLUSTRATIONS
EPA Form 2350-4 (4-80)
(PREVIOUSLY CIN. EPA FORM 337)
U.S. GOVERNMENT PRINTING OFFICE
TYPING GUIDE SHEET

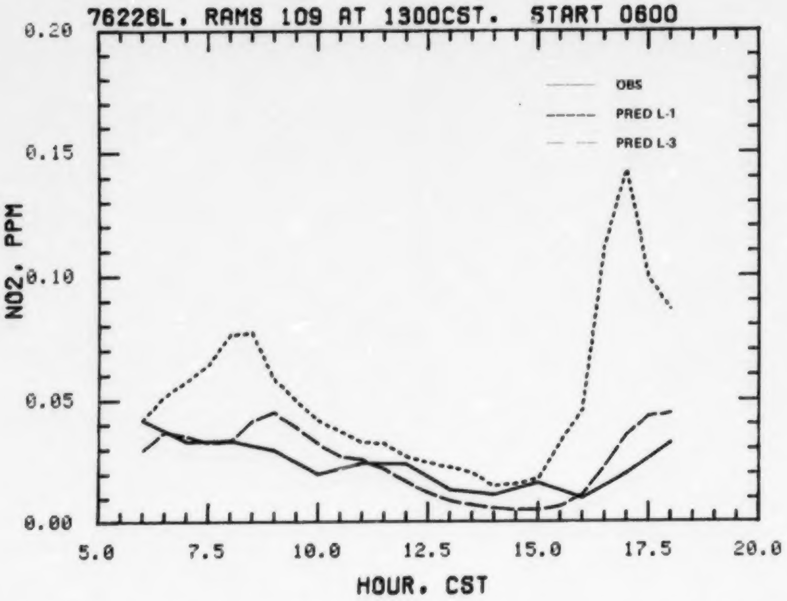

Figure 14d. LPM time series of observed and predicted NO_2 hourly concentrations on Day 226 of 1976.

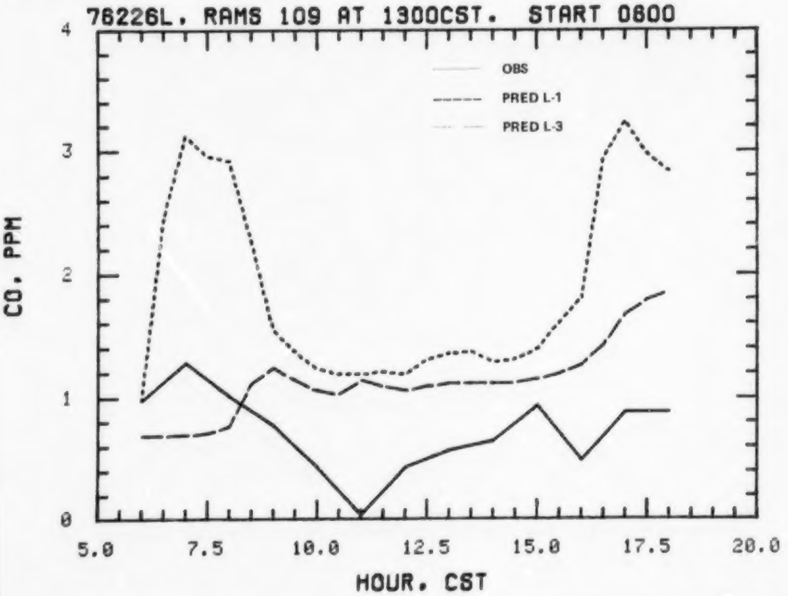

Figure 14e. LPM time series of observed and predicted CO hourly concentrations on Day 226 of 1976.

PAGE NUMBER
EPA Form 2350-4 (4-80)
(PREVIOUSLY CIN. EPA FORM 367)
U.S. GOVERNMENT PRINTING OFFICE
TYPING GUIDE SHEET

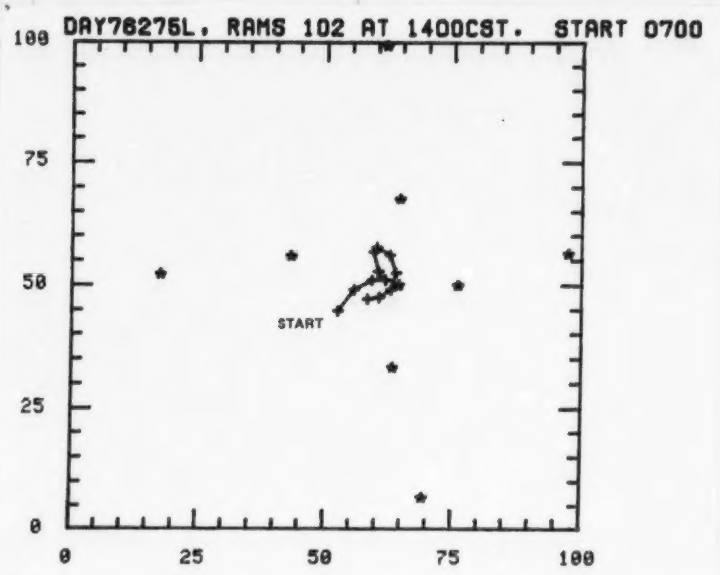

Figure 15a. LPM parcel trajectory for Day 275 of 1976.

BEGIN LAST LINE OF TEXT
BOTTOM OF IMAGE AREA; OUTSIDE DIMENSION FOR TABLES AND ILLUSTRATIONS
3/8"

PAGE NUMBER
EPA Form 2350-4 (4-80)
(PREVIOUSLY CIN. EPA FORM 287)
☆ U.S. GOVERNMENT PRINTING OFFICE: 1980-650-438
TYPING GUIDE SHEET

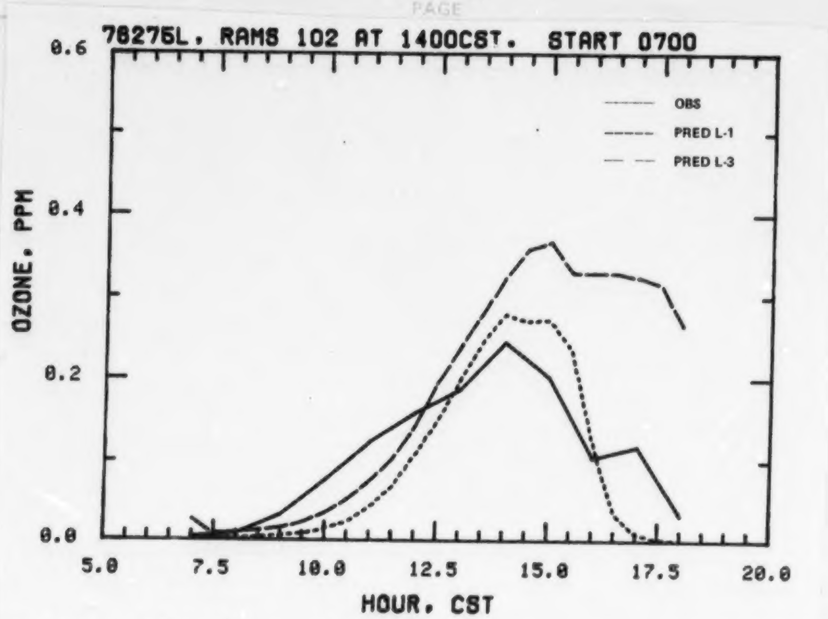

Figure 15b. LPM time series of observed and predicted O_3 hourly concentrations on Day 275 of 1976.

9-1/8"

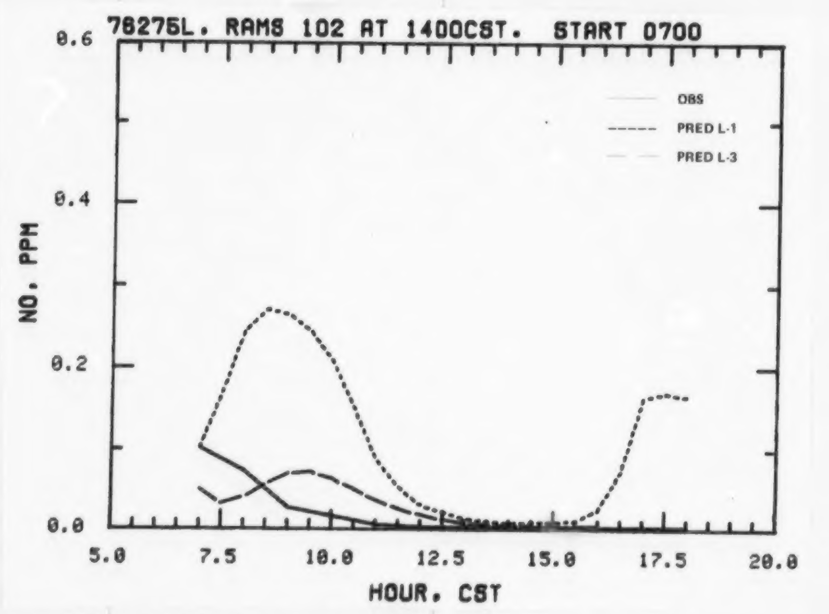

Figure 15c. LPM time series of observed and predicted NO hourly concentrations on Day 275 of 1976.

BEGIN LAST LINE OF TEXT
3/8"
BOTTOM OF IMAGE AREA, OUTSIDE DIMENSION FOR TABLES AND ILLUSTRATIONS

PAGE NUMBER
EPA Form 2350-4 (4-80)
(PREVIOUSLY CIN. EPA FORM 257)
U.S. GOVERNMENT PRINTING OFFICE 1980-060-620
TYPING GUIDE SHEET

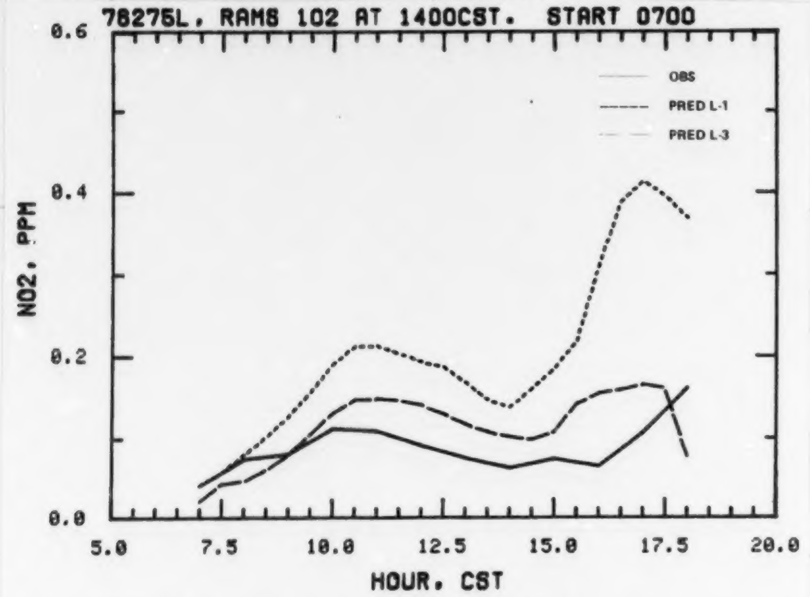

Figure 15d. LPM time series of observed and predicted NO_2 hourly concentrations on Day 275 of 1976.

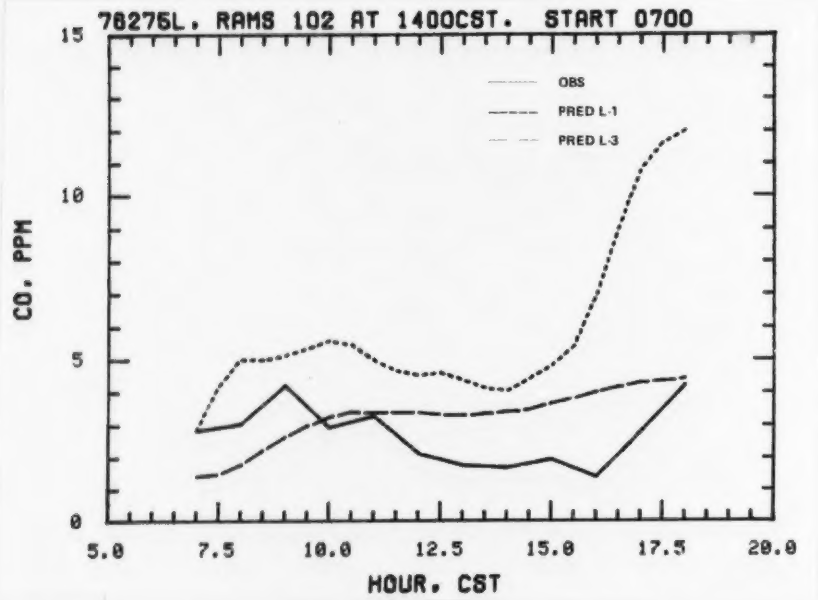

Figure 15e. LPM time series of observed and predicted CO hourly concentrations on Day 275 of 1976.

EPA Form 2350-4 (4-80)
(PREVIOUSLY CIN. EPA FORM 287)
TYPING GUIDE SHEET

SECTION 6

LIVERMORE REGIONAL AIR QUALITY MODEL

OVERVIEW

The Livermore Regional Air Quality Model (LIRAQ) was developed at Lawrence Livermore Laboratory (LLL) under funding of the National Science Foundation. The model is an Eulerian grid type and was specifically constructed for use in the San Francisco Bay area, where the Bay Area Air Quality Management District (BAAQMD) retains an interest in LIRAQ applications. Reflecting the originally intended region of study, the model has provision for generating mass consistent wind fields in complex terrain but allows only one grid cell in the vertical dimension. LIRAQ is described in detail by Duewer et al. (1978) and MacCracken et al. (1978). In 1975, EPA entered into an Interagency Agreement (IAG) with LLL to have LIRAQ adapted for use with the RAPS data base in St. Louis. Because LIRAQ uses special features of the CDC 7600 computing system, its adaptation to run on the EPA's UNIVAC 1110 was deemed impractical. Therefore, LIRAQ was transferred to the Lawrence Berkeley Laboratory (LBL) computing facility where EPA could have direct access to the model. Considerable difficulty has arisen in this project, and this section is intended as a status report on the investigations to date.

DISCUSSIONS OF RESULTS

LIRAQ is executed by submitting a series of data processors via remote terminal access to the Lawrence Berkeley Laboratory computers. The command sequences for the processors of meteorological, air quality, and emissions data are fully documented by Duewer et al. (1980). To set up a simulation of a given day requires only a few changes in the sequences relating to tape assignments, tape movements, date designations, and boundary conditions. An ample array of graphics is created automatically on microfilm both for the preprocessors and LIRAQ itself. A final verification package gives time series graphs of the various pollutants at each RAPS station and scatter diagrams of observed and predicted values over the region. Correlation coefficients are also computed.

Following attempted executions of LIRAQ on three test days, Days 195, 226, and 275 of 1976, it is apparent that there are critical, unidentified errors in the model. LIRAQ modeling was performed on a 100x100 km area centered near station 119 (see Figure 1) and using 5x5 km grid elements. Some results are presented below.

On Day 226, the wind was westerly from 0600 to 1400 CST. These winds carried emissions from St. Louis to the east where a maximum 1-hr average ozone of 0.224 ppm was recorded by station 109 for Hour 13 (1300 - 1359 CST). Time series of predicted and observed pollutants O_3, NO, NO_2, and CO are presented in Figure 16. It is clear that O_3 production is severely curtailed, and this is probably a direct consequence of the very high NO values predicted by LIRAQ. Predictions for CO, an inert pollutant which is not an active participant in the photochemistry, also are incredibly high when compared to observations. Figure 17 shows corresponding scatter diagrams for predicted and observed pollutant maxima for the interior RAPS stations. The severe underprediction of O_3 and overprediction of NO, NO_2, and CO are graphically illustrated over the entire region.

Figure 18 displays scatter diagrams of pollutant maxima for Day 195, and the same behavior is evident in the pollutant predictions.

The overprediction of both CO and NO by a factor of about 5 strongly suggest a problem in the emissions preprocessor which converts the archive tape to input for LIRAQ, although a problem in the chemistry module cannot be ruled out. The emissions preprocessor is supplied with area and point sources on separate magnetic tapes, and, if the supposed error were only in the treatment of the area sources as indicated by CO, the levels of SO_2 (coming largely from point sources) should appear reasonable. Unfortunately, the SO_2 maxima scatter diagram for Day 226 (Figure 17e) indicates the same overprediction from point sources.

Speculation on the root cause of the errors is not likely to be fruitful at this point, but the apparent factor of 5 in overpredicting the emissions brings to mind the fact that a 5x5 km grid cell is being used in the simulations. Perhaps at some point a required division by the area of the cell is mistakenly implemented by a division by the cell length.

In any case, the problem has an enormous impact on the results. Until there is a resolution of this apparent error, there is no point in further testing of LIRAQ.

OUTLOOK FOR LIRAQ

The effort to evaluate LIRAQ performance is beset with difficulties, and EPA is considering eliminating the model from its evaluation program. With limited testing, LIRAQ does not produce significant concentrations of ozone, suggesting errors in the emissions and/or chemistry module. Even if current problems are resolved, there are cost-benefit considerations centered on the adequacy of the model's theoretical framework (single vertical cell) and its inaccessibility for general use. The following points describe the present EPA judgements which tend to dissuade further investigation of LIRAQ.

1. LIRAQ was intended specifically for the San Francisco Bay area. In the model formulation, emphasis is placed on a wind field generator to produce mass consistent flows in complex terrain. This is certainly appropriate for the Bay area, but terrain is not a factor in St. Louis. To hold down the size of the model, only one cell is used in the vertical with profiles being analytically derived. This was also an appropriate decision for the Bay area, but it does not seem a sufficient treatment for St. Louis.

2. The expense of running LIRAQ is considerable. Typically, the cost of computer time for a one day simulation is $1000. The possibilities for thorough testing through sensitivity analysis are limited by budgetary considerations.

3. The remote access to LIRAQ at LBL via telephonic hook-up and the rudimentary familiarity of EPA personnel with the operating system severely limit the possiblility of analyzing and dealing with difficulties which arise. Thus, even a relatively simple error message in an execution of the programs represents a nearly intractable problem. The model is run through a series of cookbook data sets and control statement sequences.

4. Presently three days (195, 226, and 275) of 1976 have been tested on the LBL system by EPA. The Day 275 simulation produced an error in LIRAQ execution of unknown origin. On Days 195 and 226, little ozone was generated by the model, and nitrogen oxides seemed to totally dominate the photochemical system.

5. There would be a possibility of entering into another IAG with LLL to work through the apparent problems, which may be merely coding errors in the chemistry algorithm or the emissions processor. However, the prospects of success of such an endeavor are questionable, and the possible long-term benefits to EPA may be marginal. LIRAQ would still remain tied to the LBL computers.

6. Certainly EPA must take responsibility for substantial delays in the development and testing of LIRAQ. These delays were due to an unfortunate but unavoidable postponement in delivery of a final St. Louis emissions inventory, which was promised to LLL as early as 1977 but became available in August 1980. If the inventory had been delivered in a timely fashion, the problems with the model may have been identified while the IAG with LLL was still in effect.

The situation outlined above must be dealt with objectively. The LIRAQ conversion was initiated with the intent of having a complete spectrum of state-of-the-art models in existence in 1975 for testing by EPA. Events and reconsiderations of the eventual utility of the model have conspired to make LIRAQ less than attractive as an object for further research. Since LIRAQ is tied to a specific computer system, its prospects for use in a general regulatory setting - the ultimate goal of the model evaluation program - are extremely dim. EPA would like to continue a moderate research effort with the model, but it seems clear that an intensive effort would not constitute a prudent use of EPA resources. At this time, Lawrence Livermore Laboratory has agreed informally to look at LIRAQ and advise EPA if there are some easily correctable errors.

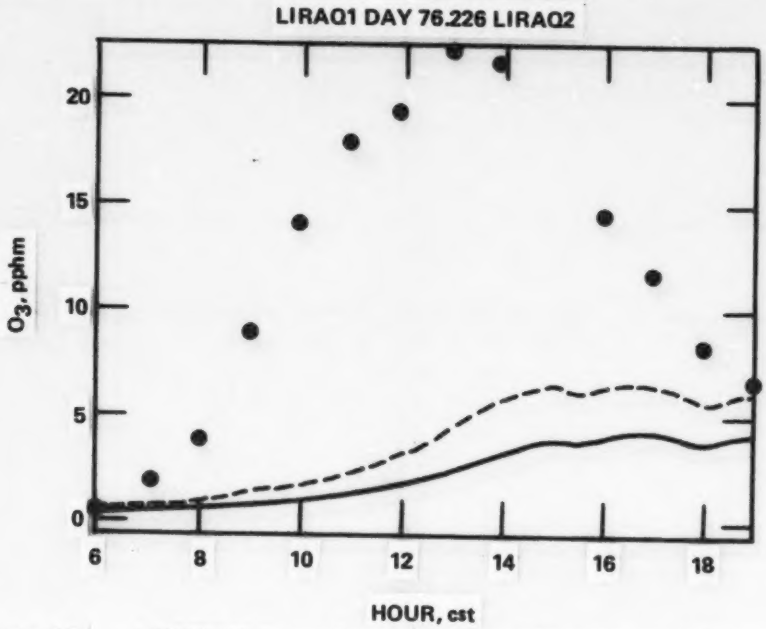

Figure 16a. LIRAQ time series of observed and predicted O_3 hourly concentrations at station 109 on Day 226 of 1976.

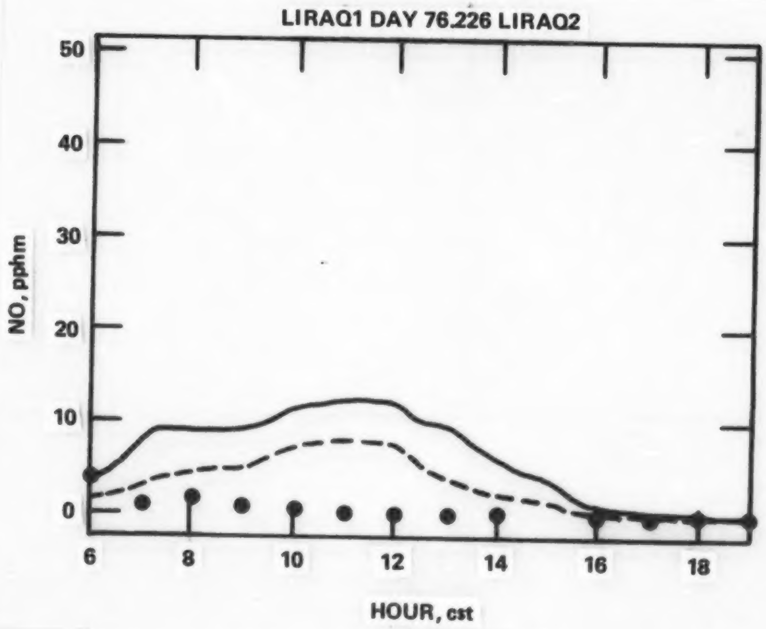

Figure 16b. LIRAQ time series of observed and predicted NO hourly concentrations at station 109 on Day 226 of 1976.

BEGIN FIRST LINE OF TEXT HERE
CENTER OF
TOP OF IMAGE AREA
DROPPED HEAD: BEGIN SECTIONS HERE
9 1/8"
BEGIN LAST LINE OF TEXT
3/8"
BOTTOM OF IMAGE AREA: OUTSIDE DIMENSION FOR TABLES AND ILLUSTRATIONS
PAGE NUMBER
EPA Form 2350-4 (4-80)
(PREVIOUSLY CIN. EPA FORM 337)
U.S. GOVERNMENT PRINTING OFFICE
TYPING GUIDE SHEET

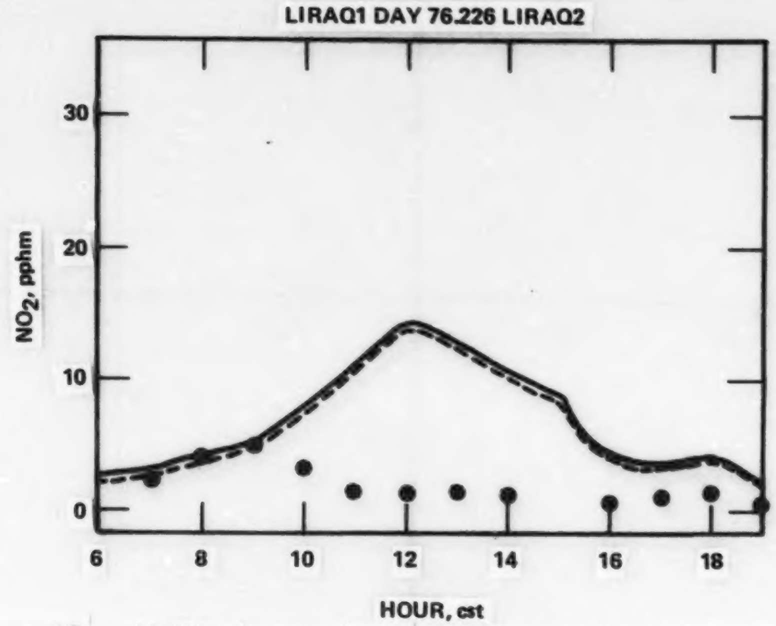

Figure 16c. LIRAQ time series of observed and predicted NO_2 hourly concentrations at station 109 on Day 226 of 1976.

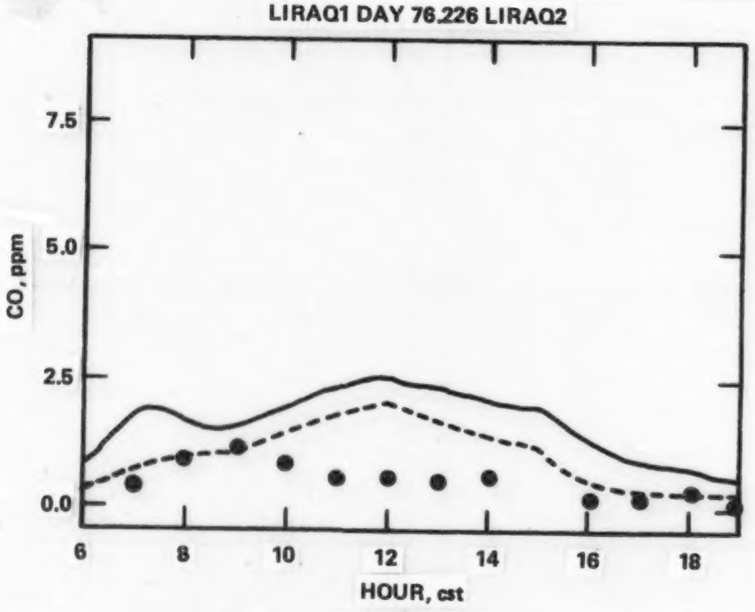

Figure 16d. LIRAQ time series of observed and predicted CO hourly concentrations at station 109 on Day 226 of 1976.

BEGIN FIRST LINE OF TEXT HERE
CENTER OF
TOP OF IMAGE AREA
DROPPED HEAD; BEGIN SECTIONS HERE
9-1/8"
BEGIN LAST LINE OF TEXT
BOTTOM OF IMAGE AREA OUTSIDE DIMENSION FOR TABLES AND ILLUSTRATIONS
3/8"
PAGE NUMBER
EPA Form 2350-4 (4-80)
(PREVIOUSLY CIN. EPA FORM 351)
U.S. GOVERNMENT PRINTING OFFICE 1980-660-629
TYPING GUIDE SHEET

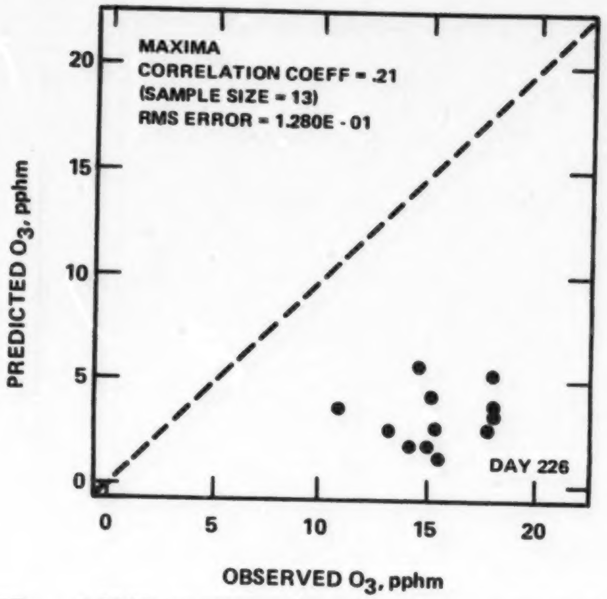

Figure 17a. LIRAQ scatter diagram of observed and predicted maximum O_3 concentrations on Day 226 of 1976.

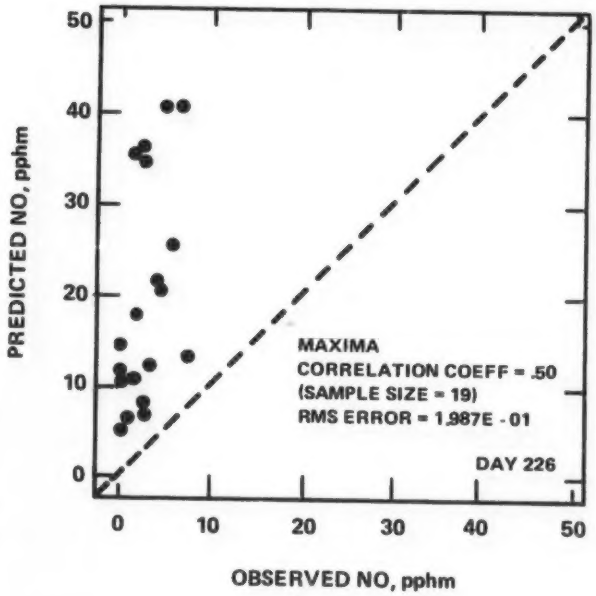

Figure 17b. LIRAQ scatter diagram of observed and predicted maximum NO concentrations on Day 226 of 1976.

BEGIN FIRST LINE OF TEXT HERE
CENTER OF PAGE
TOP OF IMAGE AREA
DROPPED HEAD; BEGIN SECTIONS HERE
9-1/8"
BEGIN LAST LINE OF TEXT
3/8"
BOTTOM OF IMAGE AREA OUTSIDE DIMENSION FOR TABLES AND ILLUSTRATIONS
PAGE NUMBER
EPA Form 2350-4 (4-80)
(PREVIOUSLY CIN. EPA FORM 287)
U.S. GOVERNMENT PRINTING OFFICE
TYPING GUIDE SHEET

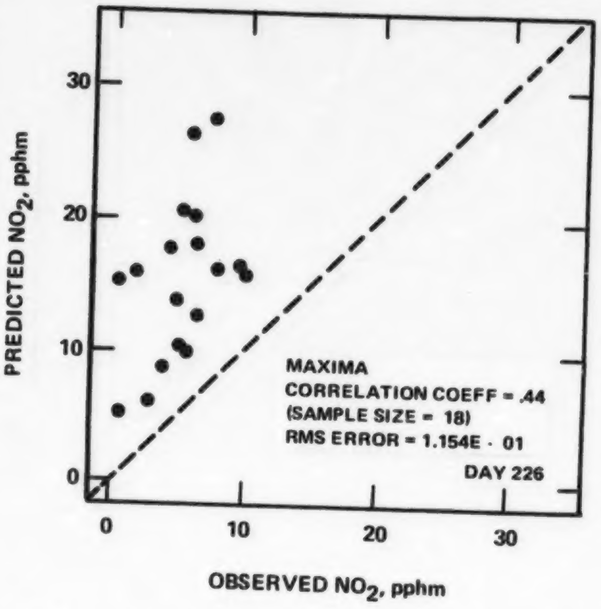

Figure 17c. LIRAQ scatter diagram of observed and predicted maximum NO_2 concentrations on Day 226 of 1976.

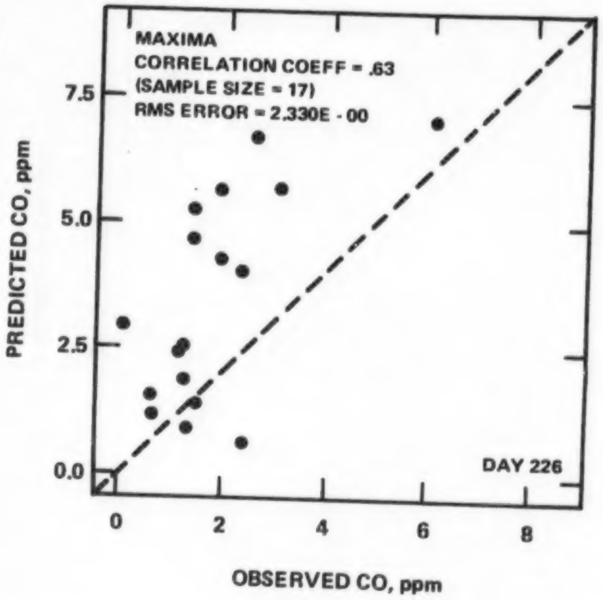

Figure 17d. LIRAQ scatter diagram of observed and predicted maximum CO concentrations on Day 226 of 1976.

EPA Form 2350-4 (4-20)
(PREVIOUSLY CIN. EPA FORM 287)
PAGE NUMBER
U.S. GOVERNMENT PRINTING OFFICE
TYPING GUIDE SHEET

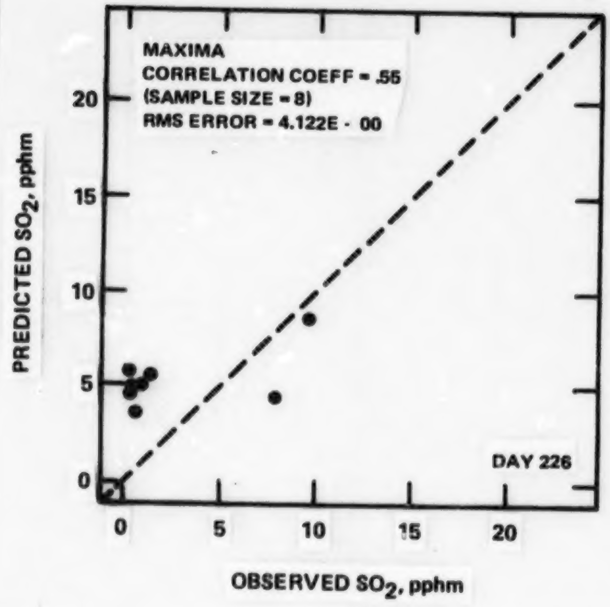

Figure 17e. LIRAQ scatter diagram of observed and predicted maximum SO_2 concentrations on Day 226 of 1976.

BEGIN LAST LINE OF TEXT
3/8"
BOTTOM OF IMAGE AREA; OUTSIDE DIMENSION FOR TABLES AND ILLUSTRATIONS

PAGE NUMBER
EPA Form 2350-4 (4-80)
(PREVIOUSLY CIN. EPA FORM 247)
U.S. GOVERNMENT PRINTING OFFICE 1980-360-830
TYPING GUIDE SHEET

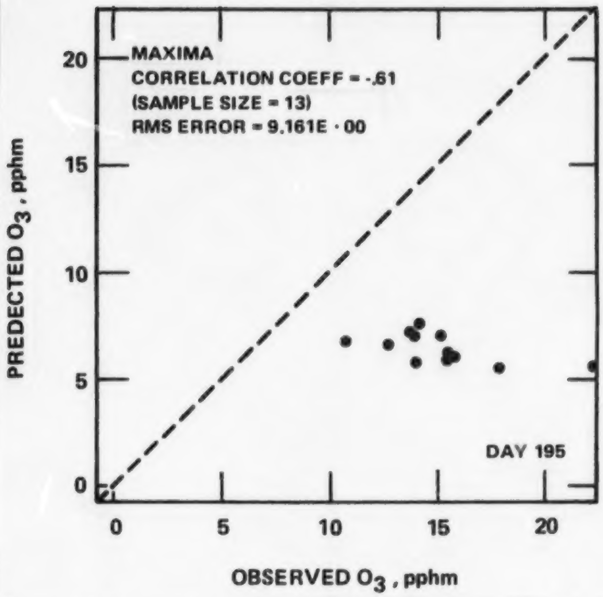

Figure 18a. LIRAQ scatter diagram of observed and predicted maximum O_3 concentrations on Day 195 of 1976.

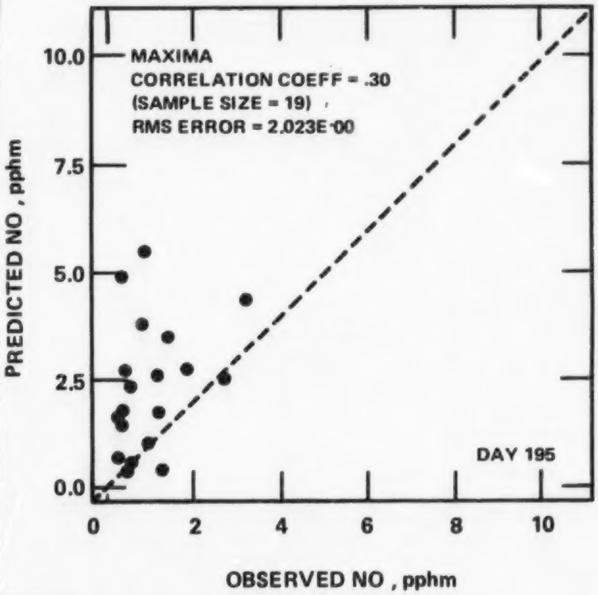

Figure 18b. LIRAQ scatter diagram of observed and predicted maximum NO concentrations on Day 195 of 1976.

EPA Form 2350-4 (4-80)
(PREVIOUSLY CIN. EPA FORM 267)
TYPING GUIDE SHEET

BEGIN FIRST LINE OF TEXT HERE
CENTER OF
TOP OF IMAGE AREA
DROPPED HEAD: BEGIN SECTIONS HERE

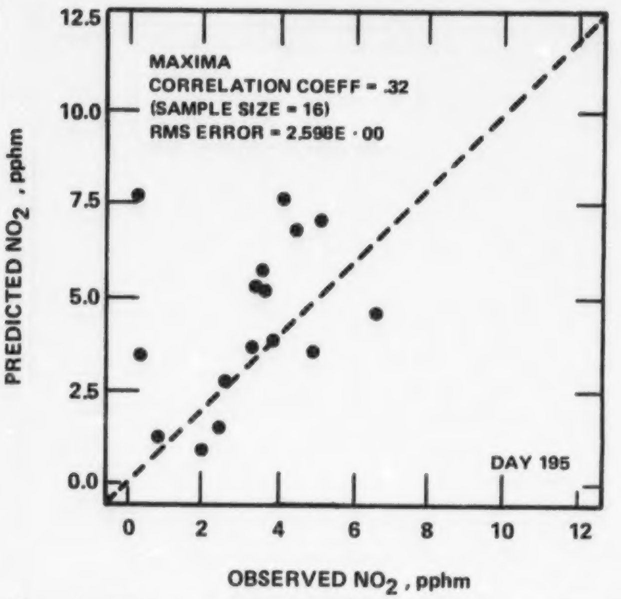

Figure 18c. LIRAQ scatter diagram of observed and predicted maximum NO_2 concentrations on Day 195 of 1976.

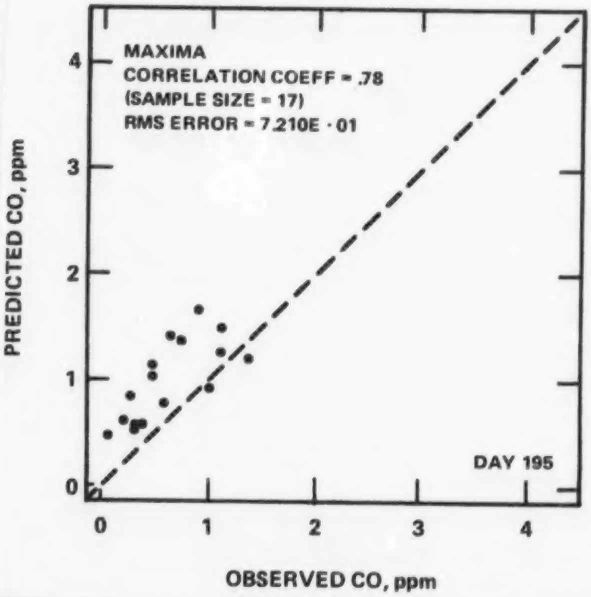

Figure 18d. LIRAQ scatter diagram of observed and predicted maximum CO concentrations on Day 195 of 1976.

BEGIN LAST LINE OF TEXT
BOTTOM OF IMAGE AREA OUTSIDE DIMENSION FOR TABLES AND ILLUSTRATIONS
3/8"

PAGE NUMBER
EPA Form 2350-4 (4-80)
(PREVIOUSLY EIN. EPA FORM 247)
TYPING GUIDE SHEET

SECTION 7

URBAN AIRSHED MODEL

OVERVIEW

The Urban Airshed Model (UAM) is a three-dimensional (3-D) grid-type or Eulerian, photochemical air quality simulation model (PAQSM) developed by Systems Applications, Inc. (SAI) of San Rafael, California. The structure of the model consists of a latticework array of cells, the total volume of which represents an urban-scale domain and in which the physical and chemical processes responsible for photochemical smog are mathematically simulated. These include the advection of pollutant species through the modeling domain, the species' entrainment from aloft by a growing mixed layer, the diffusion of material from cell to cell, the injection of primary source emissions into the modeled volume, and the chemical transformations of reactive species into intermediate and secondary products. The horizontal dimensions of each cell are constant but cell heights vary throughout a model simulation as the depth of the mixed layer in the UAM changes accordingly.

In the application of the model to the St. Louis RAPS data base, the area modeled was 60 km wide and 80 km long. Each individual cell was 4 km on a side in the horizontal. Vertically, there were four layers of cells in total; the bottom two layers simulated the mixed layer and the top two represented the region immediately above the mixed layer. The domain of the UAM was centered just west of downtown St. Louis and included the entire metropolitan area. Figure 19 shows a horizontal cross-section of the domain as applied to the RAPS monitoring network. The locations of all 25 monitoring stations are given in relation to the grid pattern. The outer ring contains the boundary cells for the model. Although model simulation does not occur in the boundary cells, they are an important part of the advective transport portion of the UAM. Four monitoring stations, 122-125, lie outside of the computational domain and are available for determining boundary concentrations. The remained of the sites lie within the domain, no two of which reside in the same cell. The 3-D grid model is a sophisticated type of PAQSM and provides both spatially and temporally resolved concentration predictions. Thus the UAM attempts to estimate the hour-average observed concentration of a pollutant species at each monitoring site within the model domain.

Model simulations were conducted using the UAM for each of the 10 test days listed in Table 1. Although a summary of results for O_3 predictions on all 10 test days will be given, detailed descriptions of model results will be presented for only 3 of these days. Emphasis will be placed on the simulation results for the pollutants CO, NO_2, and O_3 for the Julian days 142, 195, and 275.

METHOD

The package of programs constituting the UAM contains 12 data preprocessing programs as well as the simulation model. The data requirements for applying the model are rather intensive. The preprocessors (pp's) access the RAPS surface-based hour-average air quality and meteorological data base, the upper air pibal and radiosonde data, and the source emissions inventory for the necessary parameters, and process the parameters as required by the simulation model. A brief description of the pp's follows in order to convey a sense of the UAM data requirements.

The chemistry pp sets up the rate constants and other parameters related to the chemical kinetic mechanism within the model. This mechanism, named Carbon Bond II, is a state-of-the-art set of chemical reactions describing the NO_x-HC-O_3 species interactions within a photochemically active atmosphere. The mechanism was developed at SAI by Whitten et al. (1980). The terrain pp describes the spatially varying types of surfaces within the modeling domain, reflecting the transition from urban to suburban and finally to rural land uses. The spatial resolution of these land forms should be on the same scale as the grid cell size. Both the chemistry and terrain pp's need only be one executed once for a particular model application. However, all remaining pp's must be executed prior to each model simulation within the application.

The diffusion break and region top pp's describe the variations in the mixing heights and modeling region depths respectively, over the domain during the course of the simulation. Hourly values of the mixing height must be supplied for representative locations of the grid. The user must specify these depths in a meaningful manner from upper air soundings or equivalent data. The meteorological pp describes the temporal variation of vertical temperature gradients, stability class, atmospheric pressure, water vapor concentration, and the NO_2 photolysis rate constant. Values for these parameters do not vary spatially in the model. The top concentration pp specifies the concentrations of principal species at the top of the modeled region throughout the simulation. In most cases these concentrations will be close to the clean air background values for these species, although substantial concentrations of O_3 can be advected over the region. Its value is determined from the O_3 measurements at the far upwind surface monitoring sites after the nocturnal temperature inversion has eroded and the air aloft mixes through the atmosphere to the surface.

The air quality, temperature and wind speed pp's all require data from the surface monitoring network. Hour averages of observed species concentrations are objectively interpolated across the model grid to produce a field of initial concentrations for the UAM by the air quality pp. Typically this initial field is applied at a near-sunrise time. As the density of monitoring locations increases, the reliability of the objective interpolation does likewise. The temperature pp produces gridded fields of surface temperature at each hour of model simulation. These are required for both the wind and emissions point source pp's. Finally, the wind pp assimilates all available surface and upper air wind speed and direction measurements and produces a gridded field of u and v wind components at each of the model's four vertical levels. This objective wind field analysis routine was developed by Anderson of SAI (Killus et al., 1977). Vertical wind velocities are calculated internally by the UAM from mass continuity considerations. Anderson's interpolation routine smooths the data such that it eliminates unrealistic vertical motions. It simulates the mesoscale urban circulation patterns through the use of the surface temperature patterns. The boundary concentration pp determines the modeled species concentrations along each of the domain's borders for each hour of model simulation. A vertical concentration gradient is also described. In the model application reported here, data from the four outermost RAMS sites were employed in these concentration calculations.

The last two programs before the model itself are the source emission pp's. The area sources, including highway and line sources, and the point sources are treated separately. Hourly rates of emission of all primary pollutants for each grid are calculated. Organic hydrocarbon emissions must be distributed into particular structural classes. The contents and level of detail contained in the RAPS emissions inventory are described by Littman (1979).

Each pp forms a data file required by the UAM. Model simulations begin at 0500 CST and continue through 1700 CST. The model numerically calculates the rates of change of species concentrations at time steps on the order of several minutes, and then determines from these the hour-average predicted concentrations. The execution time for the model and its pp's for such a 12-h simulation on EPA's UNIVAC 1180 computer was approximately 145 min.

RESULTS

The 10 days from the RAPS data base selected for model simulation with the UAM included two where the afternoon observed O_3 maximum occurred at site 122, north of the UAM domain. The other days showed O_3 maxima occurring at sites within the model domain. The model simulates air quality within each cell of the grid. Species concentration predictions at particular RAPS monitoring site locations are interpolated from predictions at the closest cells by a distance-weighted (1/r) formula. Detailed simulation results are presented here for 3 of the 10 days modeled, and then summary statistics are given for O_3 alone over all the days.

The UAM provides a wealth of information from a simulation including the spatial and temporal concentration variations of all modeled species throughout the grid. It would not be practical to display the time series of predicted and observed concentrations for all RAPS sites here even for a few pollutants on a single day of simulation. A more concise method of displaying simulation results is invoked here based on an analysis of residual concentrations, observed minus predicted, over the 21 RAPS sites within the model domain (Bencala and Seinfeld, 1979). The particular analysis techniques employed here include residual histograms, hereafter denoted as 'RS', showing the general distribution of residuals for a complete simulation, and the residual vs. observed concentration plot, hereafter referred to as the 'RO' plot, demonstrating any trend toward over or underprediction by the model as a function of the observed concentration level. For a given species on one simulation day, there were 21 sites for each of 13 hours of simulation to account for, or 273 possible data points.

The first simulation day discussed is Day 142. The synoptic meteorological conditions on this day were described in Section 4. The maximum afternoon hour-average O_3 measurement occurred at noon at Site 101 in downtown St. Louis.

Figure 20a shows the RS for CO on this day. The ideal distribution for the RS would have a peak at 0.0 ppm and symmetric tails on either side sharply trailing off to 0.0 frequency. The figure displays behavior like this except for a slight shift in the peak toward overprediction. The RO plot in Figure 20b does reveal a trend toward underprediction with increasing concentration. This is especially evident in the three points corresponding to the highest observed concentrations. Since CO is a primary pollutant with a predominant source being motor vehicle emissions, it is possible for a monitor to be influenced by a nearby roadway. It would be difficult for a grid model without extremely fine spatial resolution to correctly simulate these CO hot spots. Yet, aside from the highest concentrations, it is instructive to study model performance for this species. As a relatively inert pollutant on the time scales of these model simulations, CO can reveal model deficiencies in advection and dispersion components that might not be evident with a more reactive species. The chemical interactions of reactive pollutants can mask problems with the simulation of their advection and dispersion.

The RS for NO_2 on Day 142 is presented in Figure 21a. While the distribution is symmetric near the 0.0 residual the tails are rather broad denoting a large amount of variance in the model predictions. This is substantiated in the RO for NO_2 in Figure 21b. Although the figure shows quite a bit of scatter, it is clear that at the higher observed concentrations, above 0.03 ppm, the model tends toward underprediction.

Figure 22a displays the RS for O_3 on this day. Here the distribution of residuals is unmistakably skewed toward overprediction with a peak at the 0.0 residual. The RO plot in Figure 22b shows the majority of the overpredicted concentrations to lie in the range of 0.050 to 0.125 ppm observed O_3. At the higher observed concentrations no trend is discernible. Background concentrations of O_3 on Day 142 were on the order of 0.06 ppm. The peak hour-average observation of 0.195 ppm at Site 101 at noon was simulated at the same time and location at a level of 0.164 ppm, a 16% underprediction.

Day 275 of 1976 in the RAPS data base represents an extreme stagnation episode in St. Louis. The synoptic meteorological conditions on this day were previously described in Section 4. The greatest hour-average O_3 measurement occurred at Site 102, just north of downtown St. Louis at 1400 CST, at a level of 0.243 ppm.

The RS for CO is shown in Figure 23a. The distribution peaks just on the overpredictive side of the 0.0 residual although there is some skewness toward the underpredictive with several extreme cases of underpredictions. Most likely the inability of the model to adequately resolve these hot spots of CO causes these cases. The RO plot in Figure 23b displays the trend toward underprediction of CO at higher observed concentrations and shows the worst underpredictions occur at the very highest CO levels. The extreme stability of the atmosphere on the morning of Day 275 is reflected in the elevated concentration levels of CO, on the order of 10 ppm. This is over twice the level of the observed peak on Day 142.

One problem with the UAM lies in simulating the vertical structure of a very stable atmosphere. The lower layers of cells must start out at a finite depth, such as 50 m, where the volume is assumed to be well mixed. In reality, the stability on Day 275 in the early morning suppressed any thermal mixing that might otherwise have occurred near the surface and allows for spatially distributed, high concentration peaks that are not seen in the simulation results.

The NO_2 frequency distribution of residuals, shown in Figure 24a, appears normally distributed about the 0.0 residual. The RO plot in Figure 24b shows a trend toward underprediction at observed concentrations greater than about 0.10 ppm. The O_3 residual analysis appears in Figures 25a and 25b and indicates the model is performing quite well in the overall predictions for the day. The RO plot for O_3 on Day 275 does not demonstrate any clear trends toward over or underprediction and most of the residuals are seen to fall within 0.05 ppm of the 0.0 residual. Background concentrations of O_3 on this day were on the order of 0.06 ppm. The hour-average maximum O_3 measurement occurred at site 102 at 1400 CST at 0.243 ppm. The model estimate at this place and time was 0.171 ppm, a 30% underprediction.

Of the 10 days included in the model evaluation exercises Day 195 has the distinction of having the largest transport wind measured near the surface and the warmest temperatures. The synoptic meteorological situation for Day 195 contained an upper air ridge over the center of the country with a warm front to the northeast of St. Louis. Winds near the surface were from the southeast during the day averaging just over 2.0 m s^{-1}. Skies were mostly clear with some occasional high level cloudiness. The maximum hour-average O_3 observation was taken at RAPS site 114, just west of the confluence of the Mississippi and Missouri rivers and north of the city of St. Louis.

CO concentrations were rather low on this day, mostly less than 1.0 ppm. Figure 26a shows the RS of the CO distribution is rather narrow, peaking slightly on the overpredictive side of the 0.0 residual. In the RO plot in Figure 26b, it is seen that this peak is indicative of the many very low observed concentrations, often near the detectable limits of the monitoring instrumentation. At higher concentrations the model tends to underpredict, especially at the two distinct data points representing CO hot spots.

The NO_2 residual distribution seen in Figure 27a is symmetric about the 0.0 residual and broader than that of the CO. It is weighted somewhat more on the underpredictive side. This is further substantiated by the RO plot for NO_2 in Figure 27b where the majority of the residuals are on the underpredicted side of the 0.0 residual and tend toward more severe underprediction at higher concentrations.

The RS for O_3 in Figure 28a displays a narrow distribution skewed toward underprediction. The RO plot for O_3 in Figure 28b shows the model to be performing well up to observed concentrations on the order of 0.10 ppm and tending to underpredict concentrations above that point. On Day 195, background concentrations of O_3 were approximately 0.08 ppm. The hour-average maximum O_3 measurement occurred at site 114 at 1500 CST at 0.222 ppm. The model estimate was 0.108, a 51% underprediction.

Figure 29 illustrates a potentially serious flaw in any grid model. It is apparently exemplified for the UAM in the Day 195 simulation. Presented in the figure is the model-predicted lowest layer concentration field of O_3, in ppb, averaged between the hours of 1400 and 1500 CST. Note that the maximum predicted O_3 concentration occurs along the northern border of the domain at 0.172 ppm. With a southeasterly wind flow, that area of high concentrations will be advected out of the model domain, and, in theory, could grow to yet higher concentrations during the next hour. However it is precisely at this time that the maximum observed O_3 occurred at site 114, within the model domain. Assuming that the maximum predicted O_3 level shown in Figure 29 did not change at the next hour and that it had been located at site 114, the model underprediction would be 23%, or a 28% improvement over the existing case. The most likely cause of the problem relates to the apparent inability of the objective wind interpolation method to correctly simulate transport in all cases through a grid model. Schere (1981) discusses 3 different wind analysis methods as candidates for the UAM and concludes that the Anderson method, currently in the model, performs at least as well as the others available.

Table 5 presents a summary of the predicted and observed O_3 maxima and an elementary statistical analysis of the UAM results for all 10 modeled days. The 'specific' model predictions correspond to the same location and time as the observed maximum and the 'global' predictions represent the maximum hour-average O_3 generated by the model at any lowest layer grid cell at any time during the simulation. The global maximum is the greatest surface value the model is able to produce within its domain. The specific and global model predictions, as seen in Table 5, typically do not coincide. This indicates that the maximum value of O_3 produced by the model did not correspond either in space or time, or both, to the maximum value observed in the atmosphere. Statistics on the residual concentration, ΔC, as shown in Table 5, were computed for both the specific and global predictions. Moreover, the average signed residual, and standard deviation are presented for the analysis. It is interesting to note that the average signed residuals for the specific and global cases of O_3 maxima are quite different, 0.074 and 0.018 ppm, respectively. The global predictions evidently show more promise toward maximum O_3 simulation. The average absolute residual is much larger than the signed residual in the global case, indicating that there were overpredictions as well as underpredictions among the 10 days tested. In the specific case, however, the average signed and absolute residuals are identical, signifying that the model has underpredicted consistently over all 10 days. The standard deviations of the specific and global residuals are 0.033 and 0.054 ppm respectively. The average value of the model's underprediction for maximum O_3 over all test days is 35% in the specific and 9% in the global.

TABLE 5. A SUMMARY OF PREDICTED AND OBSERVED O_3 MAXIMA FOR THE UAM

Day[a]	Hour (CST)	Station	Observed at 4-meters (ppm)	UAM Predicted Specific (ppm)	UAM Predicted Global (ppm)
142 (1975)	12	101	0.20	0.16	0.23
178	14	112	0.20	0.16	0.21
209	11	118	0.21	0.11	0.16
231	14	121	0.23	0.14	0.18
251	12	121[b]	0.18	0.14	0.15
159 (1976)	14	114[b]	0.17	0.14	0.28
160	16	115	0.22	0.13	0.19
195	15	114	0.22	0.11	0.17
226	13	109	0.23	0.10	0.13
275	14	102	0.24	0.17	0.22

[a] Ten days selected from 1975 and 1976.

[b] Overall maximum at 122, outside UAM grid region.

For the data displayed above:

ΔC = Obs minus Specific

$\overline{\Delta C} = 0.074$

$\text{s.d.}(\Delta C) = 0.033$

$\overline{|\Delta C|} = 0.074$

ΔC = Obs minus Global

$\overline{\Delta C} = 0.018$

$\text{s.d.}(\Delta C) = 0.054$

$\overline{|\Delta C|} = 0.048$

A least squares regression analysis for all specific O_3 predictions at all RAPS sites in the model domain on each test day is given in Table 6. The correlation coefficient here represents an integrated spatial and temporal measure of model performance. Overall the correlations are quite good. Only 4 of the slopes, however, fall between 0.8 and 1.0 with the rest being smaller than 0.7, pointing toward the general underprediction in the model's specific simulation results. Intercepts should ideally be close to 0.0, and all but 4 do lie between -0.02 and +0.03. The sum of the squared error term is a relative measure of the variance about the calculated line of regression.

TABLE 6. A SUMMARY OF LEAST SQUARES REGRESSION STATISTICS FOR UAM PREDICTED AND OBSERVED O_3[a].

Julian Date[b]	Correlation Coefficient	Slope	Intercept	Sum Squared Error
142 (1975)	0.827	0.992	-0.018	0.219
178	0.827	0.856	0.020	0.174
209	0.750	0.520	0.039	0.212
231	0.823	0.660	0.017	0.145
251	0.845	0.647	0.020	0.135
159 (1976)	0.916	0.900	-0.006	0.098
160	0.884	0.651	0.052	0.291
195	0.837	0.520	0.046	0.240
226	0.839	0.484	0.053	0.394
275	0.835	0.827	0.012	0.343

[a] Includes observations and predictions for all times and locations.

[b] Ten days selected from 1975 and 1976.

The analyses presented in Tables 5 and 6 are not intended to give a complete picture of the performance of the UAM. Rather, they present two aspects of the prediction of O_3 over a variety of days chosen from the RAPS data base. Certainly some of the 10 days, such as Day 142, were simulated better than others. The use of the UAM in a regulatory capacity demands the knowledge of performance potential in specific worst-case type situations. A summary of other statistical measures of model performance over the 10 test days appears in Appendices D and E.

CURRENT WORK

Specific testing of the UAM presently being conducted by the EPA Meteorology Lab has focused upon the model component responsible for horizontal advection. The technique employed by the UAM for horizontal advection is based on the flux-corrected transport method of Boris and Book (1973) called SHASTA, or sharp and smooth transport algorithm. A question was posed concerning the extent of numerical diffusion introduced into the model by the technique. This type of diffusion, distinct from true atmospheric diffusion, is an undesirable property of all finite difference numerical advection algorithms in that it can mask the effects of atmospheric diffusion if left unchecked. Most advection schemes contain antidiffusion steps that limit the amount of computationally generated numerical diffusion. Since there were areas within the simulated fields of pollutant concentrations from the UAM where it appeared that excess diffusion existed, it seemed reasonable to propose an independent test of the advection scheme.

The test consisted of a case of pure advection through the model domain of a block of mass 3 cells long in the x and y directions and 2 cells in the z direction. Each cell was initialized at 100 units (arbitrary) and the entire block was initially located near the south central border of the domain within a field otherwise consisting of no mass. The bottom layer of cells of this initial state of the modeling domain is shown in Figure 30a. Atmospheric diffusion, deposition, chemical transformations, vertical mixed layer growth, and source emissions were all deleted from the model for this test. The only physical process effectively simulated within this context was horizontal advection by the winds. To insure that no vertical wind component was created within the domain a temporally and spatially constant wind field of $u = 0.0 \text{ m s}^{-1}$ and $v = 2.0 \text{ m s}^{-1}$ was provided for the UAM test.

After five hours of simulation the instantaneous concentration field appeared as depicted in Figure 30b. The maximum value within the original block of mass had decreased from 100 units to 67 units, or 33%. The total mass of the block in layer 1 had increased from 900 units to 1165, an increase of 29%. Moreover the spatial extent of the original block had increased considerably from the initial state. Clearly the amount of numerical diffusion produced from the SHASTA advection algorithm as implemented within the UAM is significant.

The test of advecting a 3 by 3 block of mass is admittedly a rather severe one. In the St. Louis application however, this block would represent an area 12 km square, easily the size of a large area source. A grid-type PAQSM must be able to spatially represent the ambient concentrations produced from these source emissions without degrading them through artificial diffusion. At the current time an evaluation of other candidate numerical advection algorithms for the UAM is being conducted. It would seem that the goal of substituting a routine with less inherent diffusion in place of SHASTA is a desirable one.

CONCLUSIONS

The evaluation of the UAM is continuing at the Meteorology Division of EPA. Additional test days may be added to those already done. From the work performed to this point it is clear that the potential use of a grid-type PAQSM such as the UAM is great, although the complexity of the model often makes the solution of problems that arise more difficult. Troubleshooting and initial test application exercises have taken place over the past two years at EPA after the adaptation of the UAM to St. Louis by SAI. Most of the constituent components of the model have already been investigated and the work is continuing with those that have not. The model evaluation effort discussed in this paper has shown the UAM to simulate O_3 maxima in a global sense in St. Louis quite well and not as well in a specific sense. Areas of further study that may be pursued include:

(1) Further study of the adequacy of the wind field methodology, and

(2) The sensitivity of the model to variations in selected parameters such as initial and boundary concentrations, emissions, wind fields, and solar radiation.

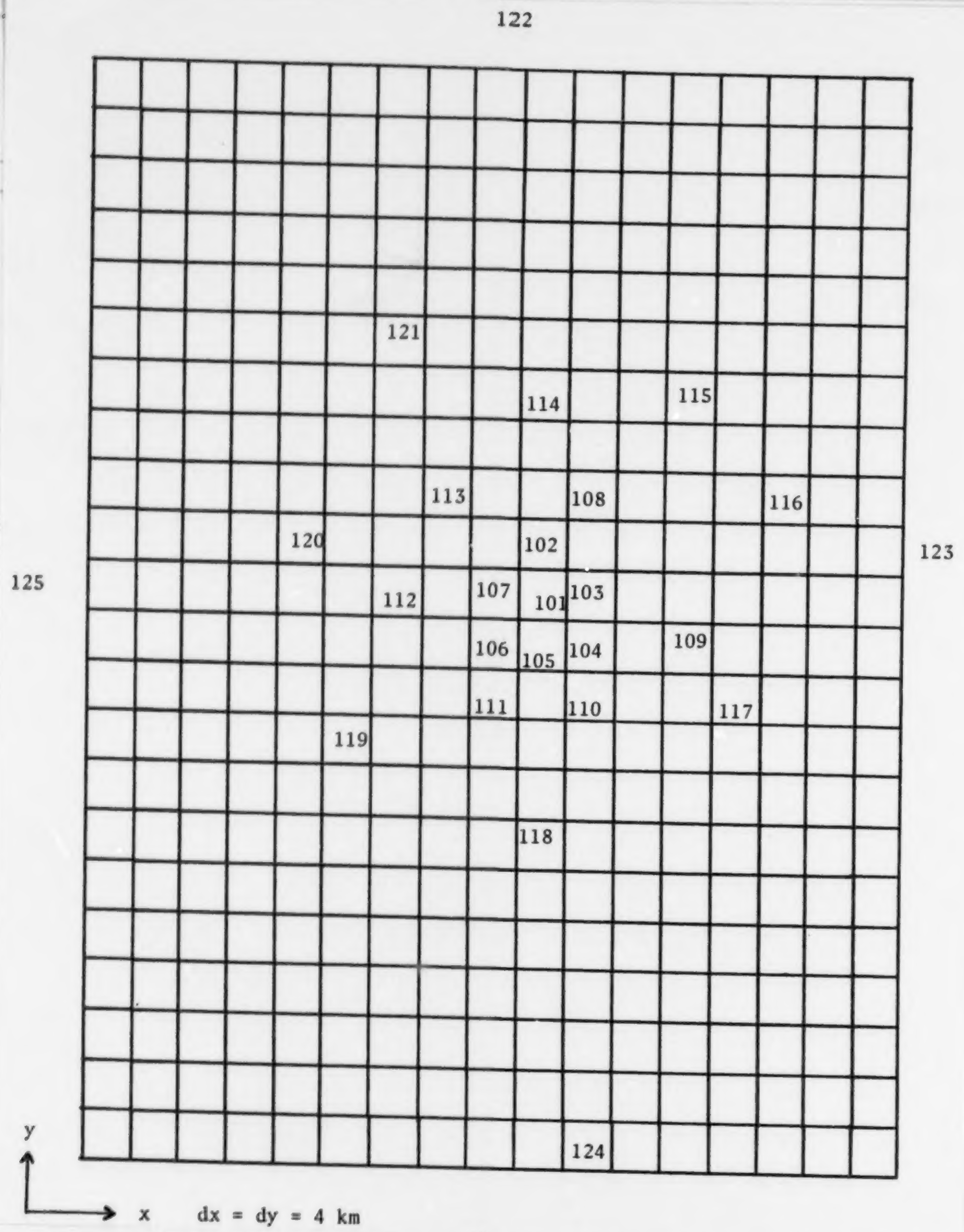
122
121
114
115
113
108
116
120
102
123
125
107
101
103
112
106
105
104
109
111
110
117
119
118
124
y
x
dx = dy = 4 km

Figure 19. Schematic drawing of horizontal section of UAM domain showing locations of RAPS monitoring sites.

BEGIN LAST LINE OF TEXT
BOTTOM OF IMAGE AREA; OUTSIDE DIMENSION FOR TABLES AND ILLUSTRATIONS
3/8"
PAGE NUMBER
EPA-287 (Cin.)
(4-76)

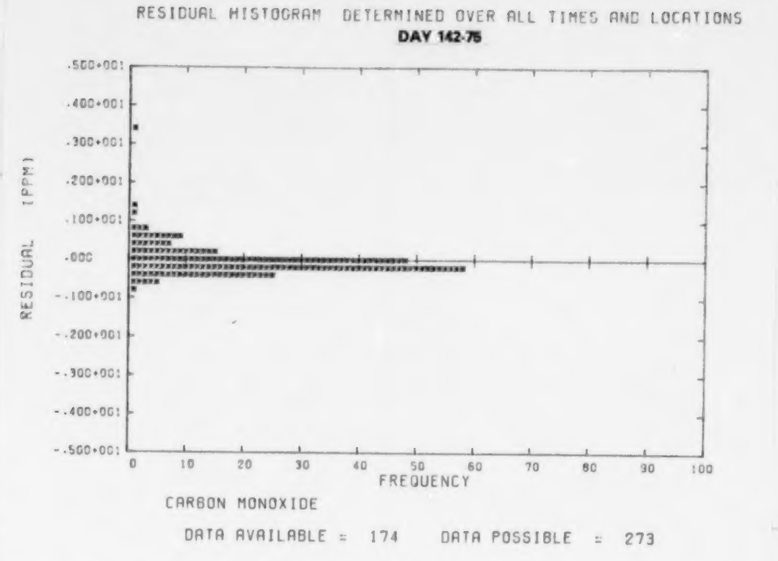

Figure 20a. Residual histogram for CO from the UAM simulation results for Day 142-75.

9-1/8"

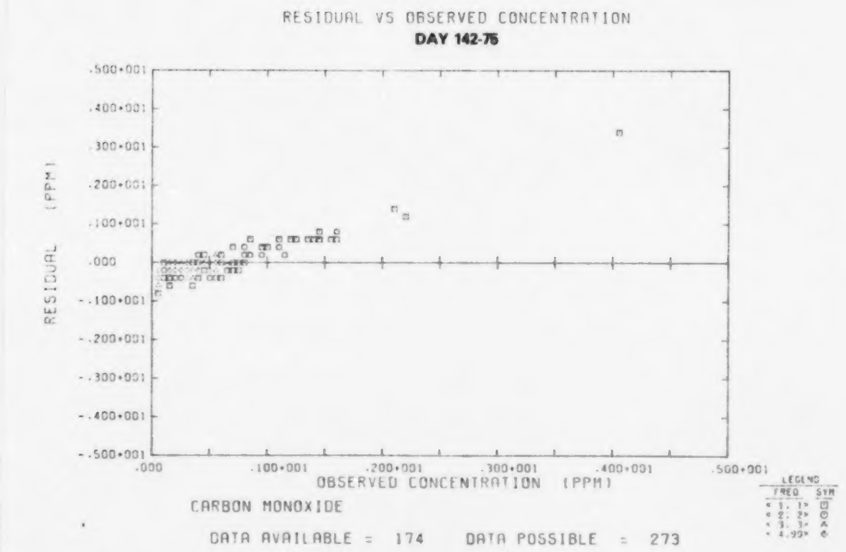

Figure 20b. Residual vs. observed plot for CO from the UAM simulation results for Day 142-75.

BEGIN LAST LINE OF TEXT
BOTTOM OF IMAGE AREA, OUTSIDE DIMENSION FOR TABLES AND ILLUSTRATIONS
3/8"

PAGE NUMBER
EPA-287 (Cin.)
(4-76)

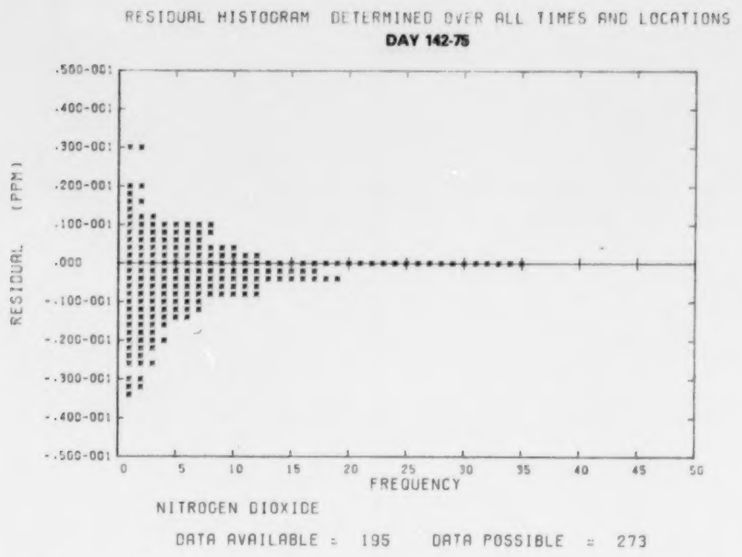

Figure 21a. Residual histogram for NO_2 from the UAM simulation results for Day 142-75.

9-1/8"

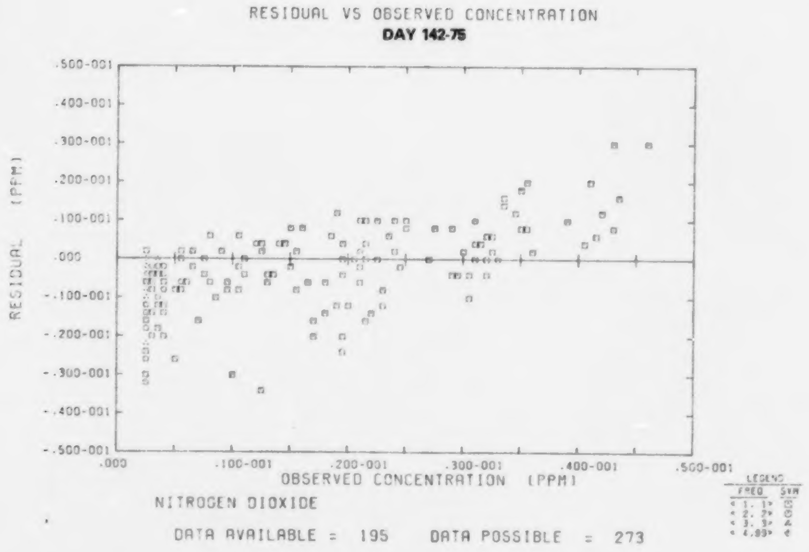

Figure 21b. Residual vs. observed plot for NO_2 from the UAM simulation results for Day 142-75.

BOTTOM OF IMAGE AREA, OUTSIDE DIMENSION FOR TABLES AND ILLUSTRATIONS
BEGIN LAST LINE OF TEXT
3/8"
PAGE NUMBER

EPA-287 (Cin.)
(4-76)

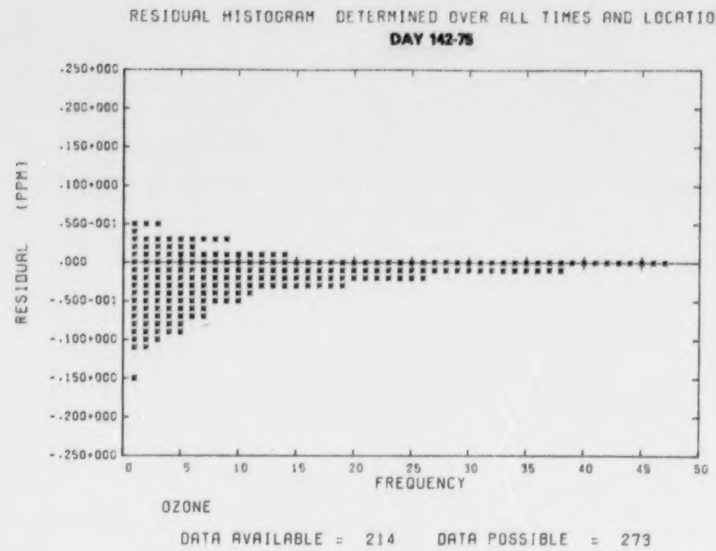

Figure 22a. Residual histogram for O_3 from the UAM simulation results for Day 142-75.

9-1/8"

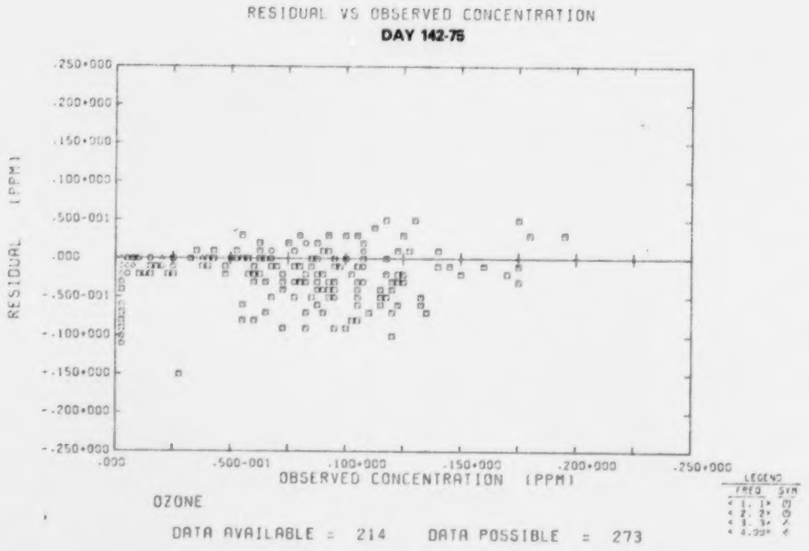

Figure 22b. Residual vs. observed plot for O_3 from the UAM simulation results for Day 142-75.

BEGIN LAST LINE OF TEXT
BOTTOM OF IMAGE AREA, OUTSIDE DIMENSION FOR TABLES AND ILLUSTRATIONS
3/8"

EPA-287 (Cin.)
(4-76)

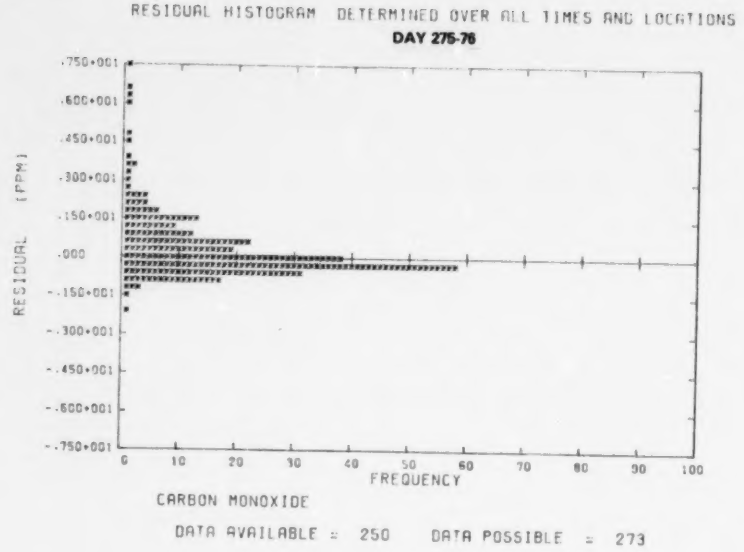

Figure 23a. Residual histogram for CO from the UAM simulation results for Day 275-76.

9-1/8"

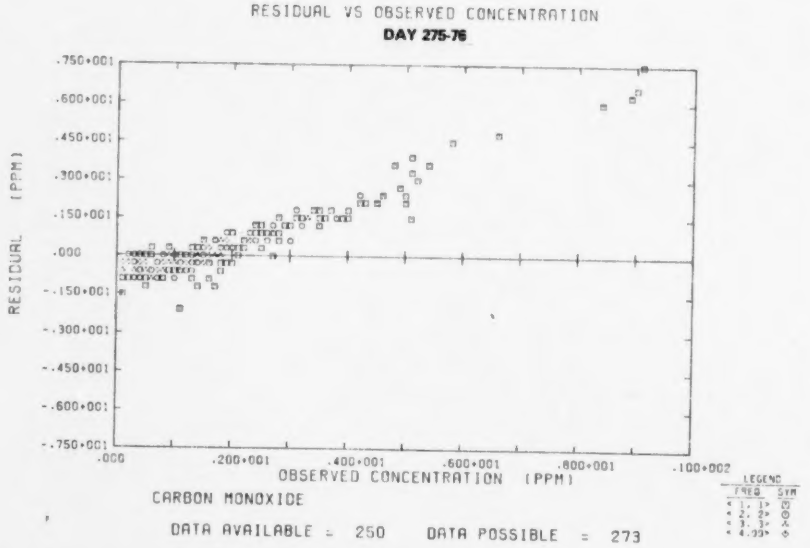

Figure 23b. Residual vs. observed plot for CO from the UAM simulation results for Day 275-76.

BEGIN LAST LINE OF TEXT
BOTTOM OF IMAGE AREA; OUTSIDE DIMENSION FOR TABLES AND ILLUSTRATIONS
3/8"

EPA-287 (Cin.)
(4-76)

TYPING GUIDE SHEET
BEGIN FIRST LINE OF TEXT HERE
CENTER OF PAGE
TOP OF IMAGE AREA
DROPPED HEAD; BEGIN SECTIONS HERE
9-1/8"

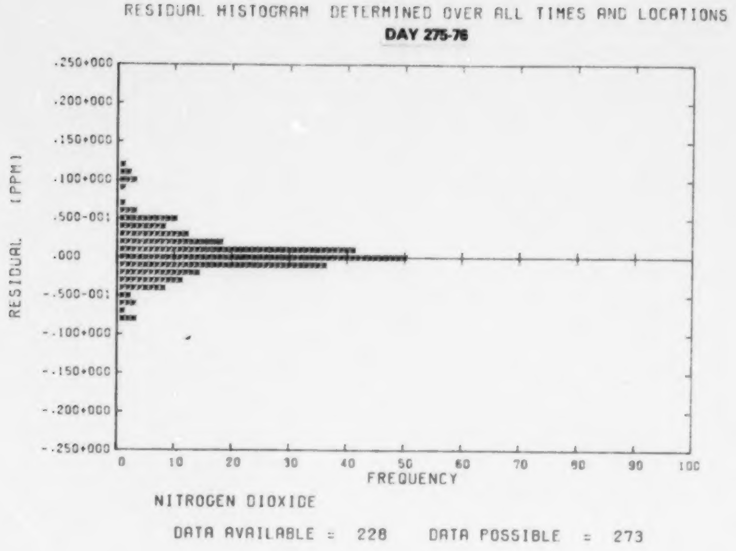

Figure 24a. Residual histogram for NO_2 from the UAM simulation results for Day 275-76.

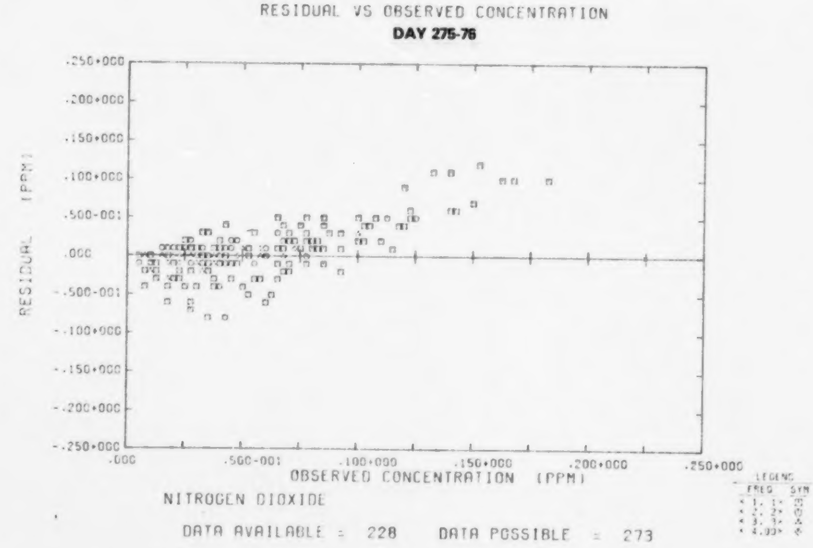

Figure 24b. Residual vs. observed plot for NO_2 from the UAM simulation results for Day 275-76.

BEGIN LAST LINE OF TEXT
BOTTOM OF IMAGE AREA; OUTSIDE DIMENSION FOR TABLES AND ILLUSTRATIONS
3/8"

PAGE NUMBER
EPA-287 (Cin.)
(4-76)

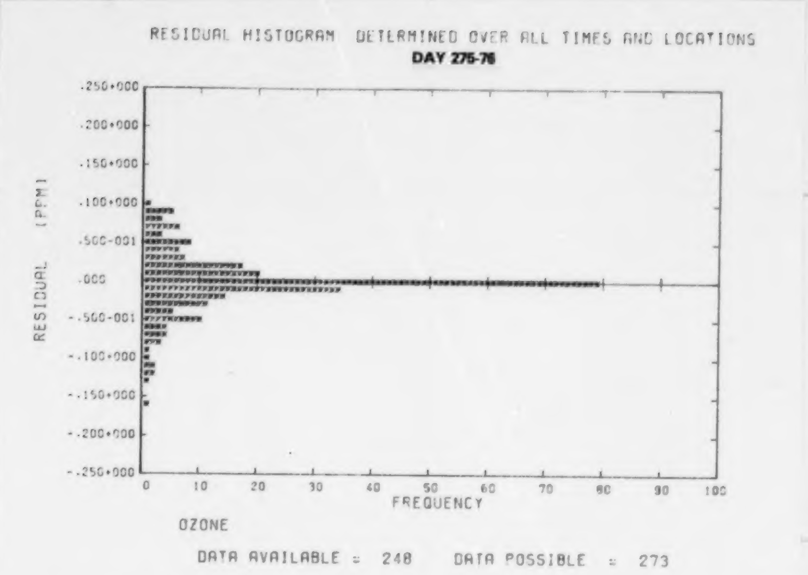

Figure 25a. Residual histogram for O_3 from the UAM simulation results for Day 275-76.

9-1/11"

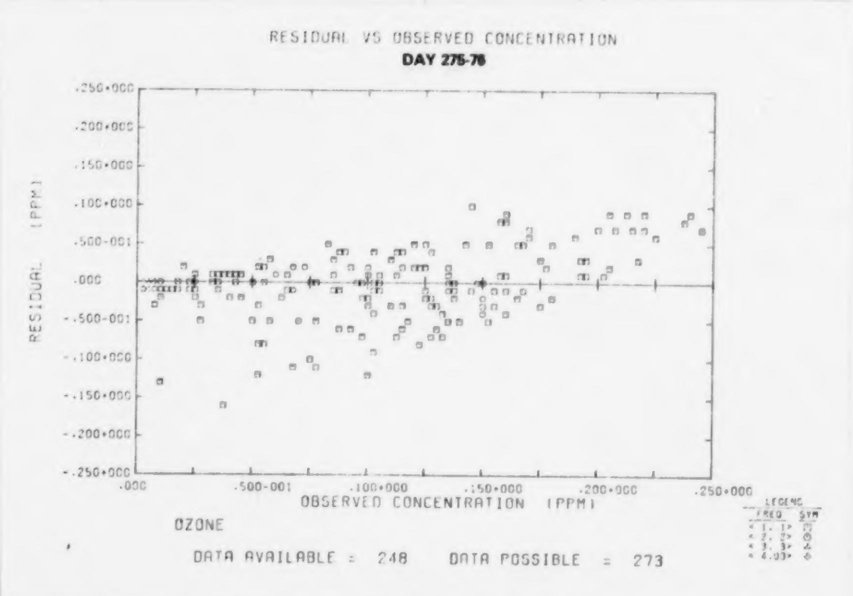

Figure 25b. Residual vs. observed plot for O_3 from the UAM simulation results for Day 275-76.

BOTTOM OF IMAGE AREA; OUTSIDE DIMENSION FOR TABLES AND ILLUSTRATIONS
BEGIN LAST LINE OF TEXT
3/8"

PAGE NUMBER
EPA-287 (Cin.)
(4-76)

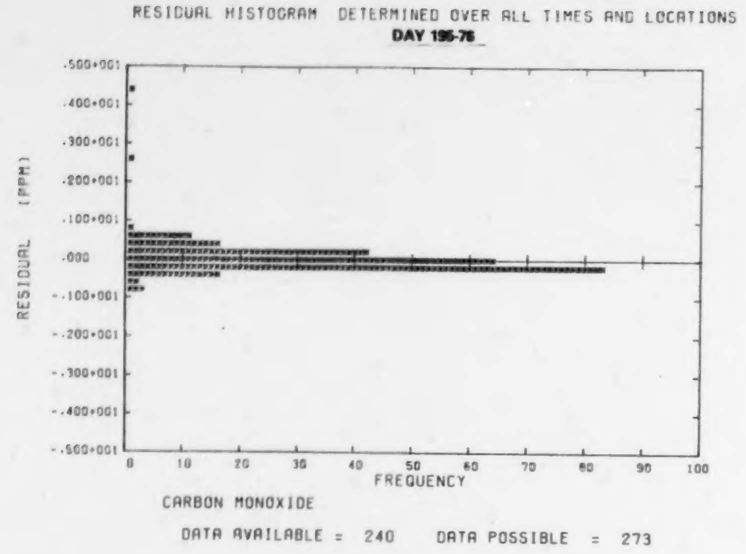

Figure 26a. Residual histogram for CO from the UAM simulation results for Day 195-76.

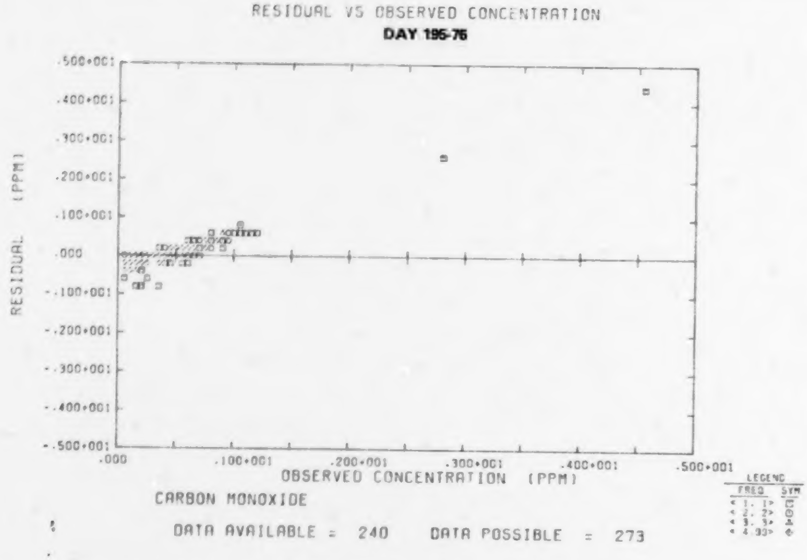

Figure 26b. Residual vs. observed plot for CO from the UAM simulation results for Day 195-76.

3/8"
PAGE NUMBER
EPA-287 (Cin.)
(4-76)

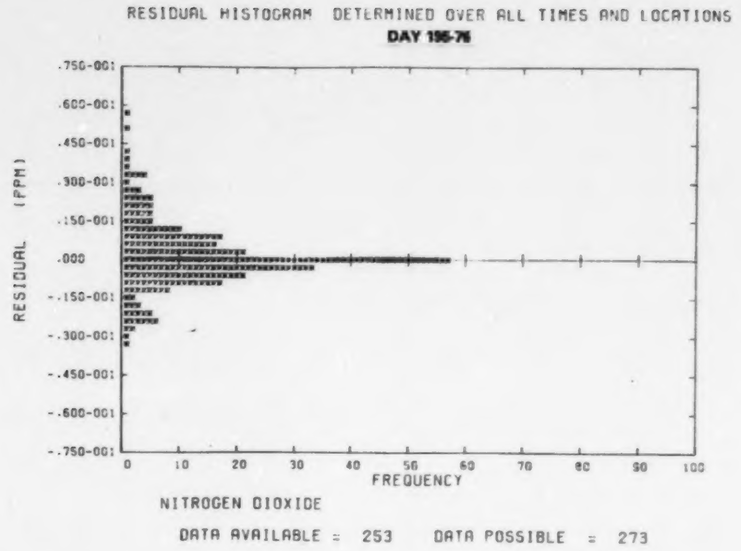

Figure 27a. Residual histogram for NO_2 from the UAM simulation results for Day 195-76.

9-1/8"

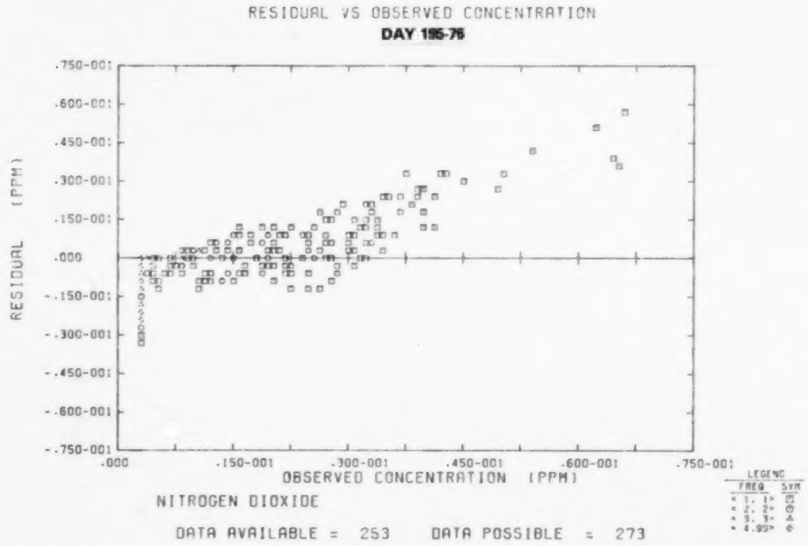

Figure 27b. Residual vs. observed plot for NO_2 from the UAM simulation results for Day 195-76.

BEGIN LAST LINE OF TEXT
BOTTOM OF IMAGE AREA; OUTSIDE DIMENSION FOR TABLES AND ILLUSTRATIONS
3/8"

PAGE NUMBER
EPA-287 (Cin.)
(4-76)

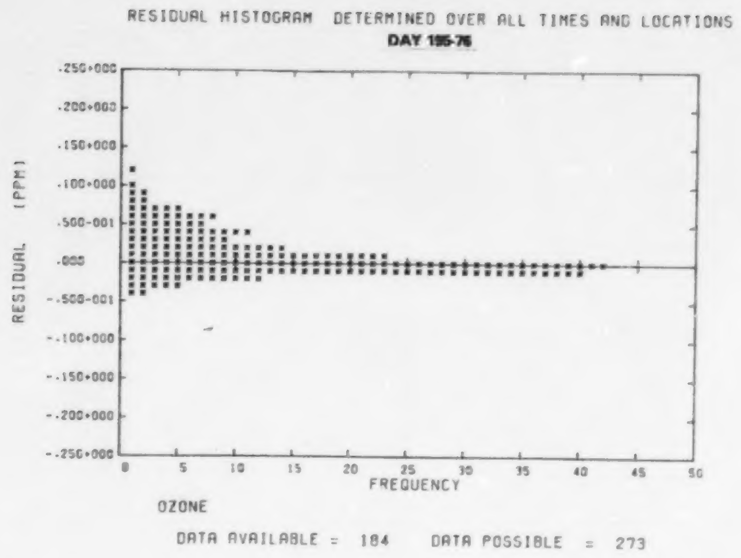

Figure 28a. Residual histogram for O_3 from the UAM simulation results for Day 195-76.

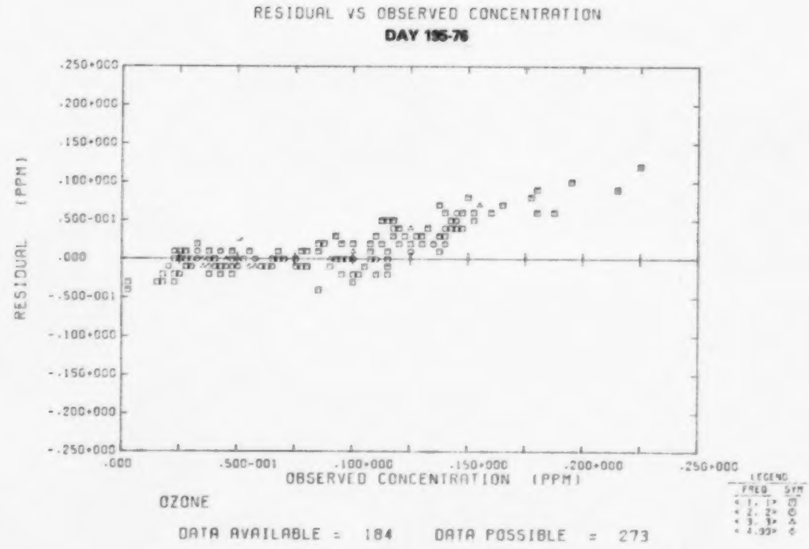

Figure 28b. Residual vs. observed plot for O_3 from the UAM simulation results for Day 195-76.

EPA-287 (Cin.)
(4-76)

118	147	168	172	172	167	158	137	118	108	110	118	117	113	110
98	133	157	168	170	168	164	134	116	104	107	117	117	110	108
93	124	140	161	164	162	150	130	110	97	101	117	118	110	101
91	117	138	162	157	154	149	124	108	92	97	118	120	112	102
88	110	128	142	148	148	136	118	108	97	102	117	122	114	104
86	103	117	128	138	137	128	112	98	96	104	118	124	117	108
84	97	108	118	127	128	121	108	94	92	102	120	128	121	110
83	96	103	111	118	122	116	102	90	88	101	122	131	128	113
81	94	101	106	111	113	108	96	83	83	100	122	132	128	117
81	96	101	102	104	104	101	90	77	81	97	118	131	130	121
84	96	100	101	101	98	94	83	77	82	96	113	128	128	123
83	93	98	99	98	96	94	89	86	88	94	108	119	126	122
82	89	93	94	93	89	88	86	91	91	92	100	112	118	118
81	86	90	92	88	83	84	87	90	90	91	96	108	111	113
81	87	88	81	87	80	78	83	88	90	90	91	96	103	108
82	87	88	88	87	77	74	78	88	90	90	90	93	87	101
82	88	88	86	86	78	76	79	86	90	81	90	90	82	96
83	89	90	90	90	89	86	83	86	90	82	91	91	91	92
86	91	91	91	90	92	90	87	87	60	82	92	92	91	92
84	93	93	93	93	93	93	92	91	92	93	94	94	93	93

Figure 29. Hour-average O_3 concentrations predicted by the UAM in the lowest layer of cells from the simulation of Day 195-76 at 1400 CST.

BEGIN LAST LINE OF TEXT
BOTTOM OF IMAGE AREA, OUTSIDE DIMENSION FOR TABLES AND ILLUSTRATIONS
3/8"
PAGE NUMBER
EPA-287 (Cin.)
(4-76)

0	0	0	0	0	0	0	0	0	0	0	0	0	0	0
0	0	0	0	0	0	0	0	0	0	0	0	0	0	0
0	0	0	0	0	0	0	0	0	0	0	0	0	0	0
0	0	0	0	0	0	0	0	0	0	0	0	0	0	0
0	0	0	0	0	0	0	0	0	0	0	0	0	0	0
0	0	0	0	0	0	0	0	0	0	0	0	0	0	0
0	0	0	0	0	0	0	0	0	0	0	0	0	0	0
0	0	0	0	0	0	0	0	0	0	0	0	0	0	0
0	0	0	0	0	0	0	0	0	0	0	0	0	0	0
0	0	0	0	0	0	0	0	0	0	0	0	0	0	0
0	0	0	0	0	0	0	0	0	0	0	0	0	0	0
0	0	0	0	0	0	0	0	0	0	0	0	0	0	0
0	0	0	0	0	0	0	0	0	0	0	0	0	0	0
0	0	0	0	0	0	0	0	0	0	0	0	0	0	0
0	0	0	0	0	0	0	0	0	0	0	0	0	0	0
0	0	0	0	0	0	0	0	0	0	0	0	0	0	0
0	0	0	0	0	0	100	100	100	0	0	0	0	0	0
0	0	0	0	0	0	100	100	100	0	0	0	0	0	0
0	0	0	0	0	0	100	100	100	0	0	0	0	0	0
0	0	0	0	0	0	0	0	0	0	0	0	0	0	0

Figure 30a. Instantaneous concentrations (arbitrary units) within the lowest layer of cells from the UAM advection-only test at the initial state.

0	0	0	0	0	0	0	0	0	0	0	0	0	0	0
0	0	0	0	0	0	0	0	0	0	0	0	0	0	0
0	0	0	0	0	0	0	0	0	0	0	0	0	0	0
0	0	0	0	0	0	0	0	0	0	0	0	0	0	0
0	0	0	0	0	1	2	2	2	1	0	0	0	0	0
0	0	0	0	2	6	9	11	9	6	2	0	0	0	0
0	0	0	0	5	14	26	29	26	14	5	0	0	0	0
0	0	0	1	8	26	44	52	44	26	8	1	0	0	0
0	0	0	1	11	32	58	67	58	32	11	1	0	0	0
0	0	0	1	10	31	54	64	54	31	10	1	0	0	0
0	0	0	1	7	21	37	44	37	21	7	1	0	0	0
0	0	0	0	3	9	16	19	16	9	3	0	0	0	0
0	0	0	0	1	2	3	3	3	2	1	0	0	0	0
0	0	0	0	0	0	0	0	0	0	0	0	0	0	0
0	0	0	0	0	0	0	0	0	0	0	0	0	0	0
0	0	0	0	0	0	0	0	0	0	0	0	0	0	0
0	0	0	0	0	0	0	0	0	0	0	0	0	0	0
0	0	0	0	0	0	0	0	0	0	0	0	0	0	0
0	0	0	0	0	0	0	0	0	0	0	0	0	0	0
0	0	0	0	0	0	0	0	0	0	0	0	0	0	0

Figure 30b. Instantaneous concentrations (arbitrary units) within the lowest layer of cells from the UAM advection-only test after 5 hrs of simulation.

REFERENCES

Bencala, K. E. and J. H. Seinfeld, 1979: An air quality model performance assessment package. Atmospheric Environment, 13, 1181-1185.

Boris, J. P. and D. L. Book, 1973: Flux-corrected transport. I. SHASTA, A fluid transport-algorithm that works. Journal of Computational Physics, 11, 38-69.

Demerjian, K. L. and K. L. Schere, 1979: Application of a photochemical box model for O_3 air quality in Houston, Texas. In Proceedings of Ozone/Oxidants: Interactions With the Total Environment II, Houston, Texas, October 1979, Air Pollution Control Association, pp. 329-352.

Duewer, W. H., J. J. Walton, K. E. Grant, and H. Walker, 1980: Livermore Regional Air Quality Model (LIRAQ) - Transfer to EPA. EPA-600/4-80-041. NTIS, Order No.80-221591.

Duewer, W. H., M. C. MacCracken, and J. J. Walton, 1978: The Livermore Regional Air Quality Model, II. Verification and Sample Application in the San Francisco Bay Area, J. Appl. Met., 17, 274-311.

Killus, J. P., J. P. Meyer, D. R. Durran, G. E. Anderson, T. N. Jerskey and G. Z. Whitten, 1977: Continued research in mesoscale air pollution simulation modeling: Volume V--Refinements in numerical analysis, transport, chemistry, and pollutant removal. Report No. ES77-142, Systems Applications, Inc., San Rafael, CA 94903.

Littman, F. E., 1979: Regional Air Pollution Study--Emission inventory summarization. Report No. EPA-600/4-79-004, U.S. Environmental Protection Agency, Research Triangle Park, NC 27711.

Lurmann, F., D. Godden, A. C. Lloyd, and R. A. Nordsieck, 1979: A Lagrangian Photochemical Air Quality Simulation Model. Vol. I-Model Formulation, Vol. II-Users Manual. EPA-600/8-79-015a,b (available NTIS).

MacCracken, M. C., D. J. Wuebbles, J. J. Walton, W. H. Duewer, and K. E. Grant, 1978: The Livermore Regional Air Quality Model, I. Concept and development. J. Appl. Met., 17, 254-272.

Schere, K. L. 1981: Air quality model response to objectively analyzed wind fields. In Proceedings of the Fifth Symposium on Turbulence, Diffusion, and Air Pollution, American Meteorological Society, Atlanta, GA, March 9-13, 1981.

Schiermeier, F. A., 1978: air monitoring milestones: RAPS field measurements are in. Environmental Science and Technology, 12, 664-651.

Shreffler, J. H., 1979: Urban-rural differences in tower-measured winds. J. Appl. Met., 18, 829-835.

Shreffler, J. H. and R. B. Evans, 1981: The surface ozone record from the Regional Air Pollution Study, 1975-1976. Atm. Environment (In press).

Venkatram, A., 1978: An examination of box models for air quality simulation. Atmospheric Environment, 12, 2243-2249.

Whitten, G. Z., J. P. Killus, and H. Hogo, 1980: Modeling of simulated photochemical smog with kinetic mechanisms - Vol. 1. Report No. EPA-600/3-80-028a, U. S. Environmental Protection Agency, Research Triangle Park, NC 27711.

APPENDIX A

PBM - TIME SERIES FOR REMAINING TEST DAYS

This appendix contains the time series plots for the pollutant species CO, NO_2, and O_3 from the PBM test results for those days that were not specifically discussed within the body of this report. The plots presented here are from test days 178-75, 209-75, 231-75, 159-76, 160-76, 195-76, and 226-76 of the RAPS data base.

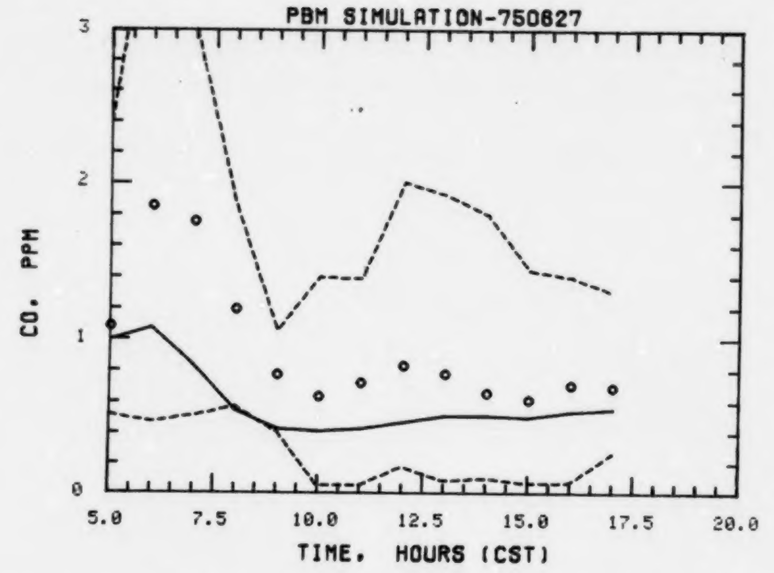

Figure A-1a. PBM simulation results for Day 178 of 1975. Time series of average observed (circles), range of observed (dashed lines), and model simulated (solid line) hour-average concentrations of CO.

BEGIN LAST LINE OF TEXT
BOTTOM OF IMAGE AREA; OUTSIDE DIMENSION FOR TABLES AND ILLUSTRATIONS
3/8"

PAGE NUMBER
EPA-287 (Cin.)
(4-76)

TYPING GUIDE SHEET
BEGIN FIRST LINE OF TEXT HERE
CENTER
TOP OF IMAGE AREA
DROPPED HEAD; BEGIN SECTIONS HERE

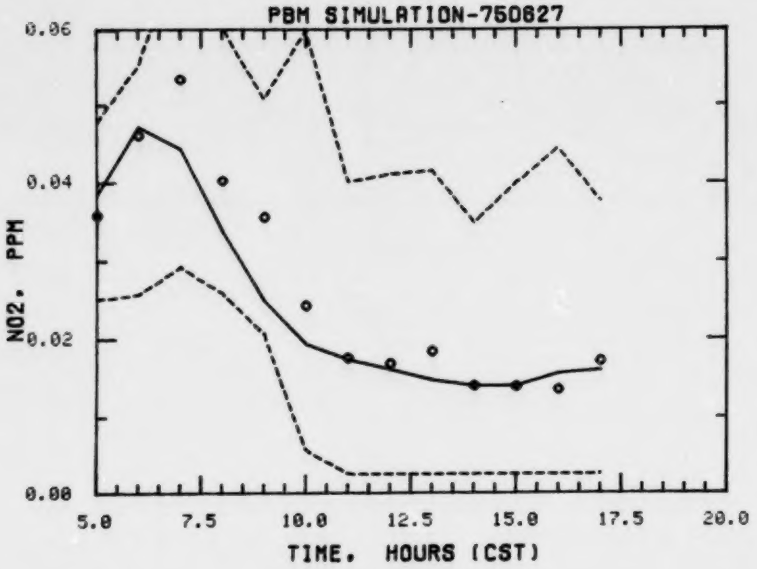

Figure A-1b. PBM simulation results for NO_2 - Day 178 of 1975. Keys to figure described in A-1a.

9-1/8"

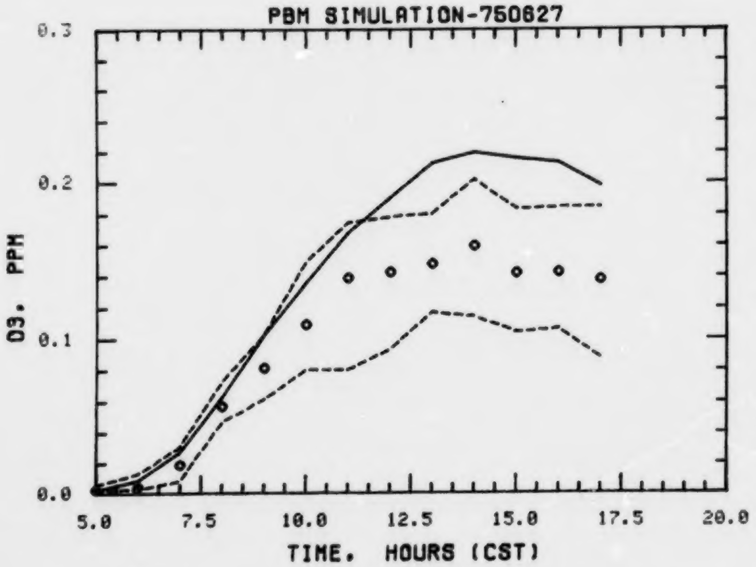

Figure A-1c. PBM simulation results for O_3 - Day 178 of 1975. Keys to figure described in A-1a.

BEGIN LAST LINE OF TEXT
BOTTOM OF IMAGE AREA; OUTSIDE DIMENSION FOR TABLES AND ILLUSTRATIONS
3/8"

PAGE NUMBER
EPA-287 (Cin.)
(4-76)

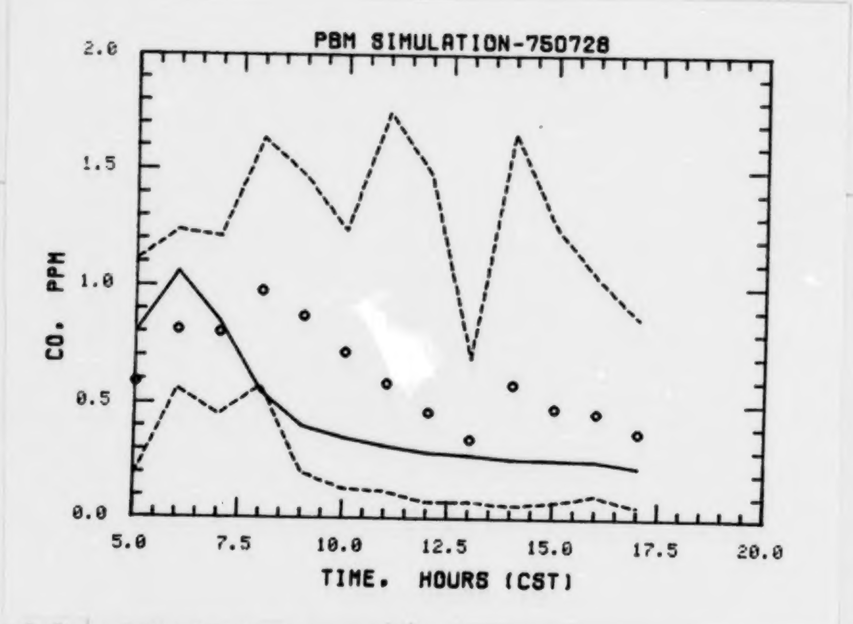

Figure A-2a. PBM simulation results for Day 209 of 1975. Time series of average observed (circles), range of observed (dashed lines), and model simulated (solid line) hour-average concentrations of CO.

BEGIN LAST LINE OF TEXT
3/8"
BOTTOM OF IMAGE AREA; OUTSIDE DIMENSION FOR TABLES AND ILLUSTRATIONS
PAGE NUMBER
EPA-287 (Cin.)
(4-76)

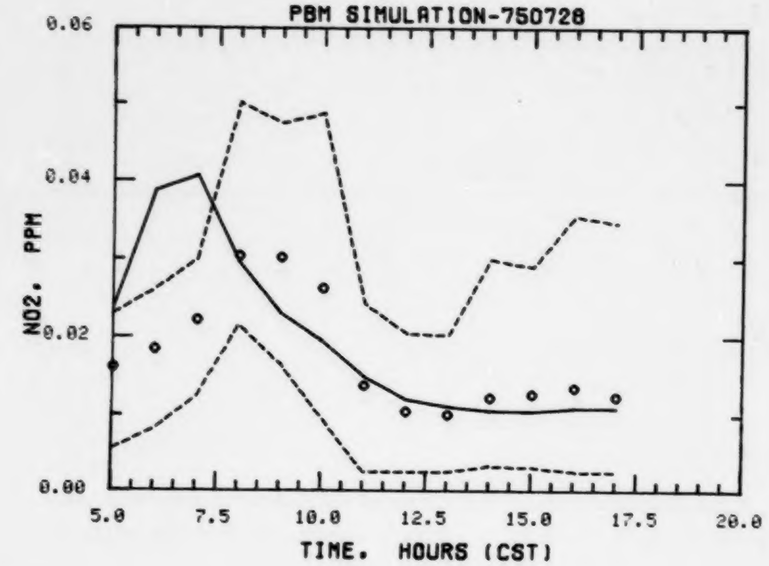

Figure A-2b. PBM simulation results for NO_2 - Day 209 of 1975. Keys to figure described in A-2a.

9-1/8"

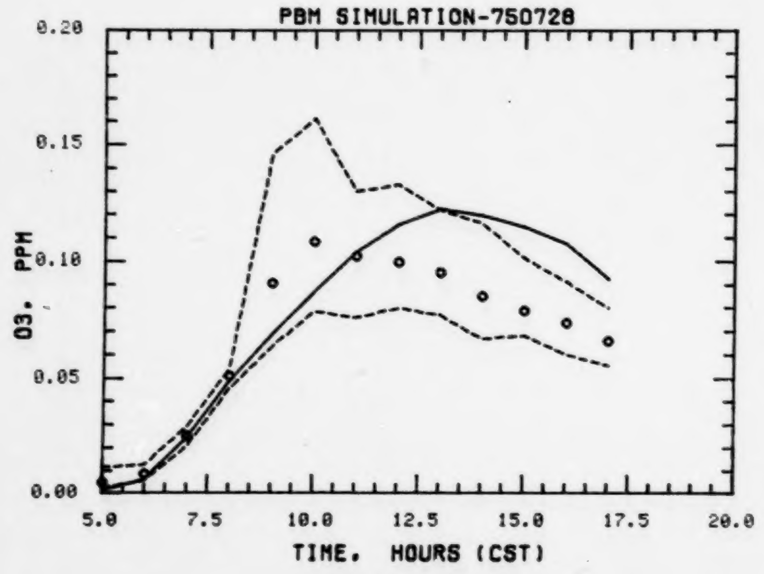

Figure A-2c. PBM simulation results for O_3 - Day 209 of 1975. Keys to figure described in A-2a.

BEGIN LAST LINE OF TEXT
BOTTOM OF IMAGE AREA; OUTSIDE DIMENSION FOR TABLES AND ILLUSTRATIONS
3/8"

EPA-287 (Cin.)
(4-76)

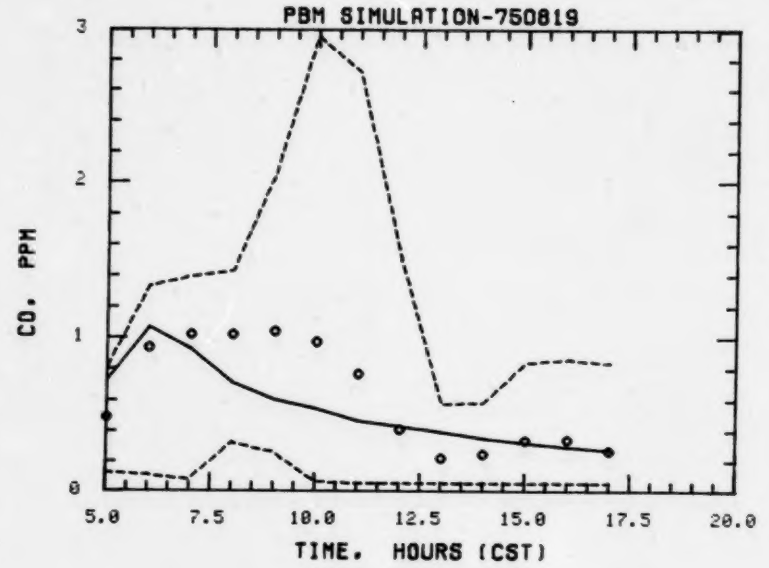

Figure A-3a. PBM simulation results for Day 231 of 1975. Time series of average observed (circles), range of observed (dashed lines), and model simulated (solid line) hour-average concentrations of CO.

BEGIN LAST LINE OF TEXT
BOTTOM OF IMAGE AREA; OUTSIDE DIMENSION FOR TABLES AND ILLUSTRATIONS
3/8"

PAGE NUMBER
EPA-287 (Cin.)
(4-76)

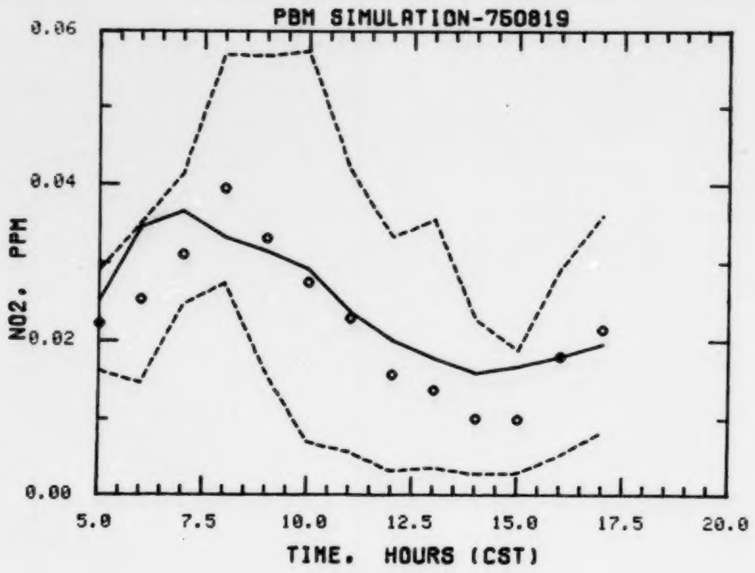

Figure A-3b. PBM simulation results for NO_2 - Day 231 of 1975. Keys to figure described in A-3a.

9-1/8"

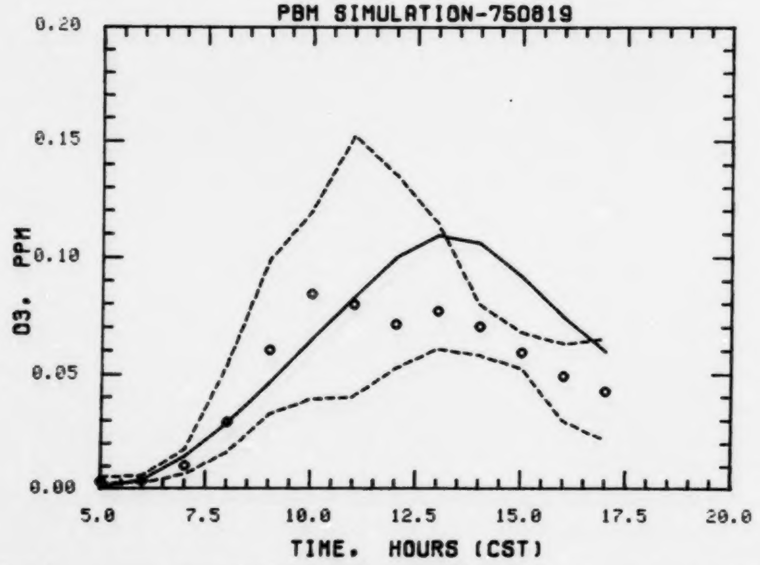

Figure A-3c. PBM simulation results for O_3 - Day 231 of 1975. Keys to figure described in A-3a.

BEGIN LAST LINE OF TEXT
BOTTOM OF IMAGE AREA, OUTSIDE DIMENSION FOR TABLES AND ILLUSTRATIONS
3/8"
PAGE NUMBER
EPA-287 (Cin.)
(4-76)

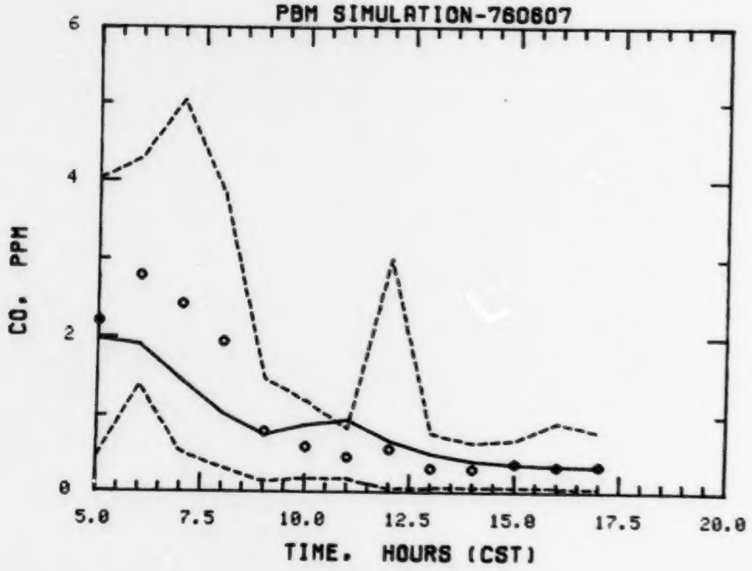

Figure A-4a. PBM simulation results for Day 159 of 1976. Time series of average observed (circles), range of observed (dashed lines), and model simulated (solid line) hour-average concentrations of CO.

BEGIN LAST LINE OF TEXT
BOTTOM OF IMAGE AREA; OUTSIDE DIMENSION FOR TABLES AND ILLUSTRATIONS
3/8"

PAGE NUMBER
EPA-287 (Cin.)
(4-76)

TYPING GUIDE SHEET
BEGIN FIRST LINE OF TEXT HERE
CENTER OF PAGE
TOP OF IMAGE AREA
DROPPED HEAD; BEGIN SECTIONS HERE
9-1/8"

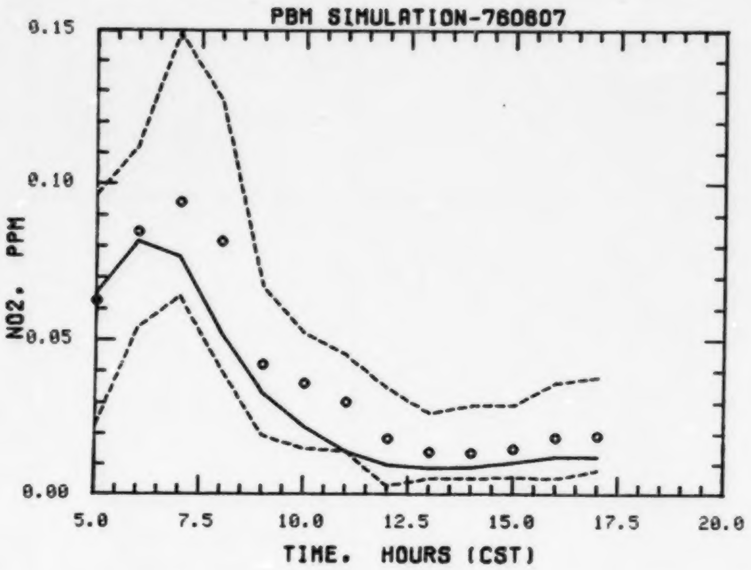

Figure A-4b. PBM simulation results for NO_2 - Day 159 of 1976. Keys to figure described in A-4a.

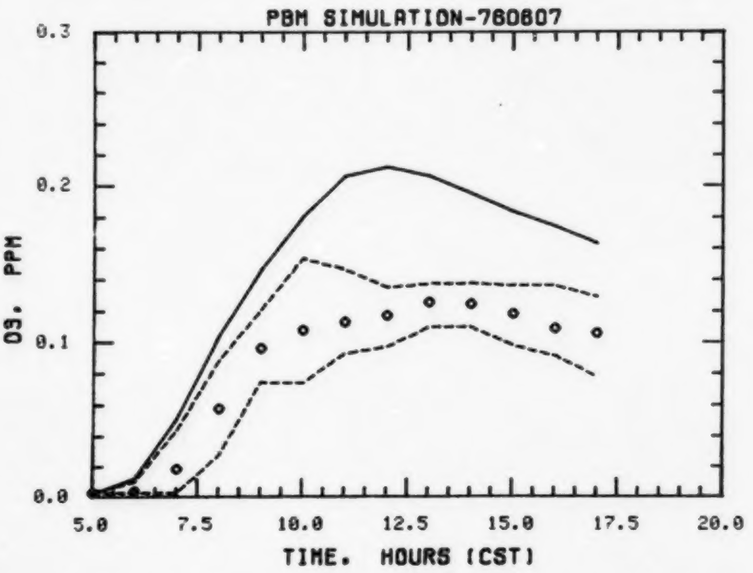

Figure A-4c. PBM simulation results for O_3 - Day 159 of 1976. Keys to figure described in A-4a.

BEGIN LAST LINE OF TEXT
BOTTOM OF IMAGE AREA, OUTSIDE DIMENSION FOR TABLES AND ILLUSTRATIONS
3/8"

PAGE NUMBER
EPA-287 (Cin.)
(4-76)

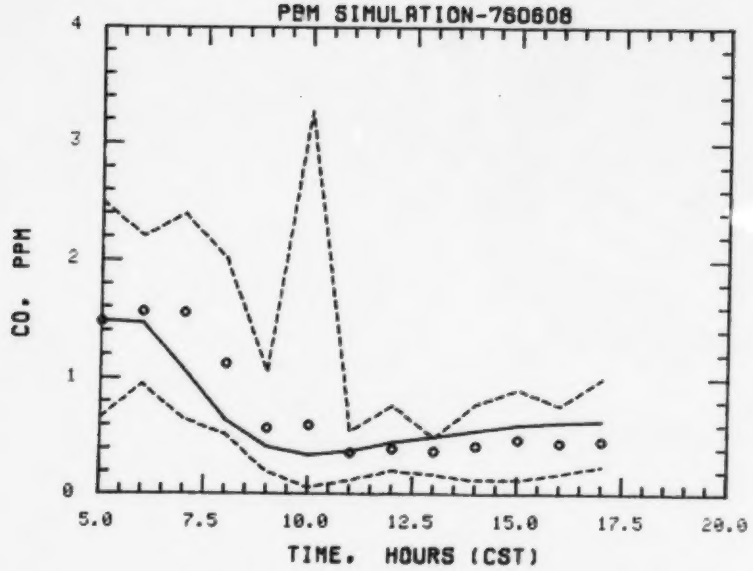

Figure A-5a. PBM simulation results for Day 160 of 1976. Time series of average observed (circles), range of observed (dashed lines), and model simulated (solid line) hour-average concentrations of CO.

BEGIN LAST LINE OF TEXT
3/8"
BOTTOM OF IMAGE AREA OUTSIDE DIMENSION FOR TABLES AND ILLUSTRATIONS

PAGE NUMBER
EPA-287 (Cin.)
(4-76)

BEGIN FIRST LINE OF TEXT HERE
TYPING GUIDE SHEET
CENTER OF PAGE
TOP OF IMAGE AREA
DROPPED HEAD. BEGIN SECTIONS HERE
9 1/8"

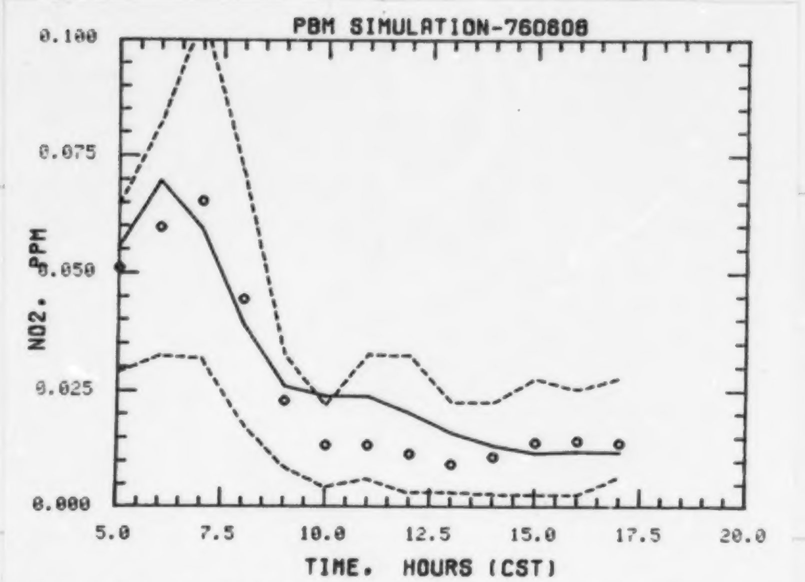

Figure A-5b. PBM simulation results for NO_2 - Day 160 of 1976. Keys to figure described in A-5a.

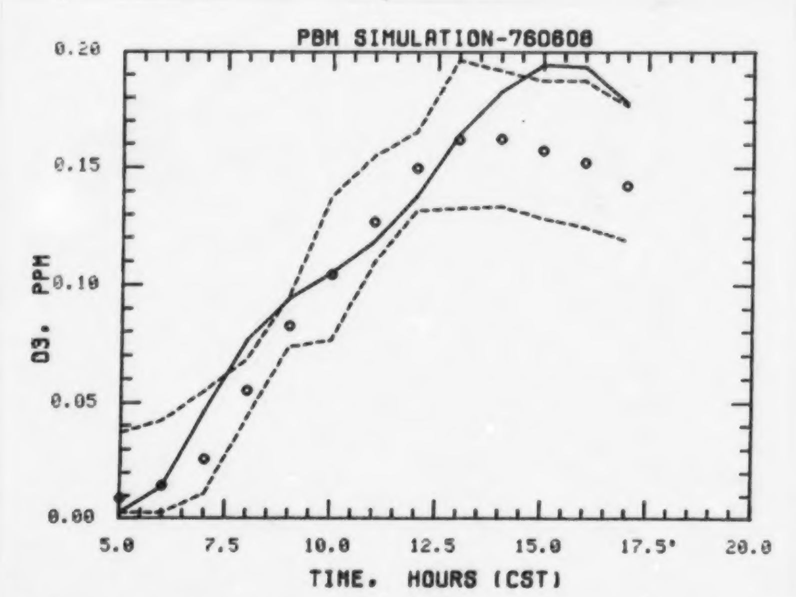

Figure A-5c. PBM simulation results for O_3 - Day 160 of 1976. Keys to figure described in A-5a.

BEGIN LAST LINE OF TEXT
BOTTOM OF IMAGE AREA. OUTSIDE DIMENSION FOR TABLES AND ILLUSTRATIONS
3/8"

PAGE NUMBER
EPA-287 (Cin.)
(4-76)

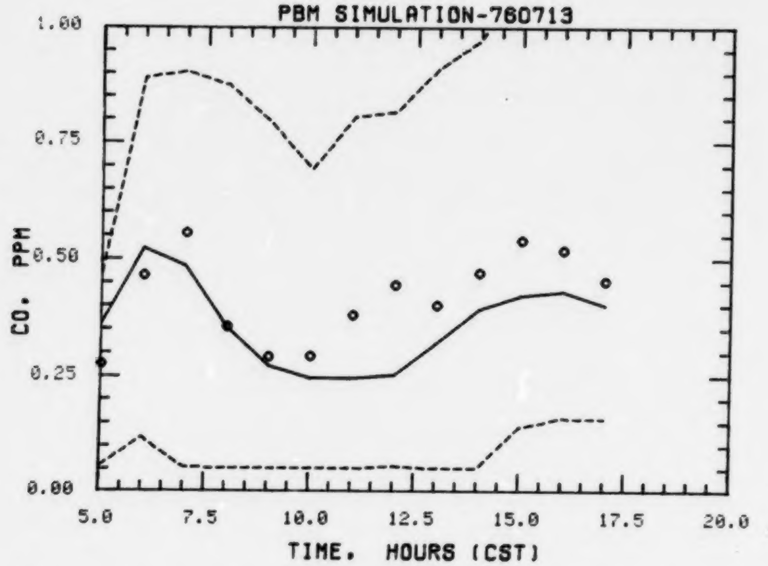

Figure A-6a. PBM simulation results for Day 195 of 1976. Time series of average observed (circles), range of observed (dashed lines), and model simulated (solid line) hour-average concentrations of CO.

BEGIN LAST LINE OF TEXT
3/8"
BOTTOM OF IMAGE AREA OUTSIDE DIMENSION FOR TABLES AND ILLUSTRATIONS
PAGE NUMBER
EPA-287 (Cin.)
(4-76)

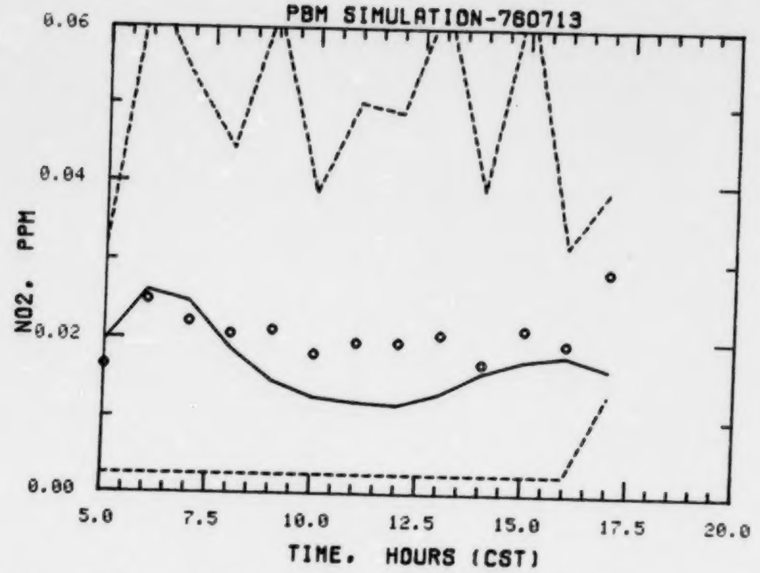

Figure A-6b. PBM simulation results for NO_2 - Day 195 of 1976. Keys to figure described in A-6a.

9 1/8"

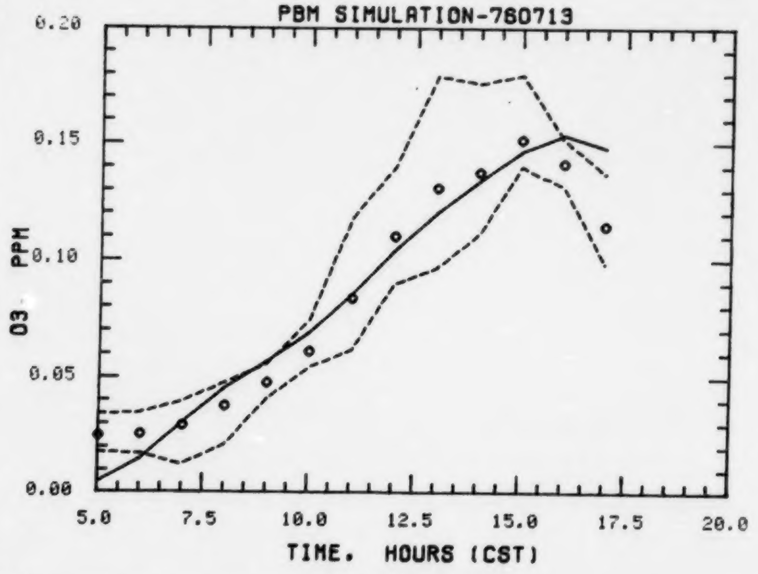

Figure A-6c. PBM simulation results for O_3 - Day 195 of 1976. Keys to figure described in A-6a.

BEGIN LAST LINE OF TEXT
BOTTOM OF IMAGE AREA OUTSIDE DIMENSION FOR TABLES AND ILLUSTRATIONS
3/8"

PAGE NUMBER
EPA-287 (Cin.)
(4-76)

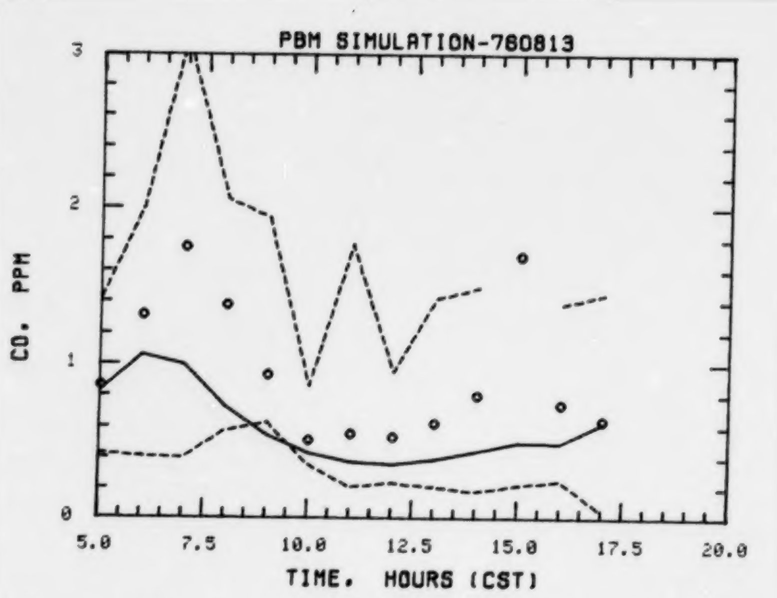

Figure A-7a. PBM simulation results for Day 226 of 1976. Time series of average observed (circles), range of observed (dashed lines), and model simulated (solid line) hour-average concentrations of CO.

BEGIN LAST LINE OF TEXT
3/8"
BOTTOM OF IMAGE AREA; OUTSIDE DIMENSION FOR TABLES AND ILLUSTRATIONS

PAGE NUMBER
EPA-287 (Cin.)
(4-76)

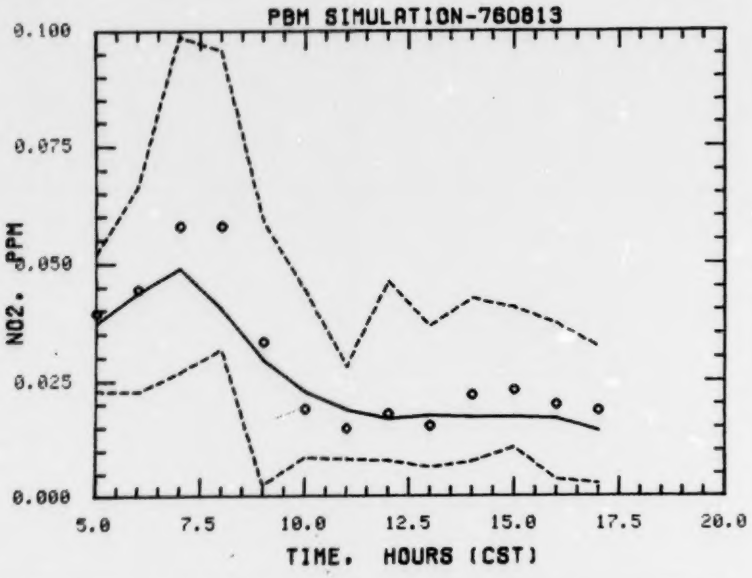

Figure A-7b. PBM simulation results for NO_2 - Day 226 of 1976. Keys to figure described in A-7a.

9-1/8"

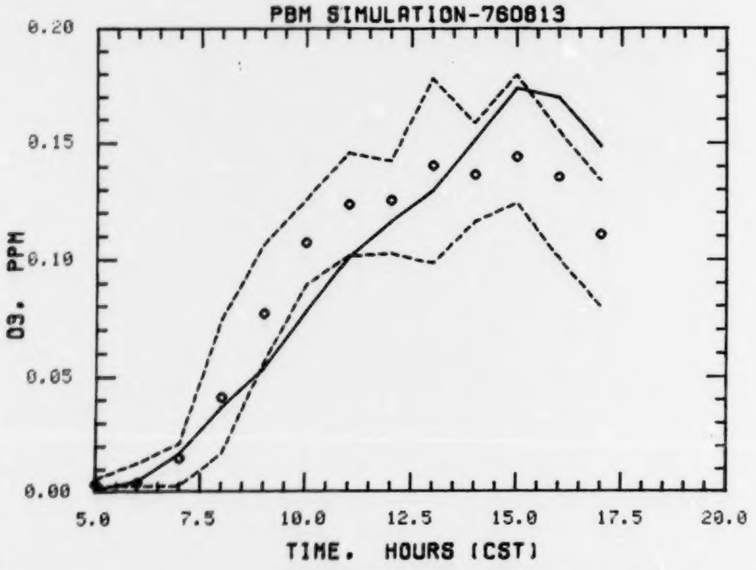

Figure A-7c. PBM simulation results for O_3 - Day 226 of 1976. Keys to figure described in A-7a.

BEGIN LAST LINE OF TEXT
BOTTOM OF IMAGE AREA; OUTSIDE DIMENSION FOR TABLES AND ILLUSTRATIONS
3/8"

PAGE NUMBER
EPA-287 (Cin.)
(4-76)

APPENDIX B

PBM - SUMMARY OF STATISTICAL RESULTS

The table presented in this appendix summarizes the statistics for the mean concentration data and the analysis of trends data obtained from PBM simulations on all of the 10 test-case days for the species NO_2, NO_x, O_3, NMHC, and CO. Note that the model internally estimates a measure of NMHC from its explicit structural classes. The table also includes summary statistics on concentration maxima data for each of the 10 test-case days for the species NO_2, O_3, and CO.

The parameters listed in the table are the same as those defined in Appendix E, except for the following:

(1) there are no separate correlation coefficients for space and time; the one correlation coefficient used here is a measure for time only, and

(2) the peak concentration data may differ only in magnitude and time of occurrence, since both peak observed and peak predicted refer to the same spatial volume.

TABLE B-1. SUMMARY OF MODEL PERFORMANCE STATISTICS FROM THE PBM[1]

Mean Concentration Data

Species	Mean observed concentration (ppm)	Mean predicted concentration (ppm)	Mean residual (ppm)	Standard deviation (ppm)	Mean residual / Mean obs. conc. (%)	Error band[2] (%)
NO_2	0.0305	0.0294	0.00106	0.00933	3.5	64.6
NO_x	0.0484	0.045	0.00302	0.0145	6.2	56.2
O_3	0.0782	0.101	-0.0225	0.0331	-28.8	43.1
NMHC	0.417	0.399	0.0184	0.175	4.4	43.8
CO	0.946	0.742	0.205	0.361	21.7	44.6

Analysis of Trends Data

Species	Correlation coefficient	Slope	Intercept (ppm)	Sum of squared error (ppm^2)
NO_2	0.901	0.796	0.00705	0.0136
NO_x	0.945	0.891	0.00798	0.0303
O_3	0.895	1.22	-0.0448	0.269
NMHC	0.856	0.724	0.128	4.84
CO	0.903	0.624	0.483	30.1

BEGIN LAST LINE OF TEXT
3/8"
BOTTOM OF IMAGE AREA; OUTSIDE DIMENSION FOR TABLES AND ILLUSTRATIONS

EPA Form 2350-4 (4-80)
(PREVIOUSLY CIN. EPA FORM 287)
U.S. GOVERNMENT PRINTING OFFICE 1980-660-1/2
TYPING GUIDE SHEET

TABLE B-1. (Continued)

SUMMARY OF MODEL PERFORMANCE STATISTICS FROM THE PBM[1]

Concentration Maxima Data

Julian date	Species	Observed Peak Concentration Value (ppm)	Observed Peak Concentration Time (CST)	Predicted Peak Concentration Value (ppm)	Predicted Peak Concentration Time (CST)	Residual (ppm)	Residual/Obs. conc. (%)
142-75	NO_2	0.0367	0600	0.0425	0700	-0.0058	-15.8
	O_3	0.137	1200	0.174	1300	-0.0370	-27.0
	CO	1.31	0700	1.18	0600	0.130	9.9
178-75	NO_2	0.0535	0700	0.0471	0600	0.0064	12.0
	O_3	0.159	1400	0.219	1400	-0.060	-37.7
	CO	1.85	0600	1.07	0600	0.780	42.2
209-75	NO_2	0.0304	0800	0.0407	0700	-0.0103	-33.9
	O_3	0.108	1000	0.122	1300	-0.0140	-13.0
	CO	0.976	0800	1.06	0600	-0.0840	-8.6
231-75	NO_2	0.0394	0800	0.0365	0700	0.0029	7.4
	O_3	0.0842	1000	0.109	1300	-0.0248	-29.5
	CO	1.04	0900	1.07	0600	-0.030	-2.9
251-75	NO_2	0.0667	0900	0.0463	0700	0.0204	30.6
	O_3	0.0841	1500	0.204	1500	-0.120	-142.7
	CO	2.85	0600	1.74	0600	1.11	38.9
159-76	NO_2	0.0938	0700	0.0814	0600	0.0124	13.2
	O_3	0.125	1300	0.212	1200	-0.0870	-69.6
	CO	2.78	0600	1.98	0500	0.800	28.8
160-76	NO_2	0.0652	0700	0.0695	0600	-0.0043	-6.6
	O_3	0.162	1400	0.194	1500	-0.0320	-19.8
	CO	1.56	0600	1.48	0500	0.080	5.1

BEGIN LAST LINE OF TEXT
BOTTOM OF IMAGE AREA; OUTSIDE DIMENSION FOR TABLES AND ILLUSTRATIONS
3/8"

EPA Form 2350-4 (4-80)
(PREVIOUSLY C.N. EPA FORM 237)
☆ U.S. GOVERNMENT PRINTING OFFICE: 1980-650-539
TYPING GUIDE SHEET

TABLE B-1. (Continued)

SUMMARY OF MODEL PERFORMANCE STATISTICS FROM THE PBM[1]

Concentration Maxima Data

Julian date	Species	Observed Peak Concentration Value (ppm)	Observed Peak Concentration Time (CST)	Predicted Peak Concentration Value (ppm)	Predicted Peak Concentration Time (CST)	Residual (ppm)	Residual / Obs. conc. (%)
195-76	NO_2	0.0287	1700	0.0260	0600	0.0027	9.4
	O_3	0.151	1500	0.153	1600	-0.0020	-1.3
	CO	0.555	0700	0.522	0600	0.033	5.9
226-76	NO_2	0.0580	0700	0.0489	0700	0.0091	15.7
	O_3	0.144	1500	0.174	1500	-0.030	-20.8
	CO	1.75	0700	1.05	0600	0.700	40.0
275-76	NO_2	0.108	1700	0.0881	1000	0.0199	18.4
	O_3	0.183	1400	0.228	1500	-0.045	-24.6
	CO	4.17	0700	3.00	0700	1.17	28.1

[1] Statistics for Mean Concentration and Analysis of Trends data are developed for all 10 test days;
Statistics for Concentration Maxima are listed for each test day.

All concentration values represent an average over the model domain.

[2] Percent of predictions within 25% of observations.

BEGIN LAST LINE OF TEXT
3/8"
BOTTOM OF IMAGE AREA; OUTSIDE DIMENSION FOR TABLES AND ILLUSTRATIONS

EPA Form 2350-4 (4-80)
(PREVIOUSLY CIN. EPA FORM 287)
☆ U.S. GOVERNMENT PRINTING OFFICE: 1980-660-619
TYPING GUIDE SHEET

APPENDIX C

LPM - TIME SERIES FOR REMAINING TEST DAYS

This appendix presents the parcel trajectories and time series plots for O_3, NO, NO_2 and CO from LPM simulations of days not discussed in the body of the report. The plots presented are from days 142, 178, and 209 of 1975 and from days 159, 160, and 195 of 1976.

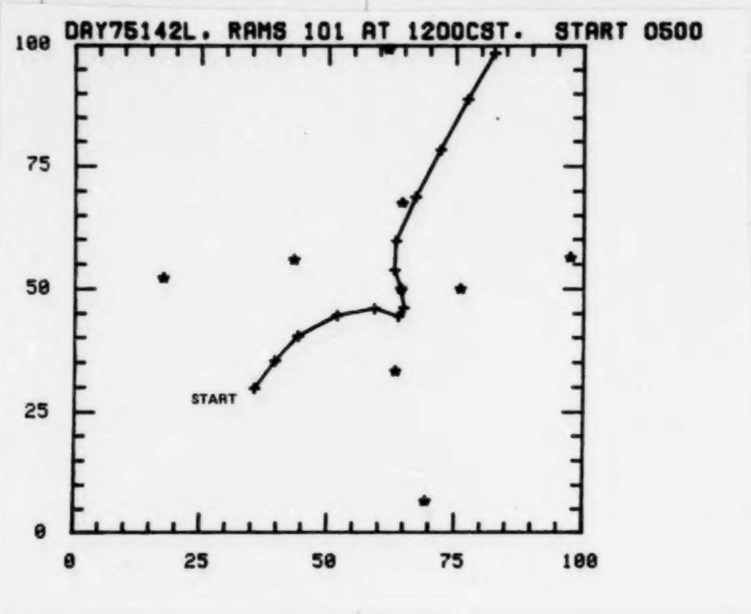

Figure C-1a. LPM parcel trajectory for Day 142 of 1975.

BEGIN LAST LINE OF TEXT
3/8"
BOTTOM OF IMAGE AREA; OUTSIDE DIMENSION FOR TABLES AND ILLUSTRATIONS

PAGE NUMBER
EPA Form 2350-4 (4-80)
(PREVIOUSLY CIN. EPA FORM 287)
U.S. GOVERNMENT PRINTING OFFICE 1980-650-620
TYPING GUIDE SHEET

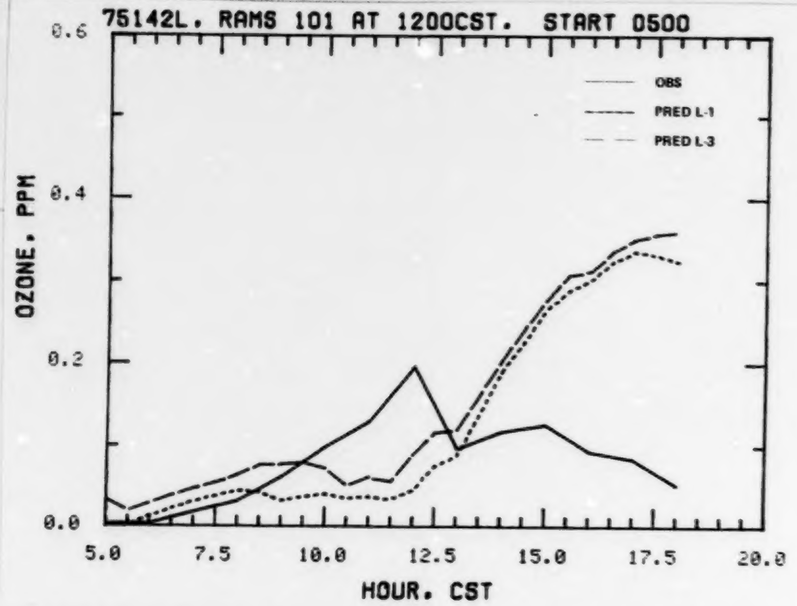

Figure C-1b. LPM time series of observed and predicted O_3 hourly concentrations on Day 142 of 1975.

9-1/8"

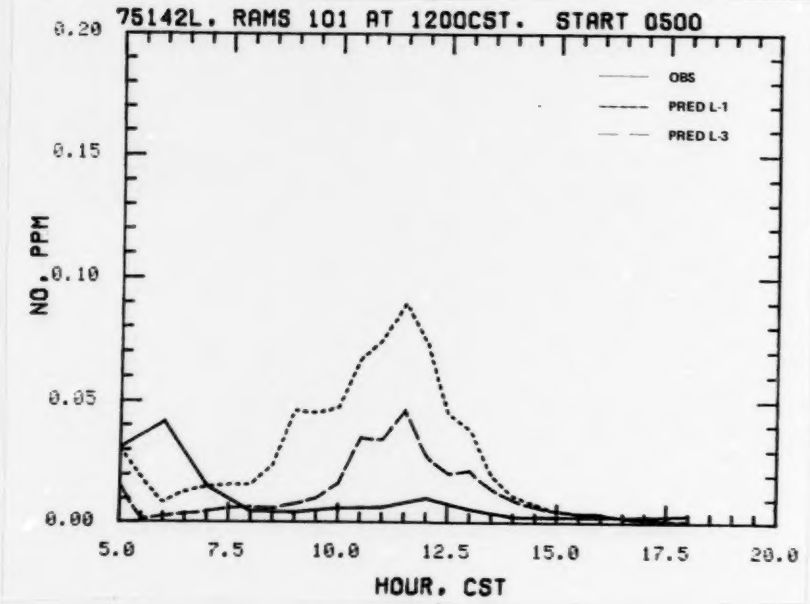

Figure C-1c. LPM time series of observed and predicted NO hourly concentrations on Day 142 of 1975.

BEGIN LAST LINE OF TEXT
BOTTOM OF IMAGE AREA; OUTSIDE DIMENSION FOR TABLES AND ILLUSTRATIONS
3/8"

PAGE NUMBER
EPA Form 2350-4 (4-80)
(PREVIOUSLY CIN. EPA FORM 287)
© U.S. GOVERNMENT PRINTING OFFICE 1980-660-639
TYPING GUIDE SHEET

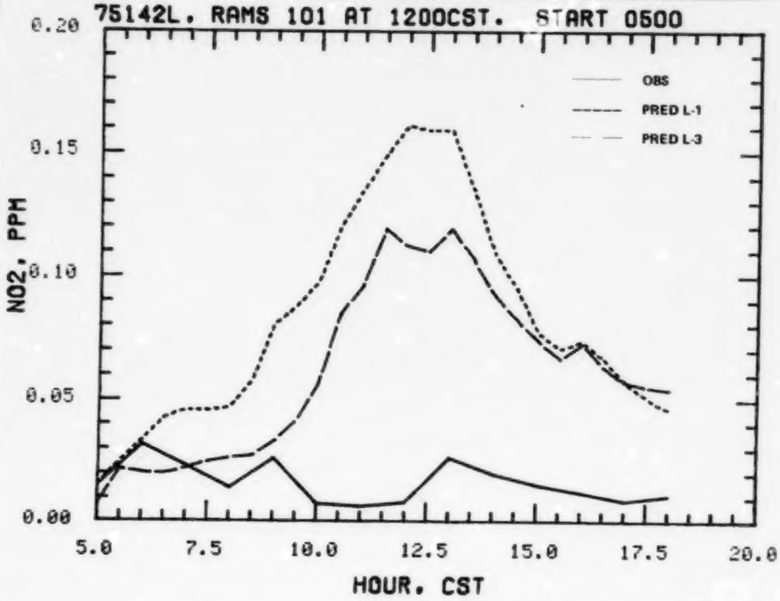

Figure C-1d. LPM time series of observed and predicted NO_2 hourly concentrations on Day 142 of 1975.

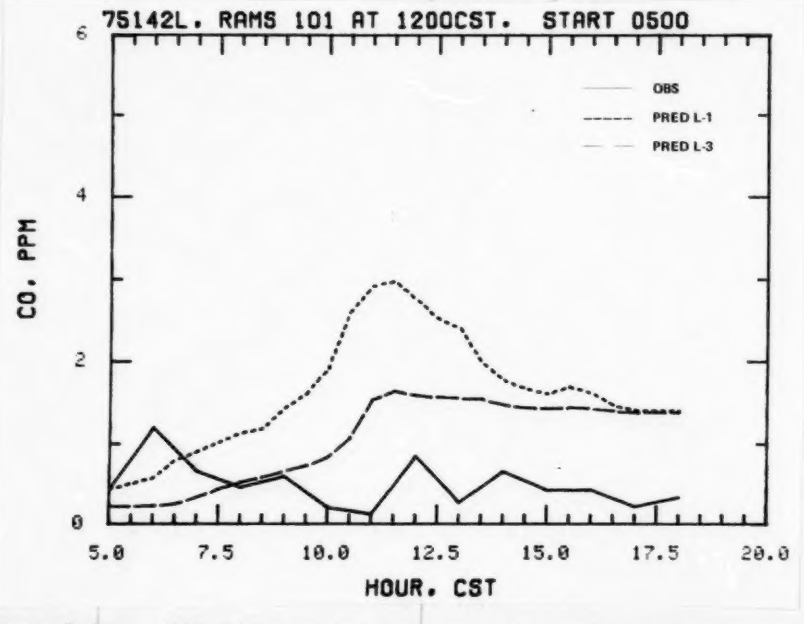

Figure C-1e. LPM time series of observed and predicted CO hourly concentrations on Day 142 of 1975.

EPA Form 2350-4 (4-80)
(PREVIOUSLY C/N EPA FORM 287)
TYPING GUIDE SHEET

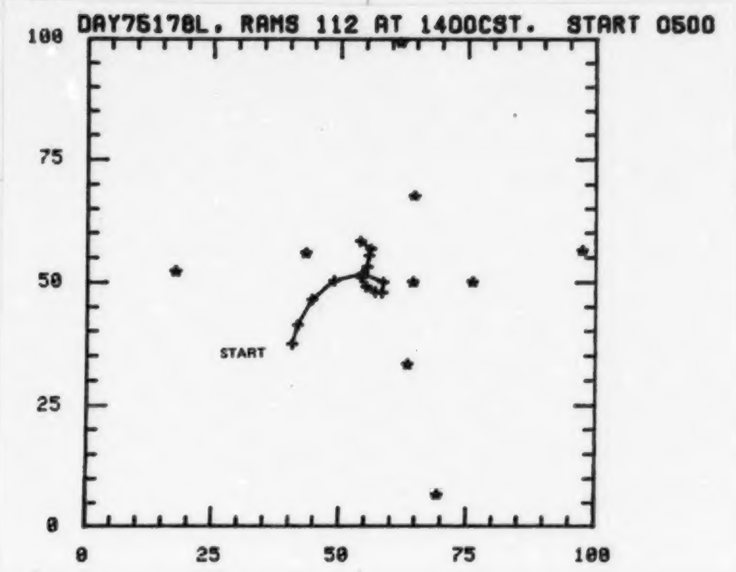

Figure C-2a. LPM parcel trajectory for Day 178 of 1975.

BEGIN LAST LINE OF TEXT
3/8"
BOTTOM OF IMAGE AREA; OUTSIDE DIMENSION FOR TABLES AND ILLUSTRATIONS

PAGE NUMBER
EPA Form 2350-4 (4-80)
(PREVIOUSLY CIN. EPA FORM 257)
☆ U.S. GOVERNMENT PRINTING OFFICE 1980-660-638
TYPING GUIDE SHEET

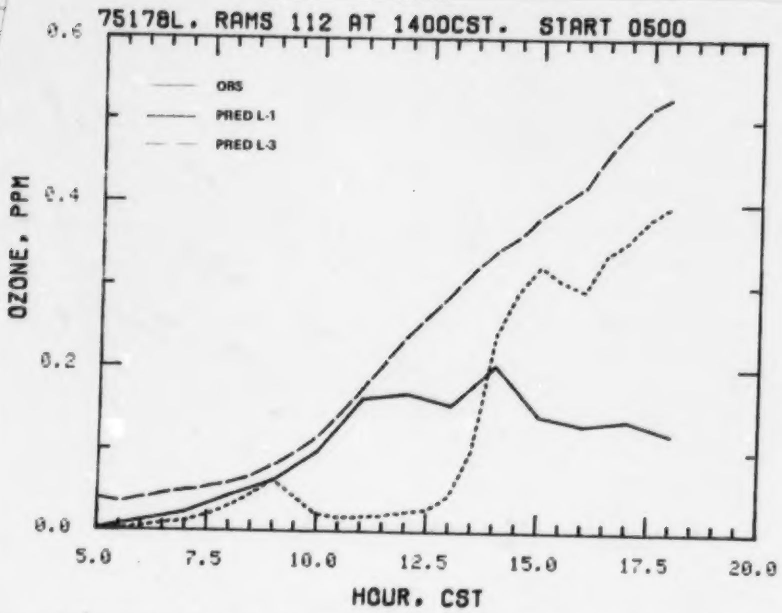

Figure C-2b. LPM time series of observed and predicted O_3 hourly concentrations on Day 178 of 1975.

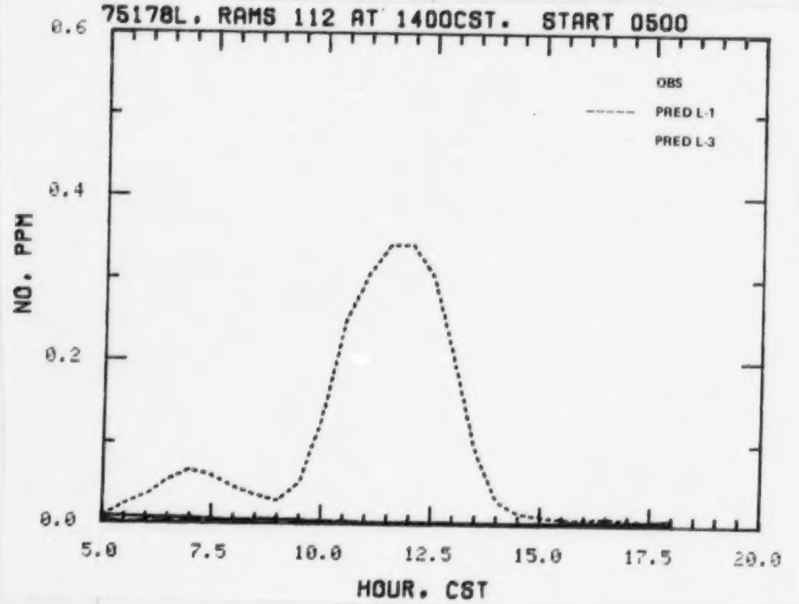

Figure C-2c. LPM time series of observed and predicted NO hourly concentrations on Day 178 of 1975.

BEGIN FIRST LINE OF TEXT HERE
CENTER OF PAGE
TOP OF IMAGE AREA
DROPPED HEAD; BEGIN SECTIONS HERE
9-1/8"
BEGIN LAST LINE OF TEXT
3/8"
BOTTOM OF IMAGE AREA OUTSIDE DIMENSION FOR TABLES AND ILLUSTRATIONS
PAGE NUMBER
EPA Form 2350-4 (4-80)
(PREVIOUSLY CIN. EPA FORM 287)
© U.S. GOVERNMENT PRINTING OFFICE 1980-
TYPING GUIDE SHEET

BEGIN FIRST LINE OF TEXT HERE
CENTER OF PAGE
TOP OF IMAGE AREA
DROPPED HEAD: BEGIN SECTIONS HERE
9 1/8"

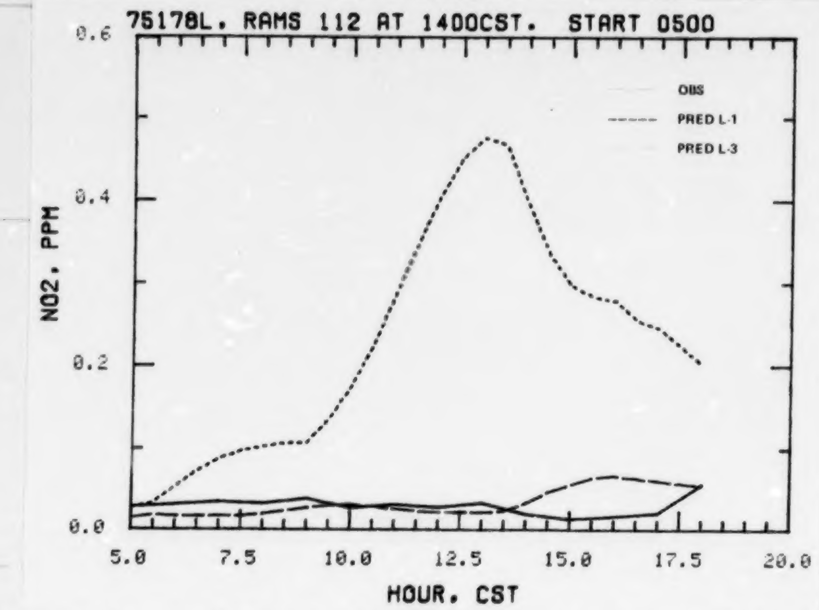

Figure C-2d. LPM time series of observed and predicted NO_2 hourly concentrations on Day 178 of 1975.

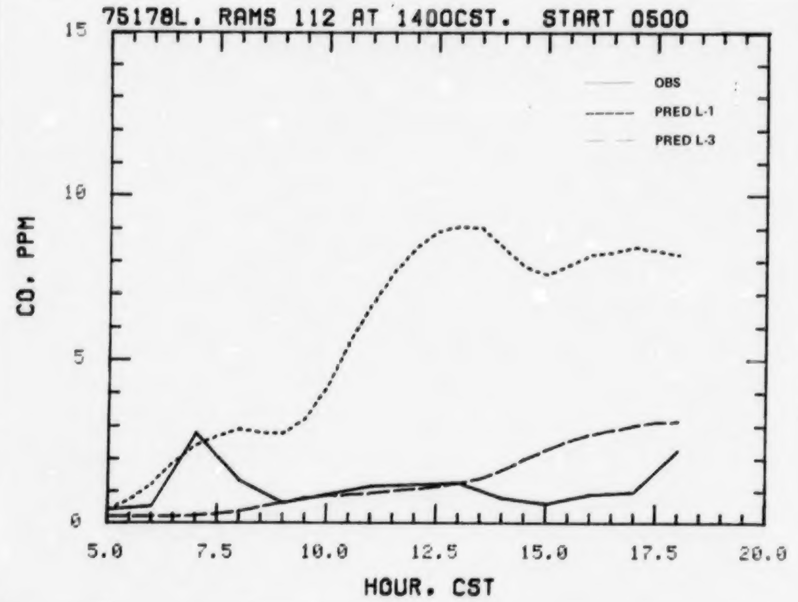

Figure C-2e. LPM time series of observed and predicted CO hourly concentrations on Day 178 of 1975.

BEGIN LAST LINE OF TEXT
BOTTOM OF IMAGE AREA OUTSIDE DIMENSION FOR TABLES AND ILLUSTRATIONS
3/8"

PAGE NUMBER
EPA Form 2350-4 (4-80)
(PREVIOUSLY CIN. EPA FORM 287)
☆ U.S. GOVERNMENT PRINTING OFFICE: 1980-680-630
TYPING GUIDE SHEET

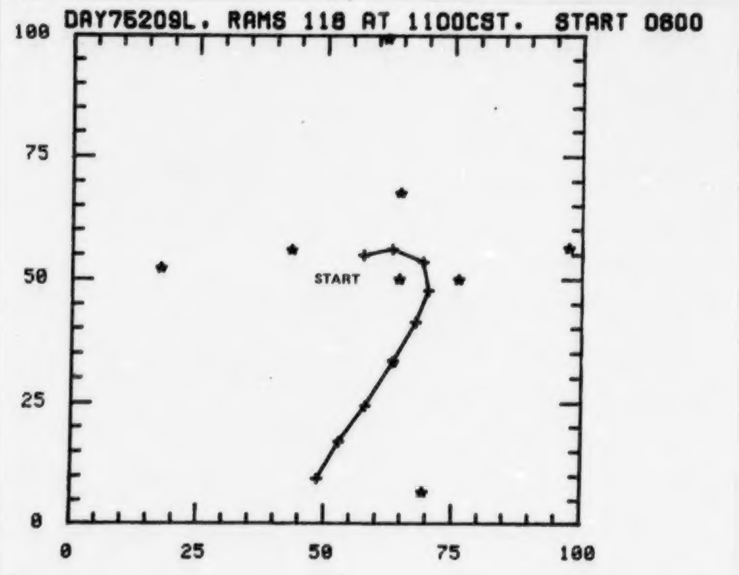

Figure C-3a. LPM parcel trajectory for Day 209 of 1975.

BEGIN LAST LINE OF TEXT
3/8"
BOTTOM OF IMAGE AREA; OUTSIDE DIMENSION FOR TABLES AND ILLUSTRATIONS

PAGE NUMBER
EPA Form 2350-4 (4-80)
(PREVIOUSLY CIN. EPA FORM 287)
☆ U.S. GOVERNMENT PRINTING OFFICE 1980-660-605
TYPING GUIDE SHEET

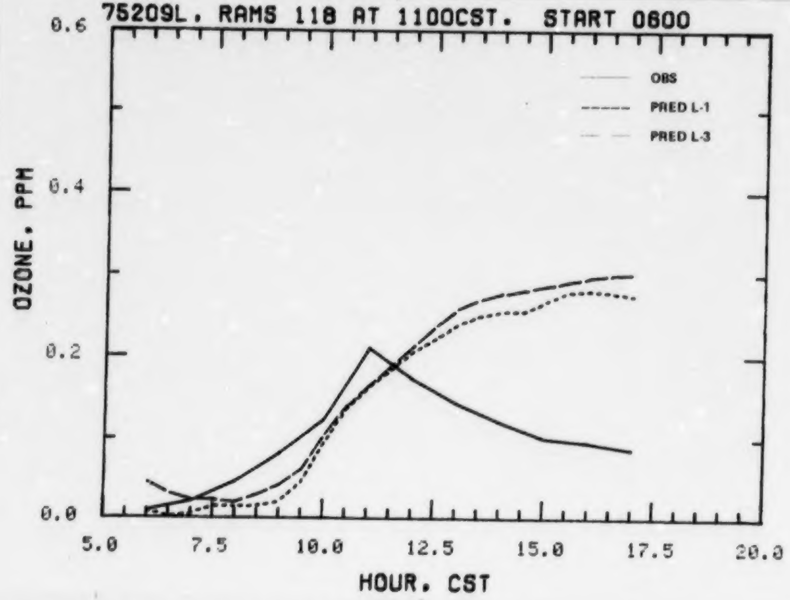

Figure C-3b. LPM time series of observed and predicted O_3 hourly concentrations on Day 209 of 1975.

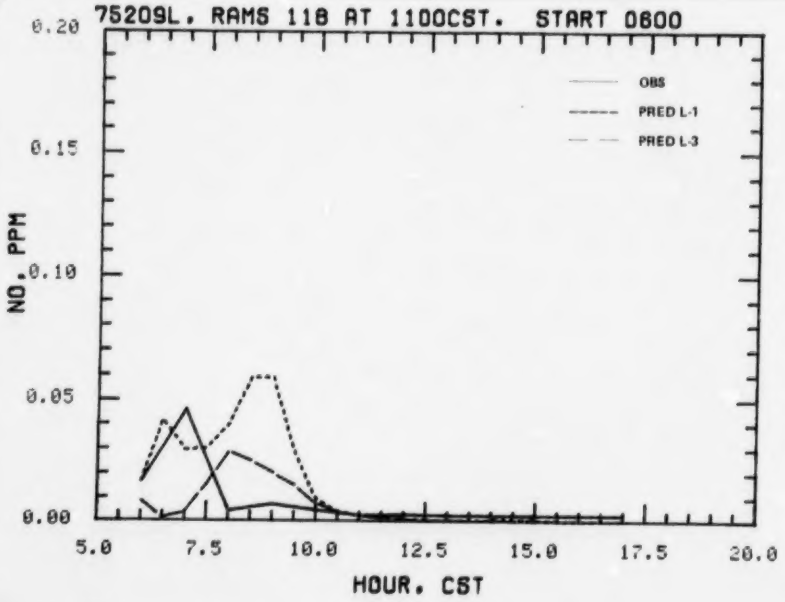

Figure C-3c. LPM time series of observed and predicted NO hourly concentrations on Day 209 of 1975.

PAGE NUMBER
EPA Form 2350-4 (4-80)
(PREVIOUSLY CIN. EPA FORM 287)
☆ U.S. GOVERNMENT PRINTING OFFICE: 1980-600-839
TYPING GUIDE SHEET

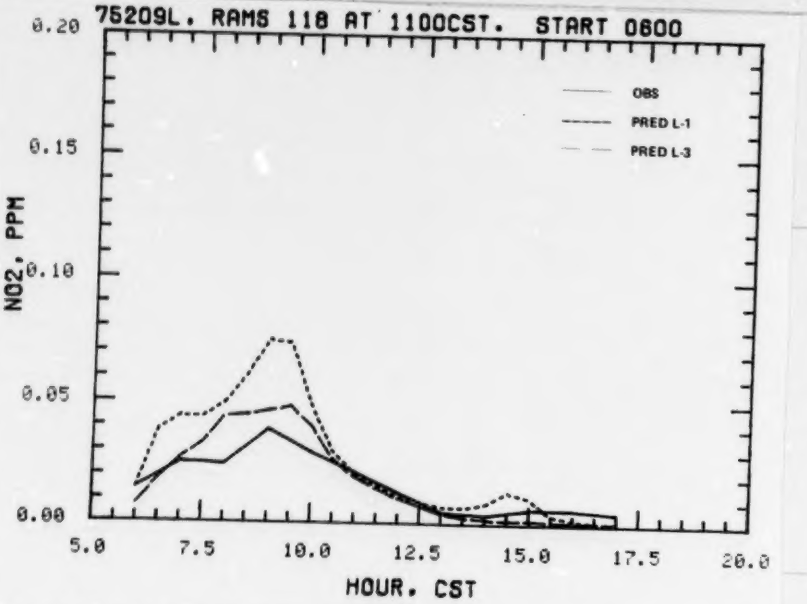

Figure C-3d. LPM time series of observed and predicted NO_2 hourly concentrations on Day 209 of 1975.

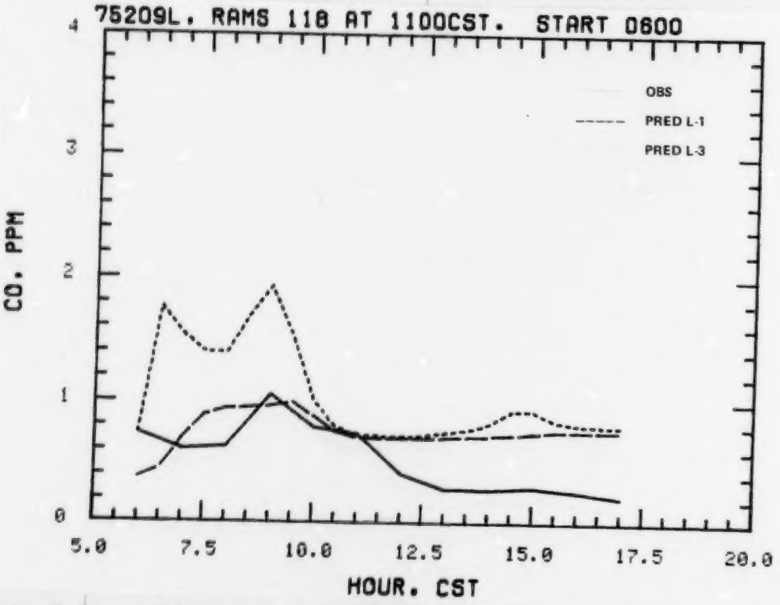

Figure C-3e. LPM time series of observed and predicted CO hourly concentrations on Day 209 of 1975.

BEGIN LAST LINE OF TEXT
3/8"
BOTTOM OF IMAGE AREA; OUTSIDE DIMENSION FOR TABLES AND ILLUSTRATIONS

PAGE NUMBER
EPA Form 2350-4 (4-80)
(PREVIOUSLY CIN. EPA FORM 287)
U.S. GOVERNMENT PRINTING OFFICE 1980-660-639
TYPING GUIDE SHEET

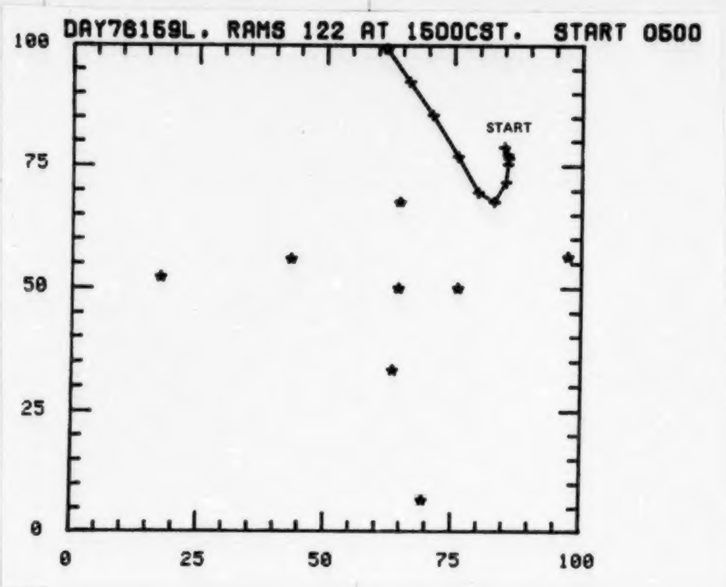

Figure C-4a. LPM parcel trajectory for Day 159 of 1976.

EPA Form 2350-4 (4-80)
(PREVIOUSLY CIN. EPA FORM 287)
TYPING GUIDE SHEET

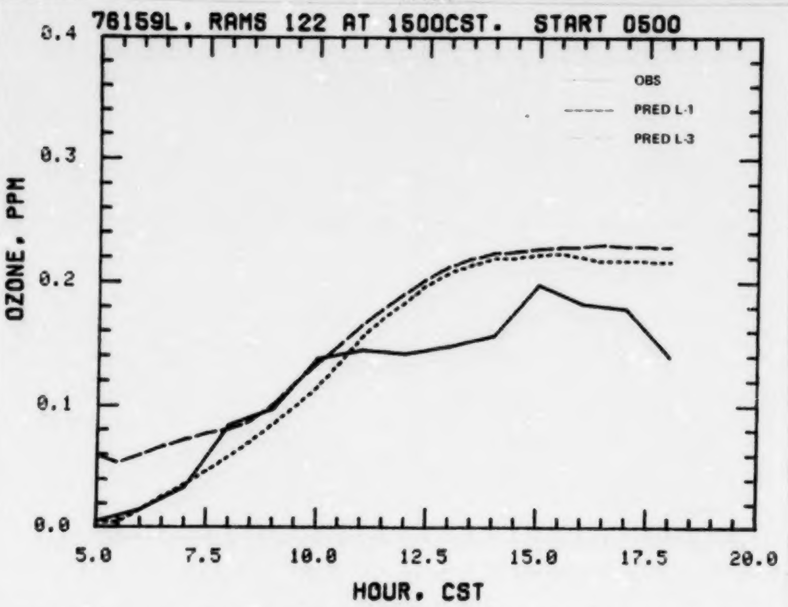

Figure C-4b. LPM time series of observed and predicted O_3 hourly concentrations for Day 159 of 1976.

9-1/8"

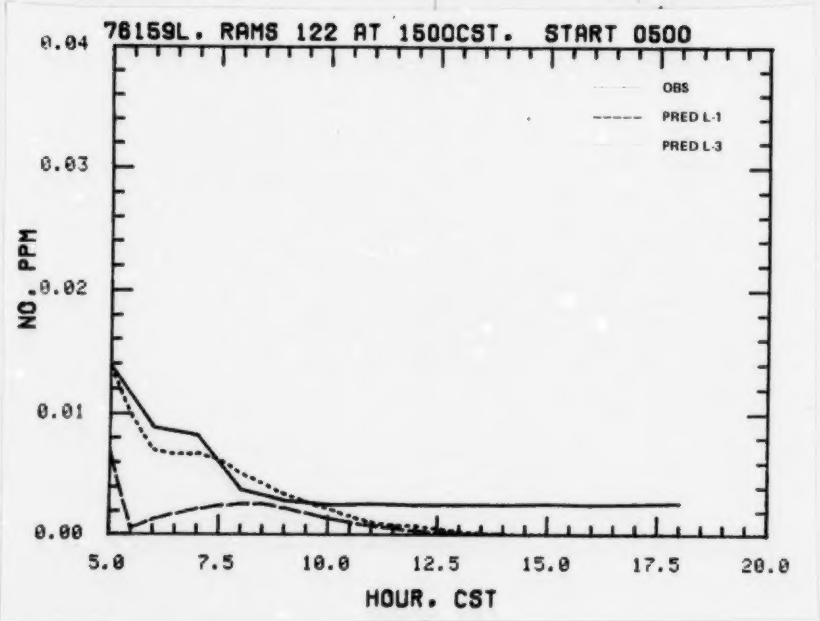

Figure C-4c. LPM time series of observed and predicted NO hourly concentrations on Day 159 of 1976.

BEGIN LAST LINE OF TEXT
BOTTOM OF IMAGE AREA; OUTSIDE DIMENSION FOR TABLES AND ILLUSTRATIONS
3/8"

PAGE NUMBER
EPA Form 2350-4 (4-80)
(PREVIOUSLY CIN. EPA FORM 287)
U.S. GOVERNMENT PRINTING OFFICE 1980-660-638
TYPING GUIDE SHEET

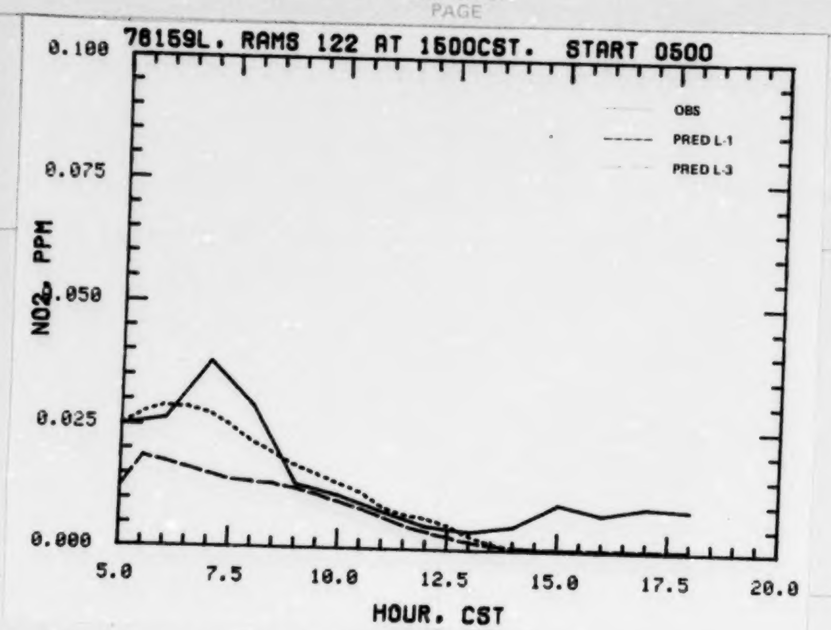

Figure C-4d. LPM time series of observed and predicted NO_2 hourly concentrations on Day 159 of 1976.

9-1/8"

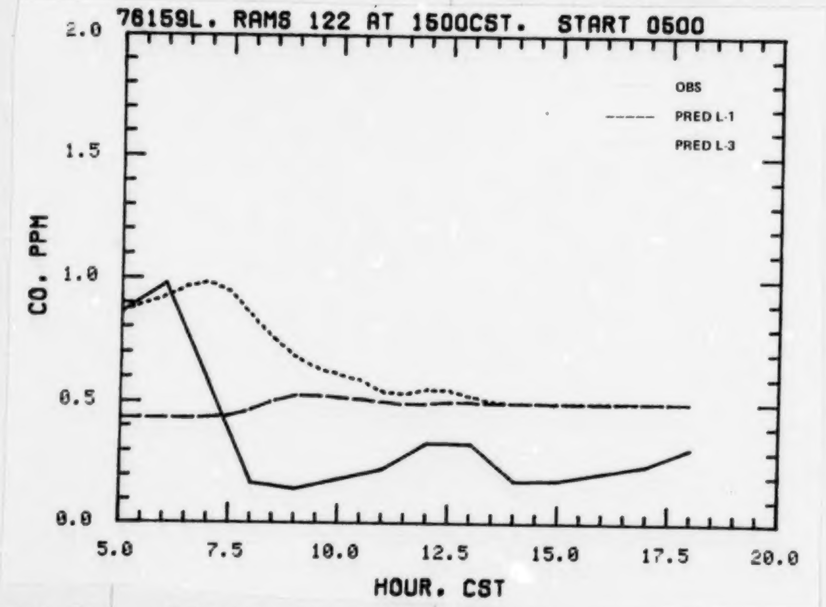

Figure C-4e. LPM time series of observed and predicted CO hourly concentrations on Day 159 of 1976.

BEGIN LAST LINE OF TEXT

3/8"

BOTTOM OF IMAGE AREA; OUTSIDE DIMENSION FOR TABLES AND ILLUSTRATIONS

PAGE NUMBER

EPA Form 2350-4 (4-80)
(PREVIOUSLY CIN. EPA FORM 2F7)

© U.S. GOVERNMENT PRINTING OFFICE 1980 660-639

TYPING GUIDE SHEET

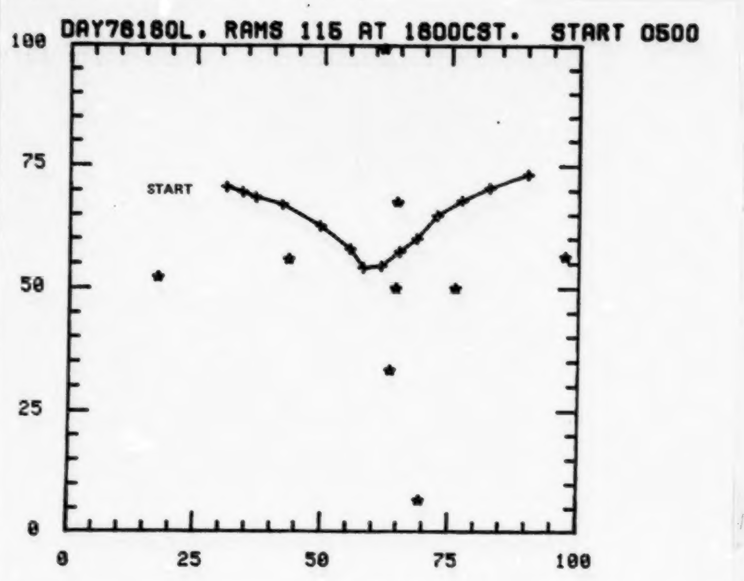

Figure C-5a. LPM parcel trajectory for Day 160 of 1976.

BEGIN LAST LINE OF TEXT
3/8"
BOTTOM OF IMAGE AREA; OUTSIDE DIMENSION FOR TABLES AND ILLUSTRATIONS

PAGE NUMBER
EPA Form 2350-4 (4-80)
(PREVIOUSLY CIN. EPA FORM 287)
☆ U.S. GOVERNMENT PRINTING OFFICE 1980-660-639
TYPING GUIDE SHEET

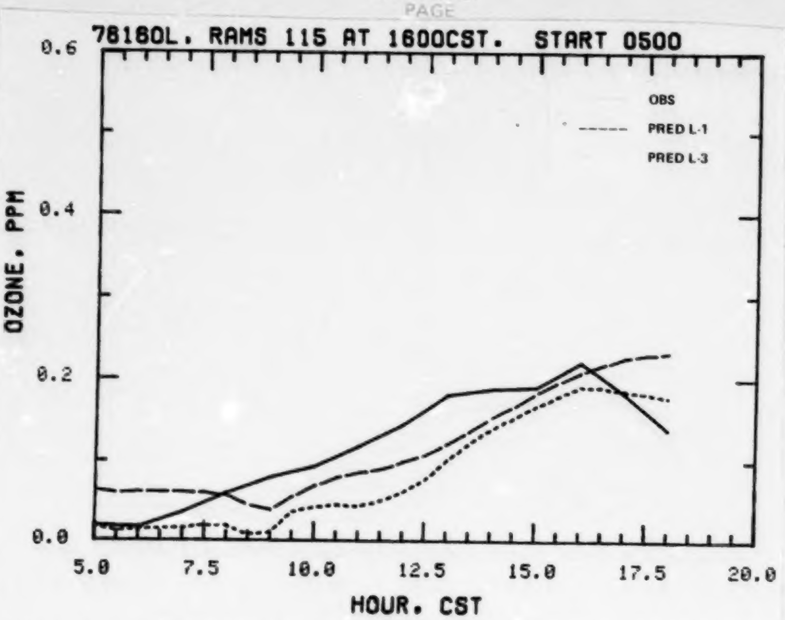

Figure C-5b. LPM time series of observed and predicted O_3 hourly concentrations on Day 160 of 1976.

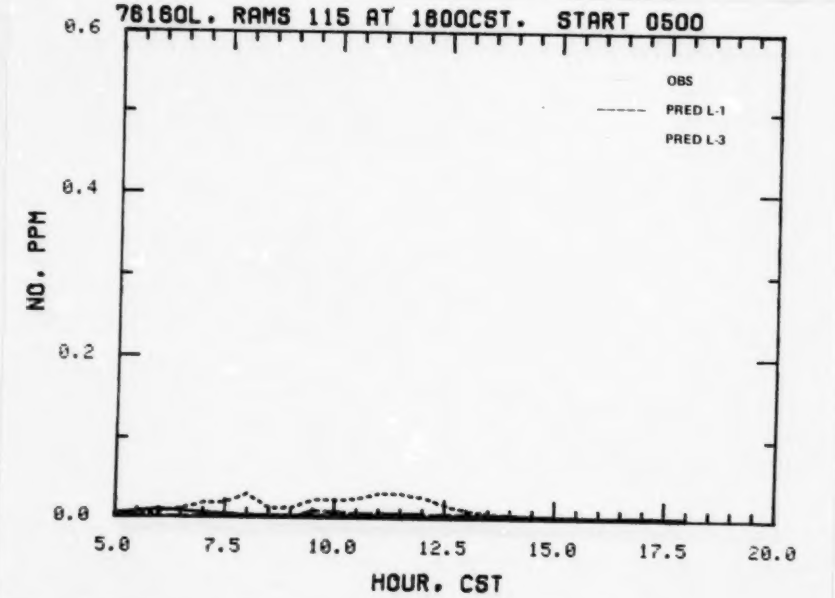

Figure C-5c. LPM time series of observed and predicted NO hourly concentrations on Day 160 of 1976.

BEGIN FIRST LINE OF TEXT HERE
CENTER OF PAGE
TOP OF IMAGE AREA
DROPPED HEAD; BEGIN SECTIONS HERE
9-1/8"
BEGIN LAST LINE OF TEXT
3/8"
BOTTOM OF IMAGE AREA; OUTSIDE DIMENSION FOR TABLES AND ILLUSTRATIONS
PAGE NUMBER
EPA Form 2350-4 (4-80)
(PREVIOUSLY CIN. EPA FORM 237)
☆ U.S. GOVERNMENT PRINTING OFFICE 1980-680-630
TYPING GUIDE SHEET

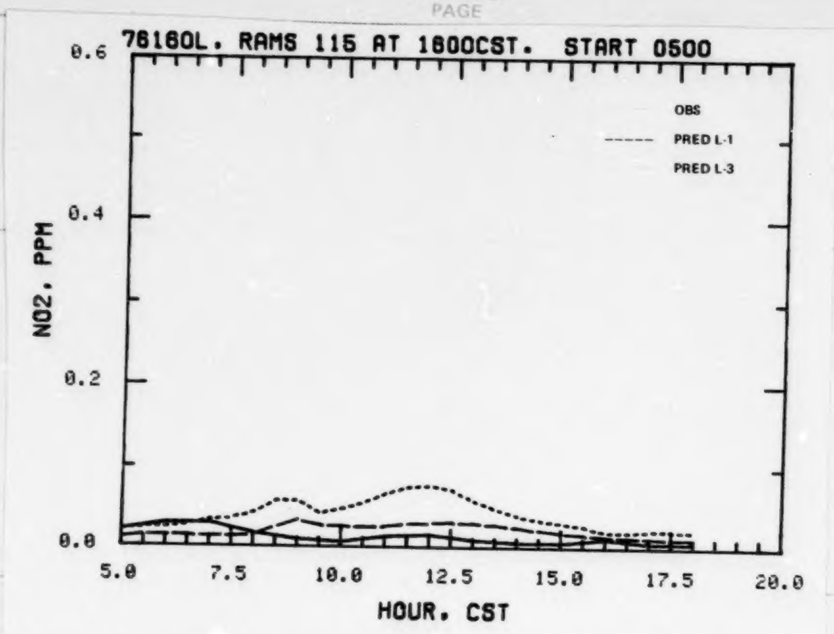

Figure C-5d. LPM time series of observed and predicted NO_2 hourly concentrations on Day 160 of 1976.

9-1/8"

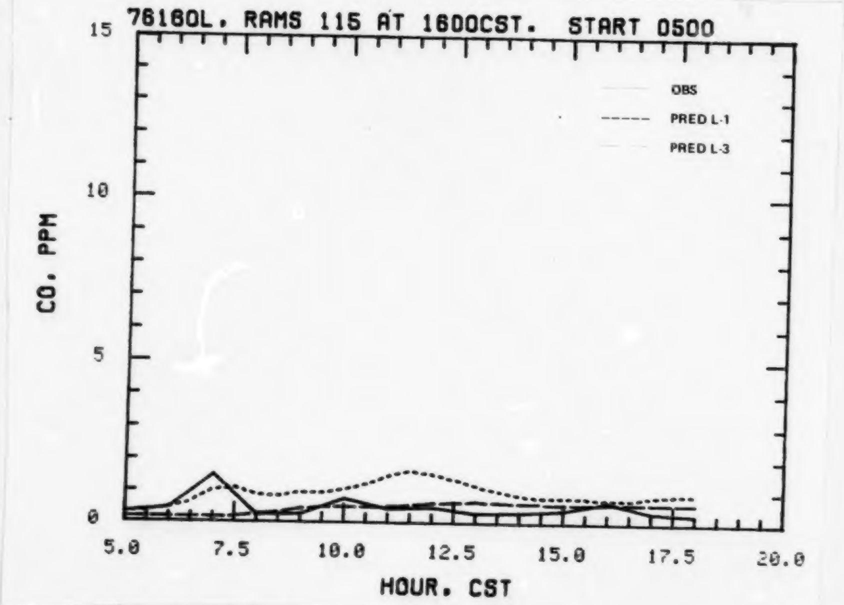

Figure C-5e. LPM time series of observed and predicted CO hourly concentrations on Day 160 of 1976.

BEGIN LAST LINE OF TEXT
BOTTOM OF IMAGE AREA, OUTSIDE DIMENSION FOR TABLES AND ILLUSTRATIONS
3/8"

PAGE NUMBER
EPA Form 2350-4 (4-80)
(PREVIOUSLY CIN. EPA FORM 287)
☆ U.S. GOVERNMENT PRINTING OFFICE 1980-660-839
TYPING GUIDE SHEET

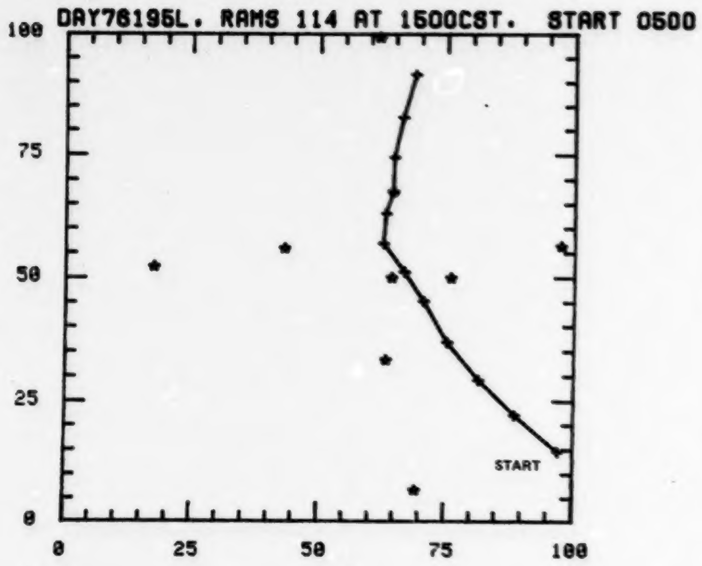

Figure C-6a. LPM parcel trajectory for Day 195 of 1976.

BEGIN LAST LINE OF TEXT
3/8"
BOTTOM OF IMAGE AREA; OUTSIDE DIMENSION FOR TABLES AND ILLUSTRATIONS

PAGE NUMBER
EPA Form 2350-4 (4-80)
(PREVIOUSLY CIN. EPA FORM 287)
☆ U.S. GOVERNMENT PRINTING OFFICE 1980-660-030
TYPING GUIDE SHEET

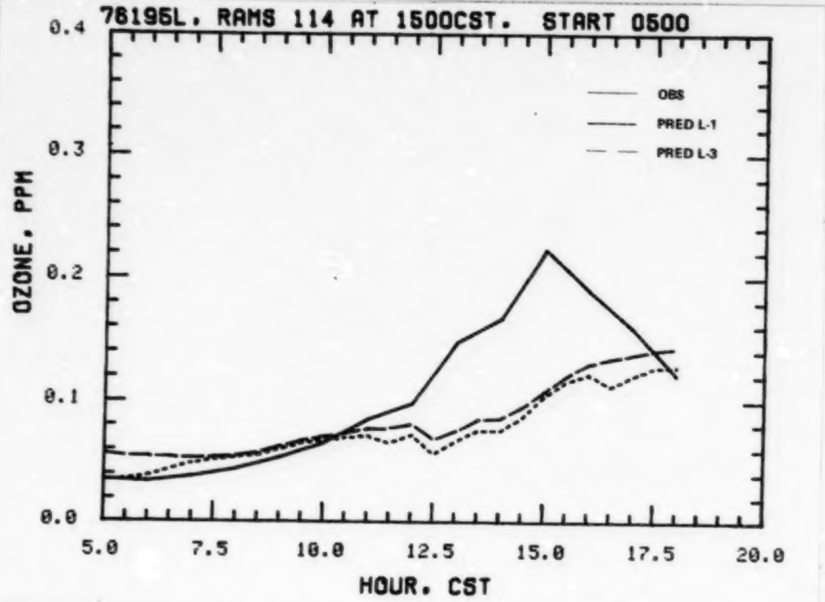

Figure C-6b. LPM time series of observed and predicted O_3 hourly concentrations on Day 195 of 1976.

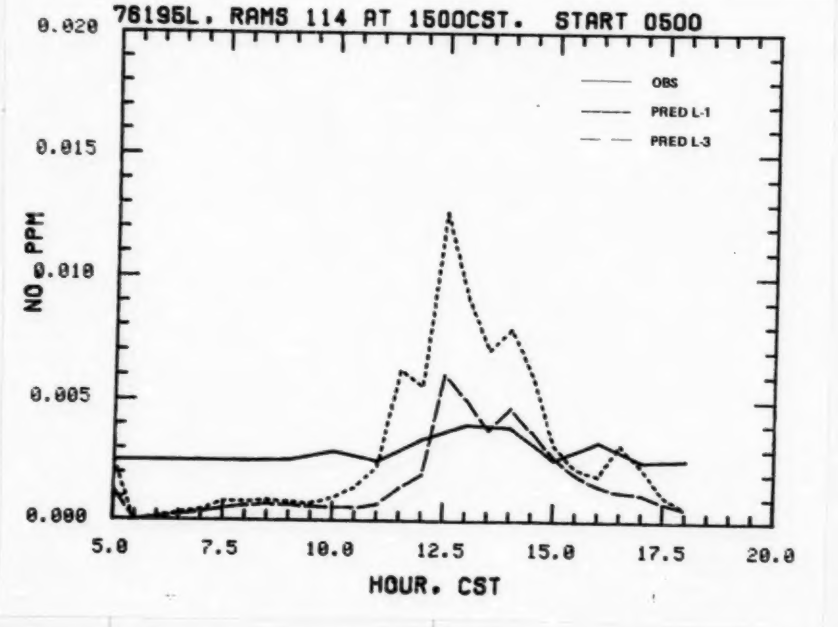

Figure C-6c. LPM time series of observed and predicted NO hourly concentrations on Day 195 of 1976.

BEGIN FIRST LINE OF TEXT HERE
CENTER OF PAGE
TOP OF IMAGE AREA
DROPPED HEAD: BEGIN SECTIONS HERE
9-1/8"
BEGIN LAST LINE OF TEXT
3/8"
BOTTOM OF IMAGE AREA, OUTSIDE DIMENSION FOR TABLES AND ILLUSTRATIONS
PAGE NUMBER
EPA Form 2350-4 (4-80)
(PREVIOUSLY CIN. EPA FORM 287)
© U.S. GOVERNMENT PRINTING OFFICE 1980-660-639
TYPING GUIDE SHEET

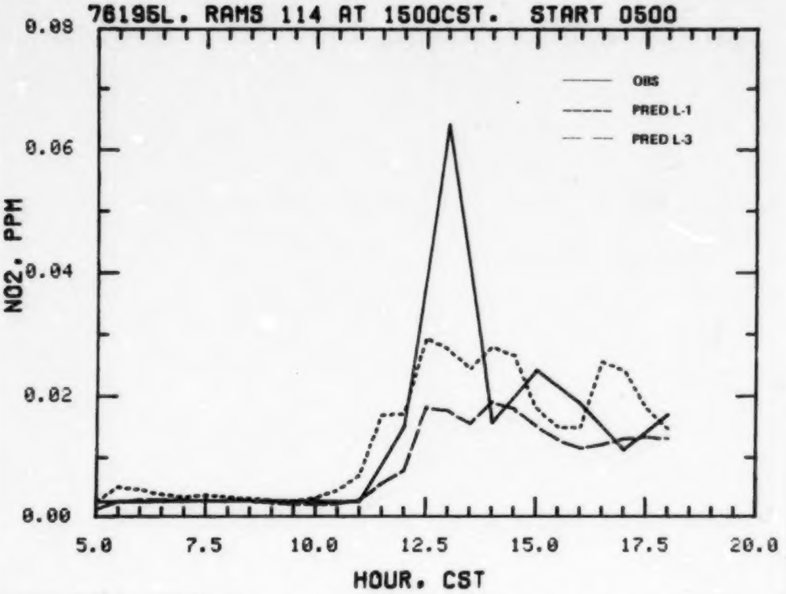

Figure C-6d. LPM time series of observed and predicted NO_2 hourly concentrations on Day 195 of 1976.

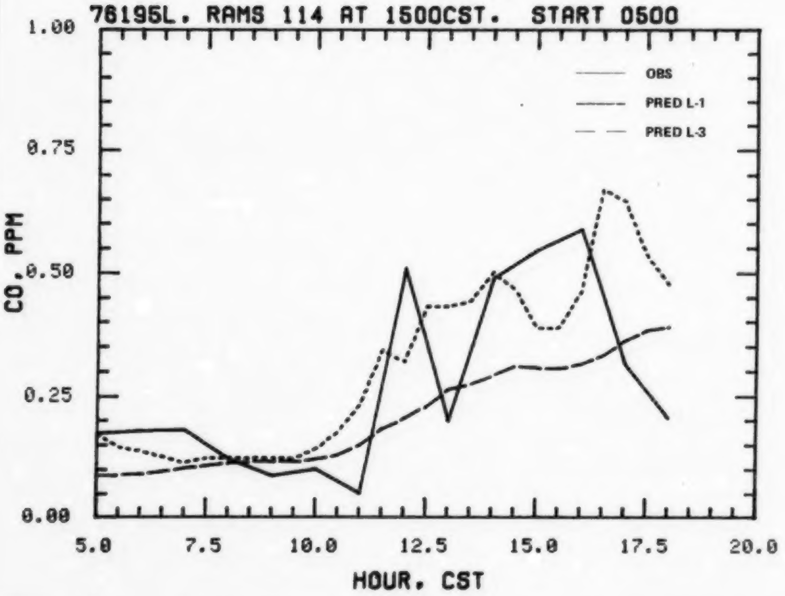

Figure C-6e. LPM time series of observed and predicted CO hourly concentrations on Day 195 of 1976.

BEGIN FIRST LINE OF TEXT HERE
CENTER OF PAGE
TOP OF IMAGE AREA
DROPPED HEAD: BEGIN SECTIONS HERE
9-1/8"
BEGIN LAST LINE OF TEXT
3/8"
BOTTOM OF IMAGE AREA; OUTSIDE DIMENSION FOR TABLES AND ILLUSTRATIONS
PAGE NUMBER
EPA Form 2350-4 (4-80)
(PREVIOUSLY CIN. EPA FORM 287)
U.S. GOVERNMENT PRINTING OFFICE 1980-660-809
TYPING GUIDE SHEET

APPENDIX D

UAM - RS AND RO PLOTS FOR REMAINING TEST DAYS

This appendix contains the residual histograms (RS) and residual vs. observed plots (RO) for the species NO_2, O_3, and CO from the UAM statistical analysis that were not specifically discussed within the body of this report. The plots presented here are from test days 178-75, 209-75, 231-75, 251-75, 159-76, 160-76, and 226-76 of the RAPS data base.

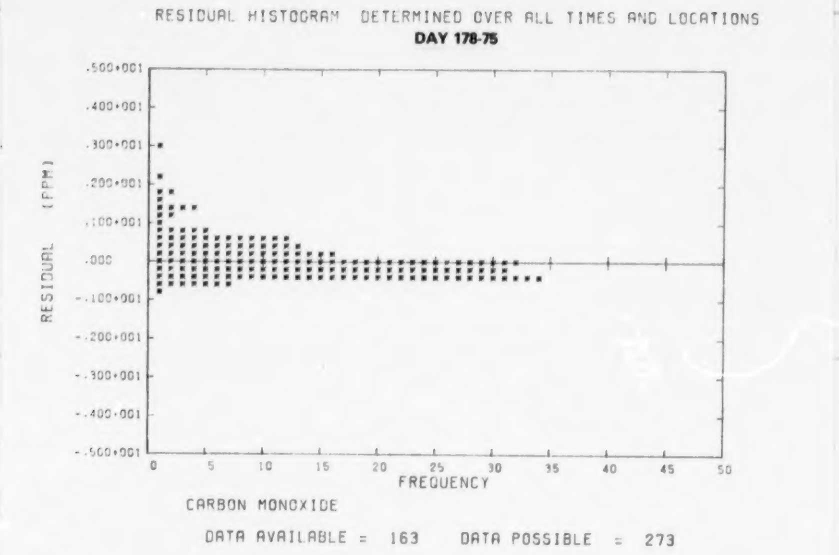

Figure D-1a. Residual histogram for CO from the UAM simulation results for Day 178-75.

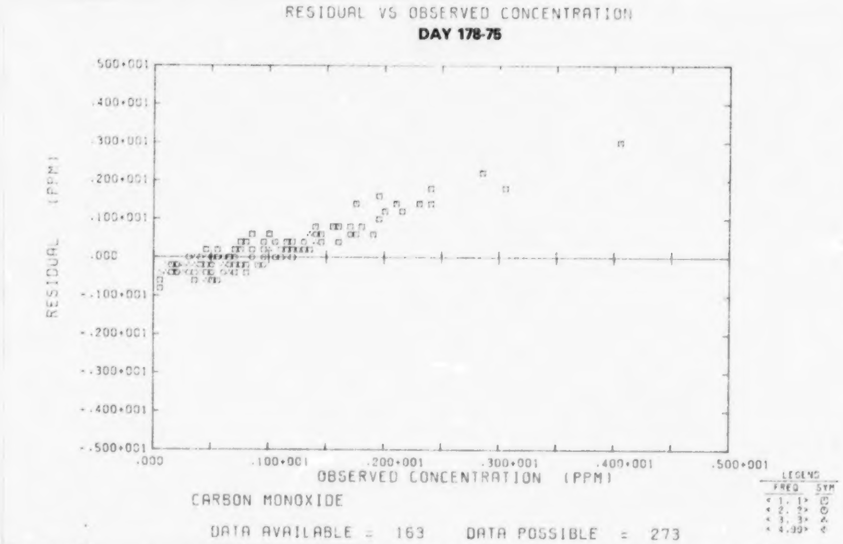

Figure D-1b. Residual vs. observed plot for CO from the UAM simulation results for Day 178-75.

BEGIN LAST LINE OF TEXT
BOTTOM OF IMAGE AREA, OUTSIDE DIMENSION FOR TABLES AND ILLUSTRATIONS
3/8"

PAGE NUMBER
EPA-287 (Cin.)
(4-76)

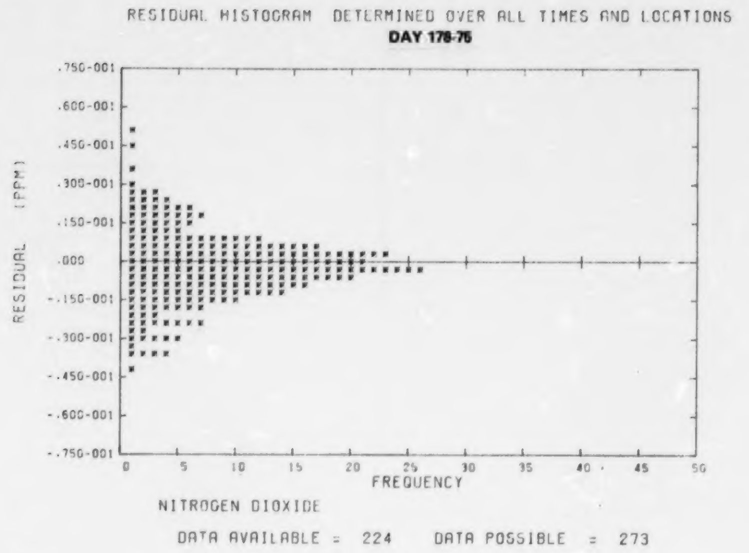

Figure D-2a. Residual histogram for NO_2 from the UAM simulation results for Day 178-75.

9-1/8"

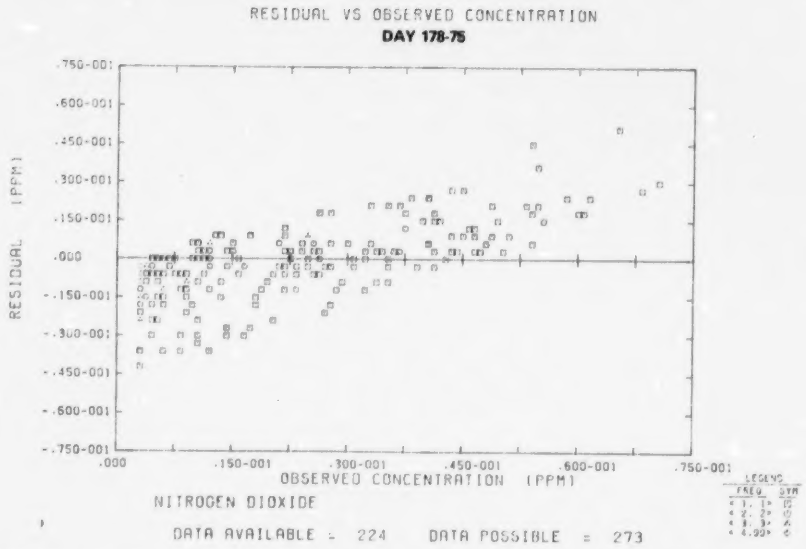

Figure D-2b. Residual vs. observed plot for NO_2 from the UAM simulation results for Day 178-75.

BEGIN LAST LINE OF TEXT
BOTTOM OF IMAGE AREA; OUTSIDE DIMENSION FOR TABLES AND ILLUSTRATIONS
3/8"

PAGE NUMBER
EPA-287 (Cin.)
(4-76)

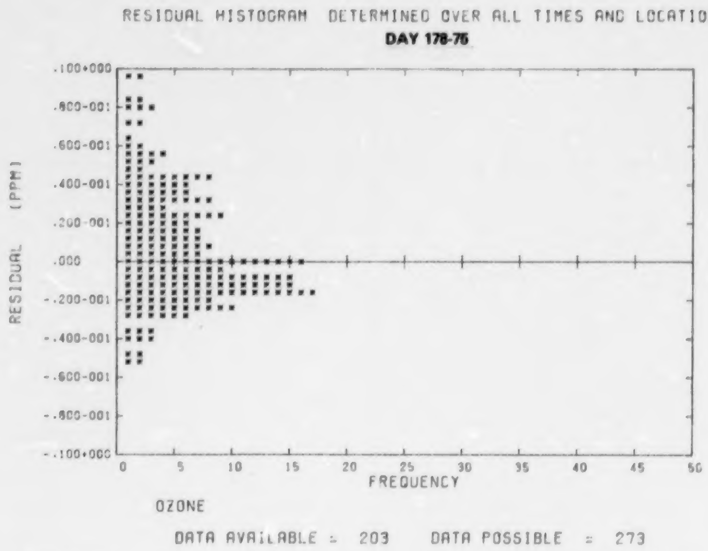

Figure D-3a. Residual histogram for O_3 from the UAM simulation results for Day 178-75.

9-1/8"

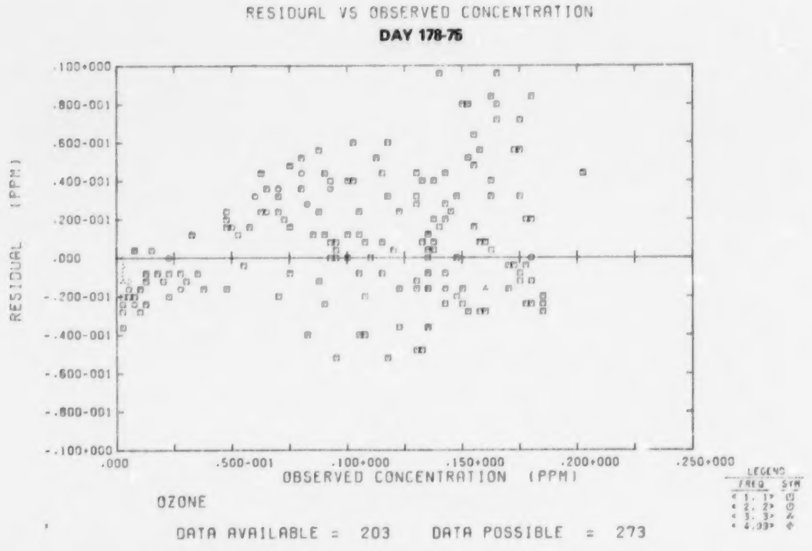

Figure D-3b. Residual vs. observed plot for O_3 from the UAM simulation results for Day 178-75.

BEGIN LAST LINE OF TEXT
BOTTOM OF IMAGE AREA; OUTSIDE DIMENSION FOR TABLES AND ILLUSTRATIONS
3/8"
PAGE NUMBER
EPA-287 (Cin.)
(4-76)

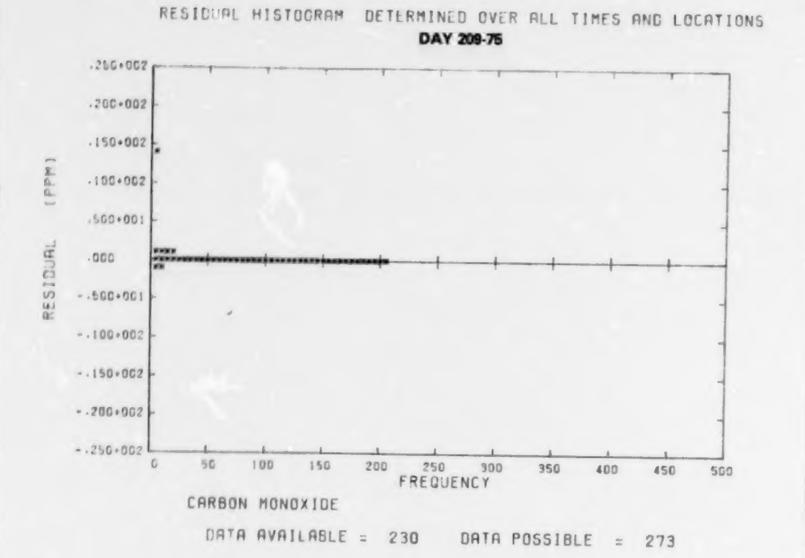

Figure D-4a. Residual histogram for CO from the UAM simulation results for Day 209-75.

9-1/8"

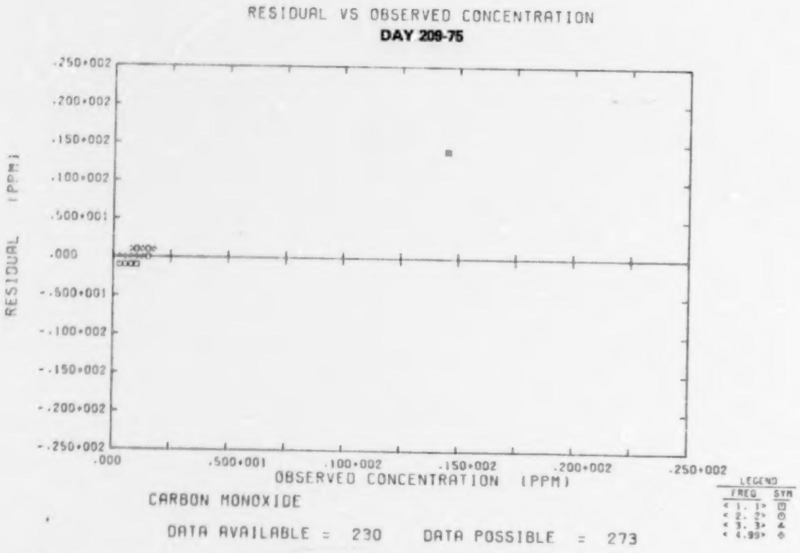

Figure D-4b. Residual vs. observed plot for CO from the UAM simulation results for Day 209-75.

BEGIN LAST LINE OF TEXT
BOTTOM OF IMAGE AREA; OUTSIDE DIMENSION FOR TABLES AND ILLUSTRATIONS
3/8"

PAGE NUMBER
EPA-287 (Cin.)
(4-76)

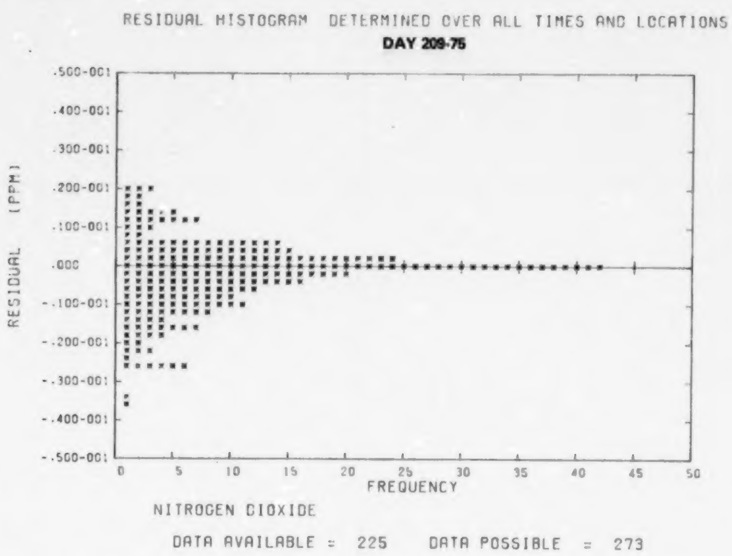

Figure D-5a. Residual histogram for NO_2 from the UAM simulation results for Day 209-75.

9-1/8"

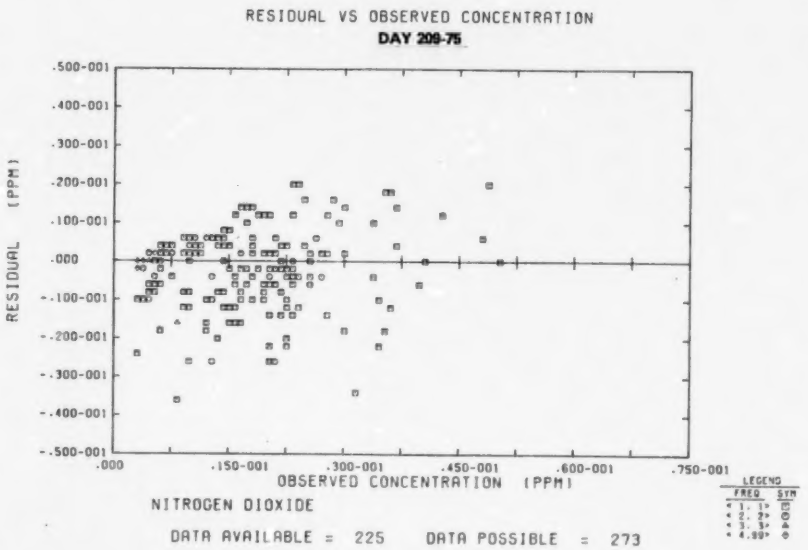

Figure D-5b. Residual vs. observed plot for NO_2 from the UAM simulation results for Day 209-75.

BEGIN LAST LINE OF TEXT
BOTTOM OF IMAGE AREA; OUTSIDE DIMENSION FOR TABLES AND ILLUSTRATIONS
3/8"

EPA-287 (Cin.)
(4-76)

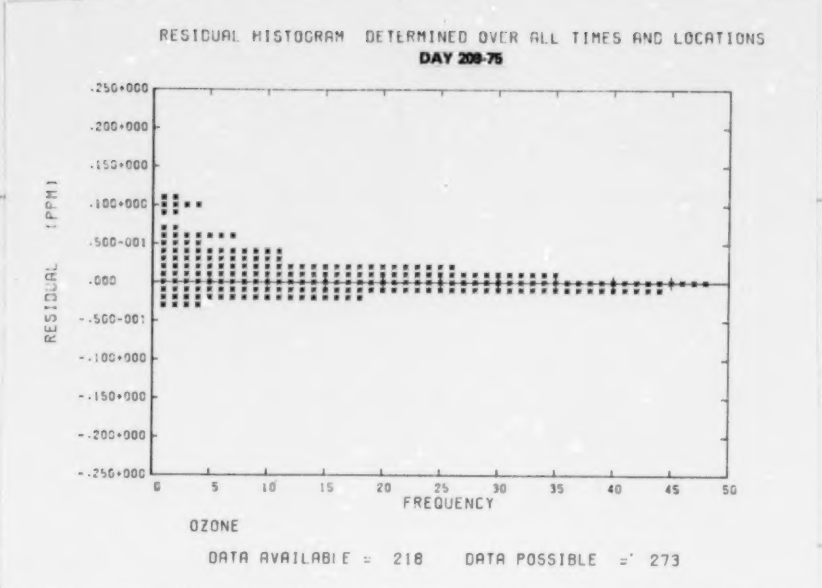

Figure D-6a. Residual histogram for O_3 from the UAM simulation results for Day 209-75.

9-1/8"

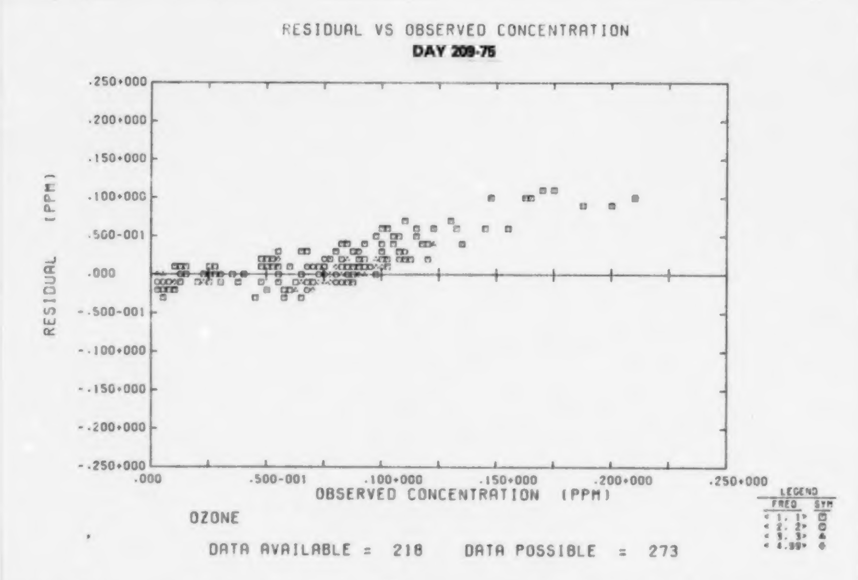

Figure D-6b. Residual vs. observed plot for O_3 from the UAM simulation results for Day 209-75.

BEGIN LAST LINE OF TEXT
BOTTOM OF IMAGE AREA: OUTSIDE DIMENSION FOR TABLES AND ILLUSTRATIONS
3/8"

PAGE NUMBER
EPA-287 (Cin.)
(4-76)

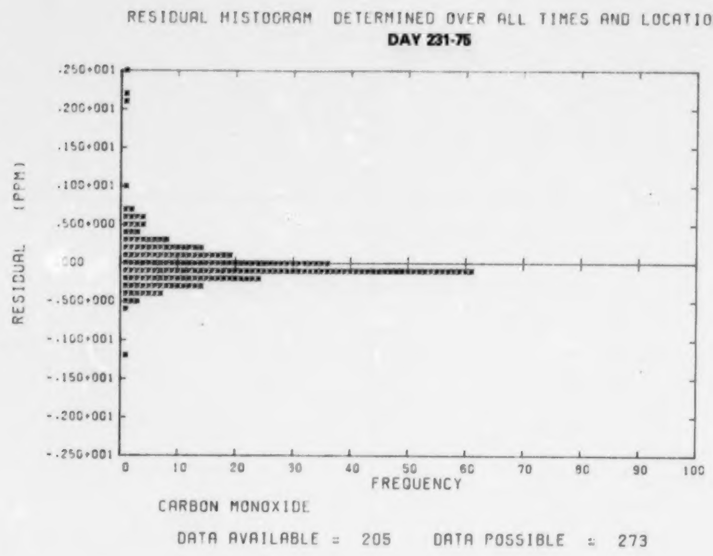

Figure D-7a. Residual histogram for CO from the UAM simulation results for Day 231-75.

9-1/8"

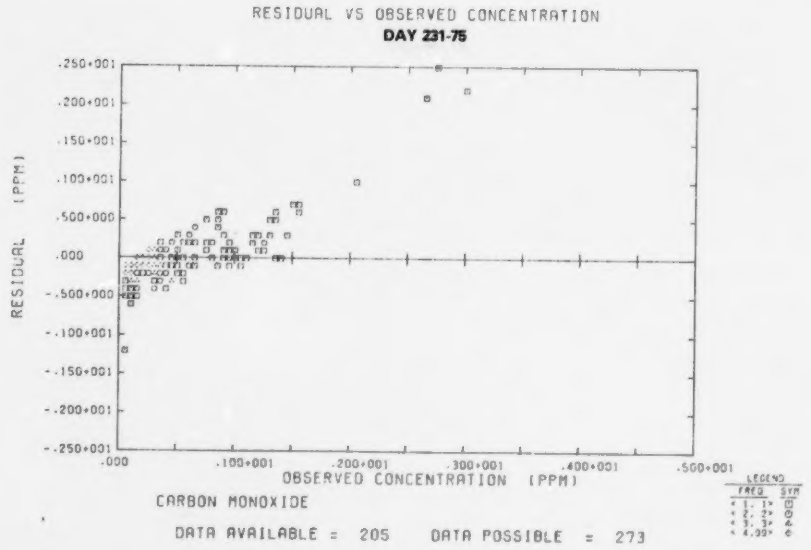

Figure D-7b. Residual vs. observed plot for CO from the UAM simulation results for Day 231-75.

BEGIN LAST LINE OF TEXT
BOTTOM OF IMAGE AREA; OUTSIDE DIMENSION FOR TABLES AND ILLUSTRATIONS
3/8"

PAGE NUMBER
EPA-287 (Cin.)
(4-76)

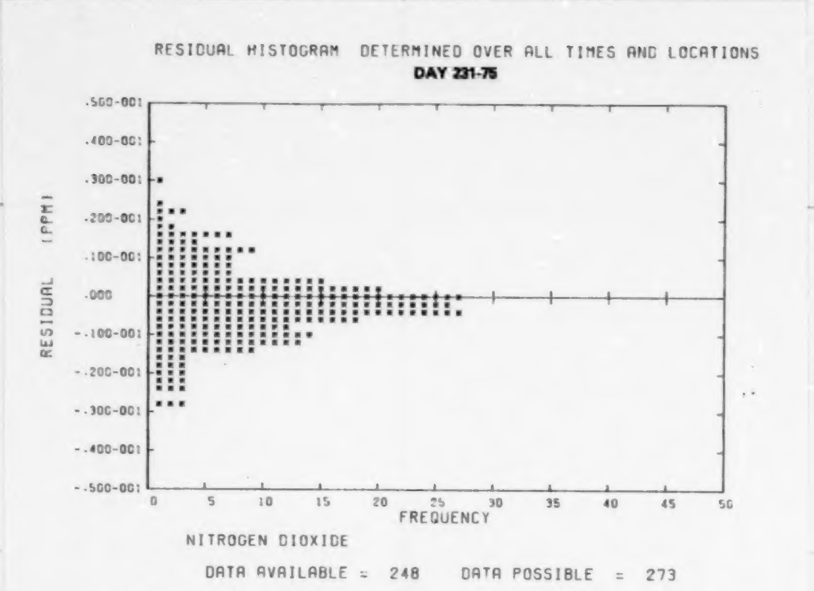

Figure D-8a. Residual histogram for NO_2 from the UAM simulation results for Day 231-75.

9-1/8"

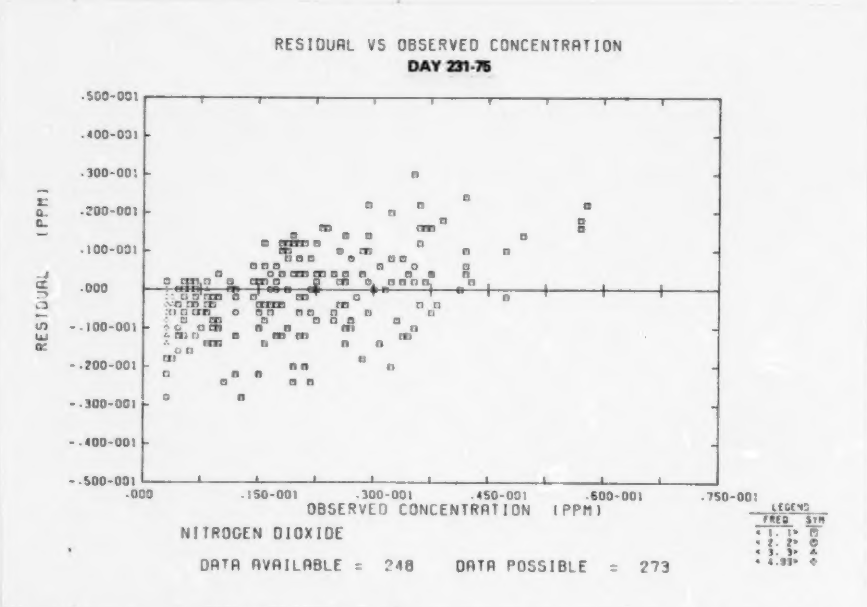

Figure D-8b. Residual vs. observed plot for NO_2 from the UAM simulation results for Day 231-75.

BEGIN LAST LINE OF TEXT
BOTTOM OF IMAGE AREA; OUTSIDE DIMENSION FOR TABLES AND ILLUSTRATIONS
3/8"

PAGE NUMBER
EPA-287 (Cin.)
(4-76)

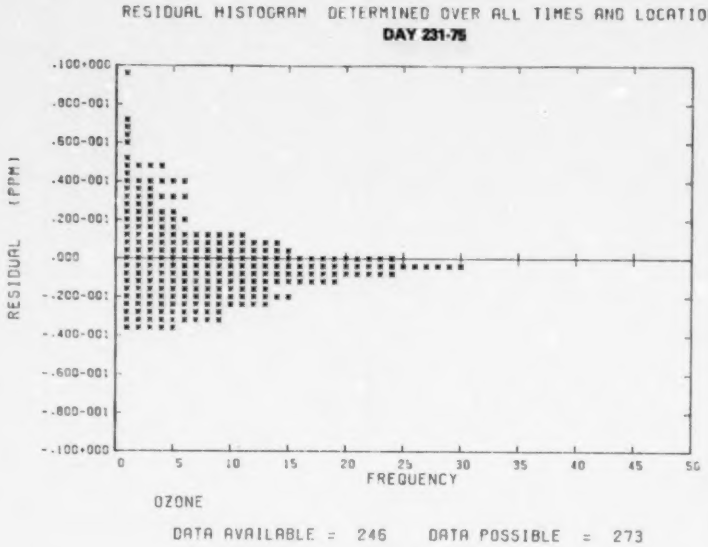

Figure D-9a. Residual histogram for O_3 from the UAM simulation results for Day 231-75.

9-1/8"

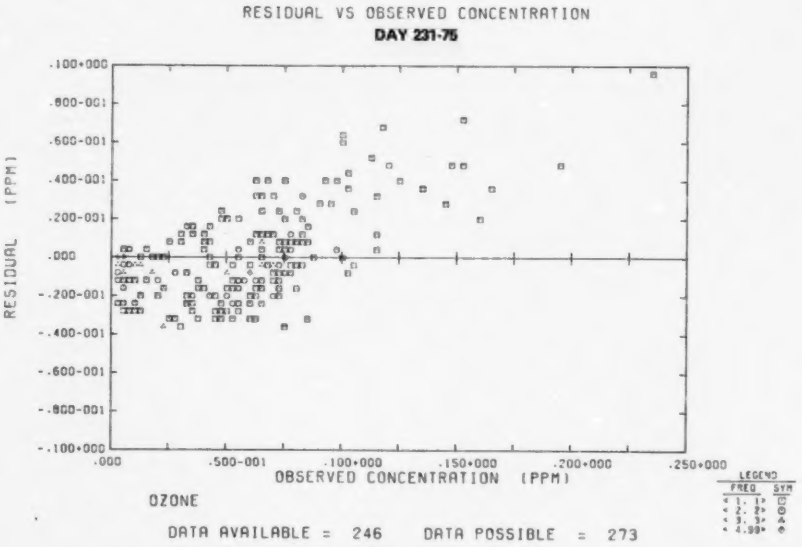

Figure D-9b. Residual vs. observed plot for O_3 from the UAM simulation results for Day 231-75.

BOTTOM OF IMAGE AREA; OUTSIDE DIMENSION FOR TABLES AND ILLUSTRATIONS
BEGIN LAST LINE OF TEXT
3/8"

PAGE NUMBER
EPA-287 (Cin.)
(4-76)

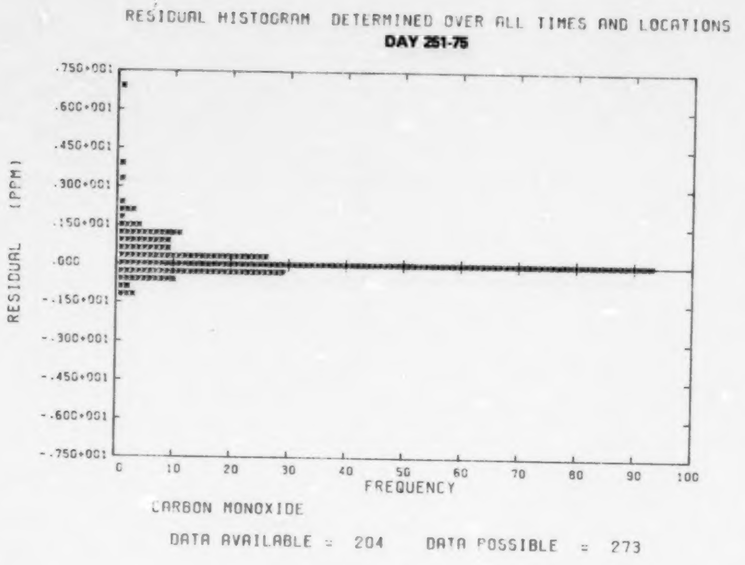

Figure D-10a. Residual histogram for CO from the UAM simulation results for Day 251-75.

9-1/8"

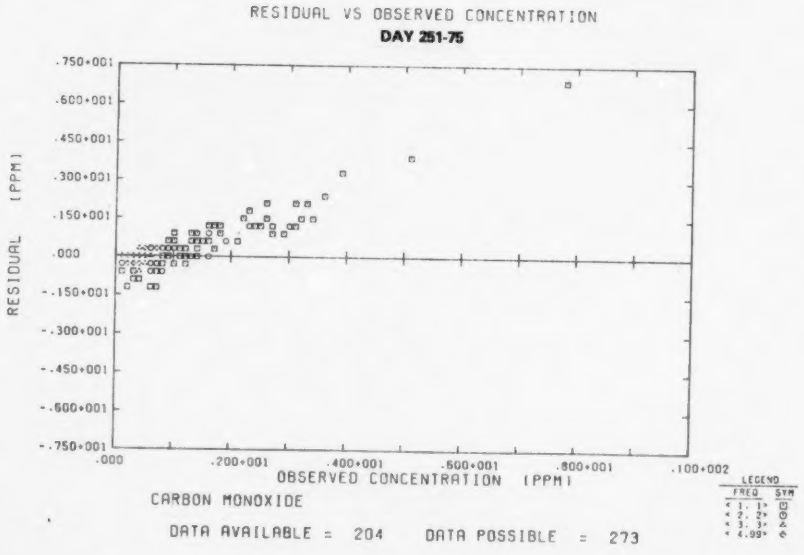

Figure D-10b. Residual vs. observed plot for CO from the UAM simulation results for Day 251-75.

BEGIN LAST LINE OF TEXT
BOTTOM OF IMAGE AREA; OUTSIDE DIMENSION FOR TABLES AND ILLUSTRATIONS
3/8"

PAGE NUMBER
EPA Form 2350-4 (4-80)
(PREVIOUSLY CIN. EPA FORM 287)
© U.S. GOVERNMENT PRINTING OFFICE 1980-660-628
TYPING GUIDE SHEET

BEGIN FIRST LINE OF TEXT HERE
CENTER OF
TOP OF IMAGE AREA
DROPPED HEAD; BEGIN SECTIONS HERE

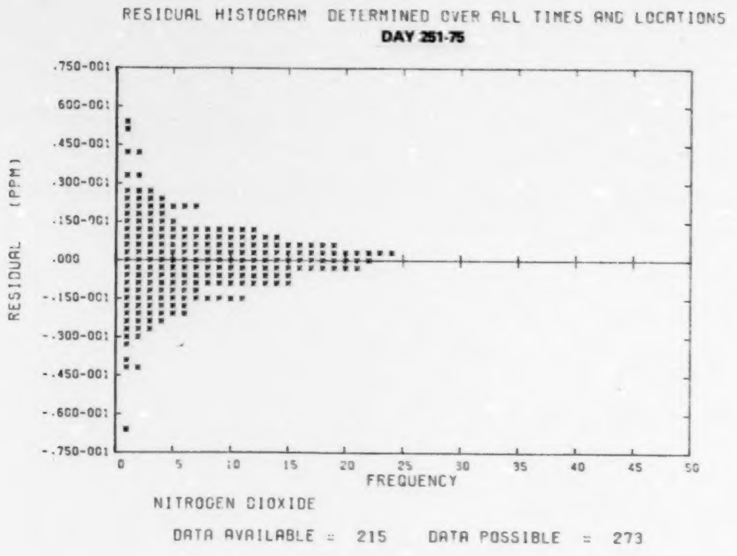

Figure D-11a. Residual histogram for NO_2 from the UAM simulation results for Day 251-75.

9-1/8"

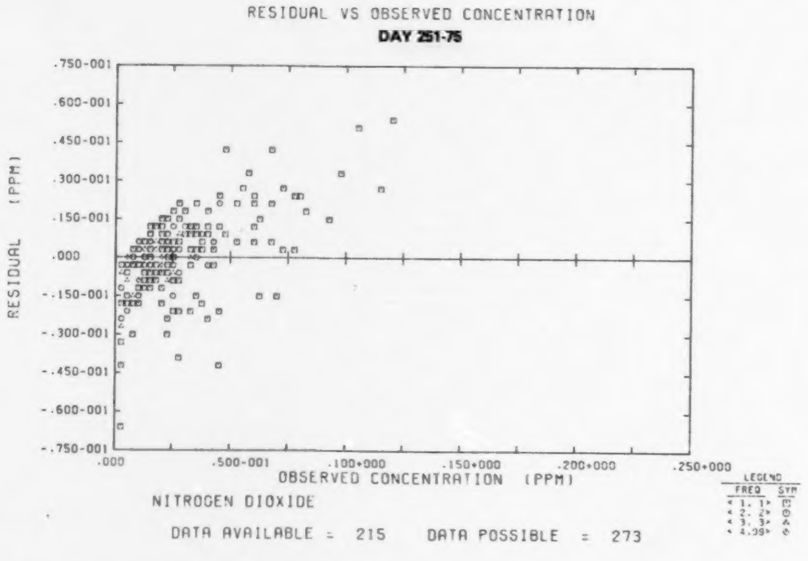

Figure D-11b. Residual vs. observed plot for NO_2 from the UAM simulation results for Day 251-75.

BEGIN LAST LINE OF TEXT
BOTTOM OF IMAGE AREA; OUTSIDE DIMENSION FOR TABLES AND ILLUSTRATIONS
3/8"

PAGE NUMBER
EPA Form 2350-4 (4-80)
(PREVIOUSLY CIN. EPA FORM 287)
☆ U.S. GOVERNMENT PRINTING OFFICE 1980-660-539
TYPING GUIDE SHEET

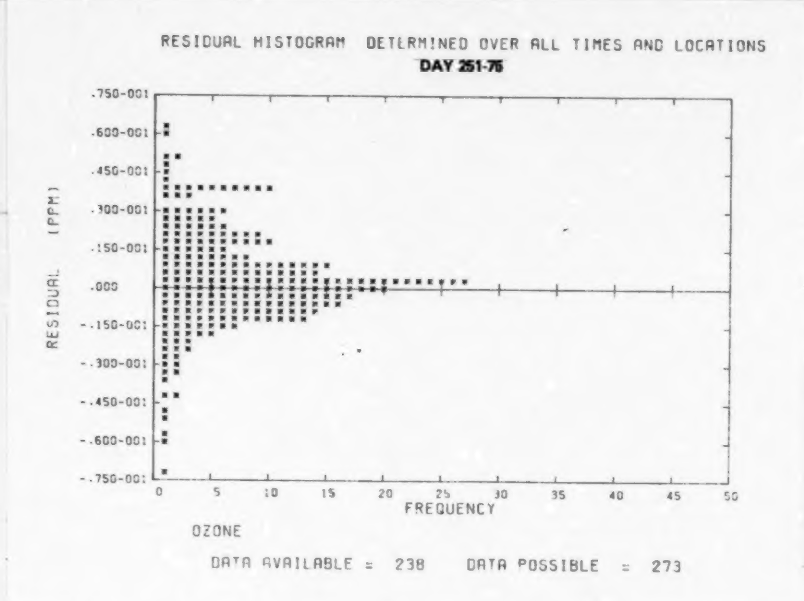

Figure D-12a. Residual histogram for O_3 from the UAM simulation results for Day 251-75.

9-1/8"

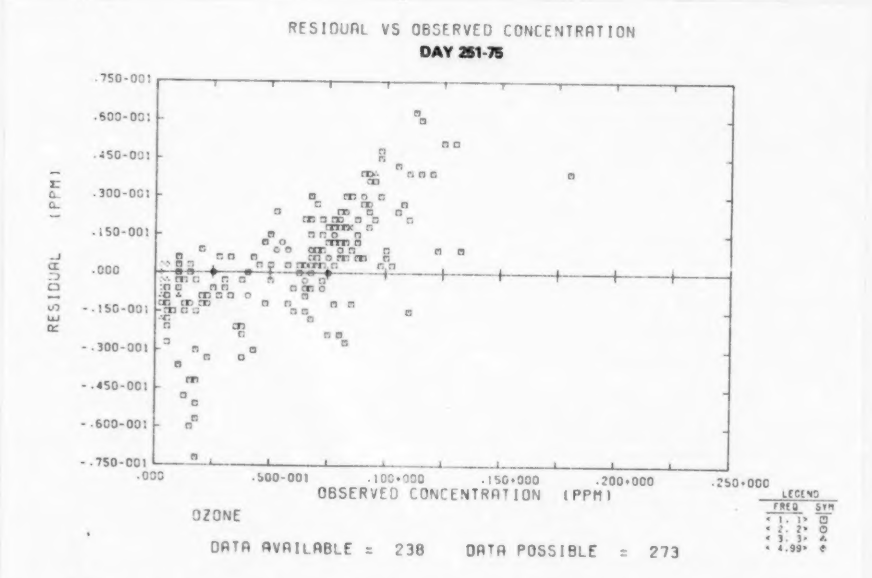

Figure D-12b. Residual vs. observed plot for O_3 from the UAM simulation results for Day 251-75.

BEGIN LAST LINE OF TEXT
3/8"
BOTTOM OF IMAGE AREA; OUTSIDE DIMENSION FOR TABLES AND ILLUSTRATIONS

PAGE NUMBER
EPA Form 2350-4 (4-80)
(PREVIOUSLY CIN. EPA FORM 287)
☆ U.S. GOVERNMENT PRINTING OFFICE: 1980-660-939
TYPING GUIDE SHEET

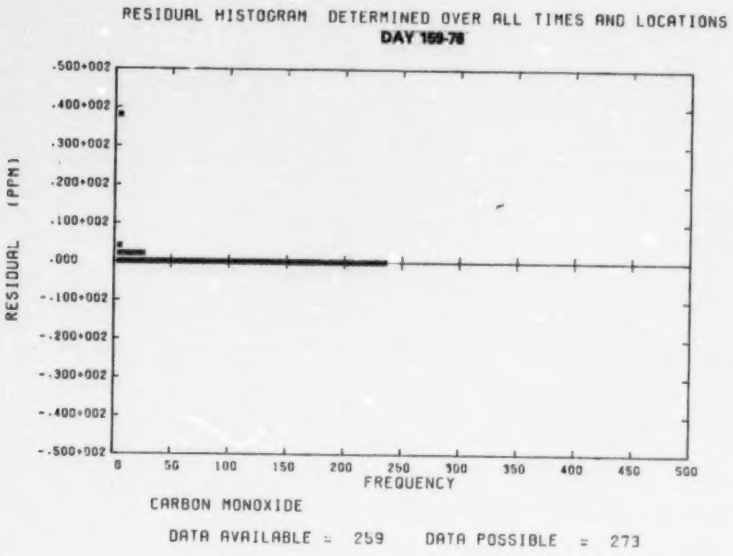

Figure D-13a. Residual histogram for CO from the UAM simulation results for Day 159-76.

9-1/8"

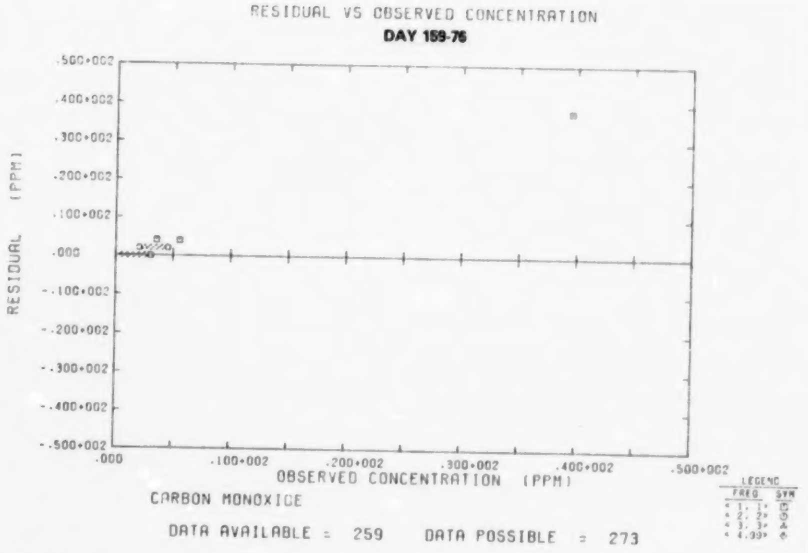

Figure D-13b. Residual vs. observed plot for CO from the UAM simulation results for Day 159-76.

BEGIN LAST LINE OF TEXT
BOTTOM OF IMAGE AREA; OUTSIDE DIMENSION FOR TABLES AND ILLUSTRATIONS
3/8"

PAGE NUMBER
EPA Form 2350-4 (4-80)
(PREVIOUSLY CIN. EPA FORM 287)
© U.S. GOVERNMENT PRINTING OFFICE 1980-660-628
TYPING GUIDE SHEET

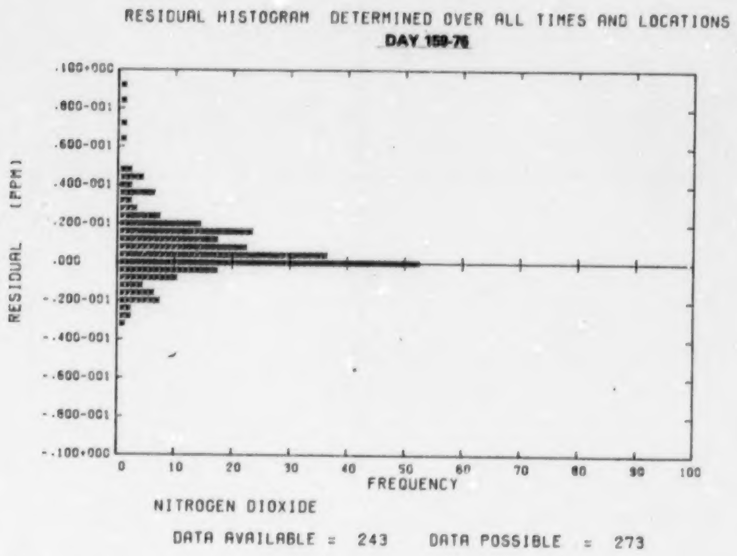

Figure D-14a. Residual histogram for NO_2 from the UAM simulation results for Day 159-76.

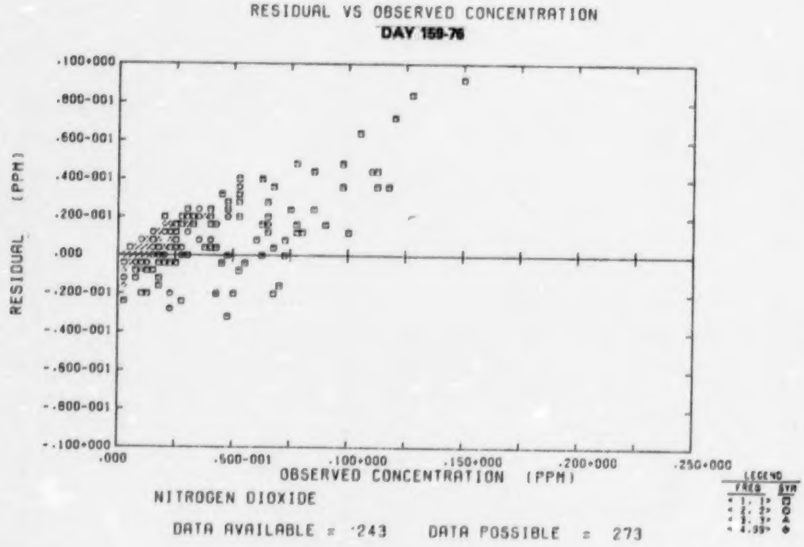

Figure D-14b. Residual vs. observed plot for NO_2 from the UAM simulation results for Day 159-76.

EPA Form 2350-4 (4-80)
(PREVIOUSLY CIN. EPA FORM 287)
TYPING GUIDE SHEET

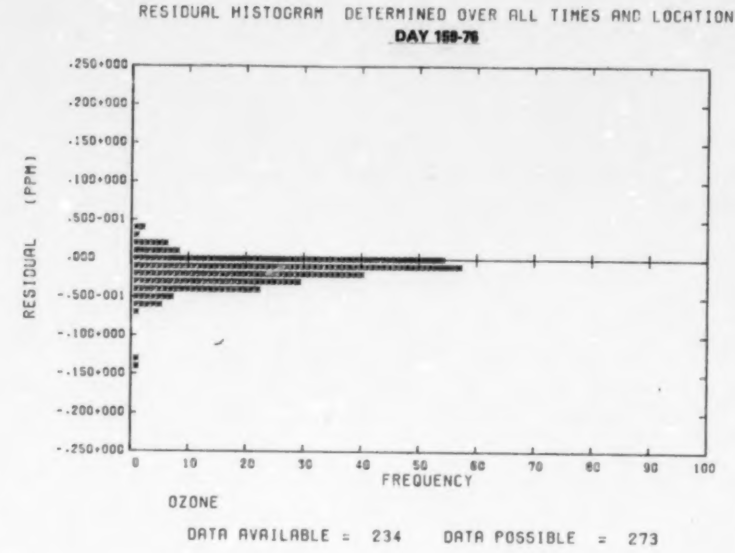

Figure D-15a. Residual histogram for O_3 from the UAM simulation results for Day 159-76.

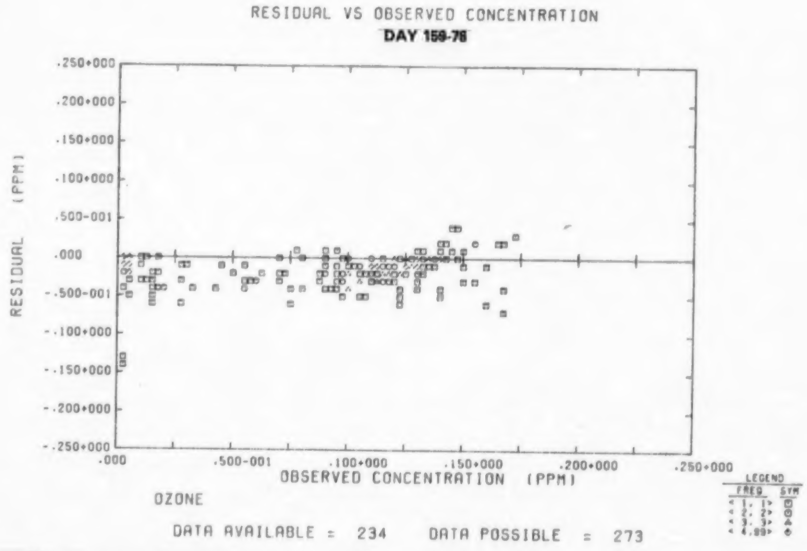

Figure D-15b. Residual vs. observed plot for O_3 from the UAM simulation results for Day 159-76.

BEGIN FIRST LINE OF TEXT HERE
CENTER OF PAGE
TOP OF IMAGE AREA
DROPPED HEAD; BEGIN SECTIONS HERE
9-1/8"
BEGIN LAST LINE OF TEXT
BOTTOM OF IMAGE AREA; OUTSIDE DIMENSION FOR TABLES AND ILLUSTRATIONS
3/8"
PAGE NUMBER
EPA Form 2350-4 (4-80)
(PREVIOUSLY CIN. EPA FORM 267)
TYPING GUIDE SHEET

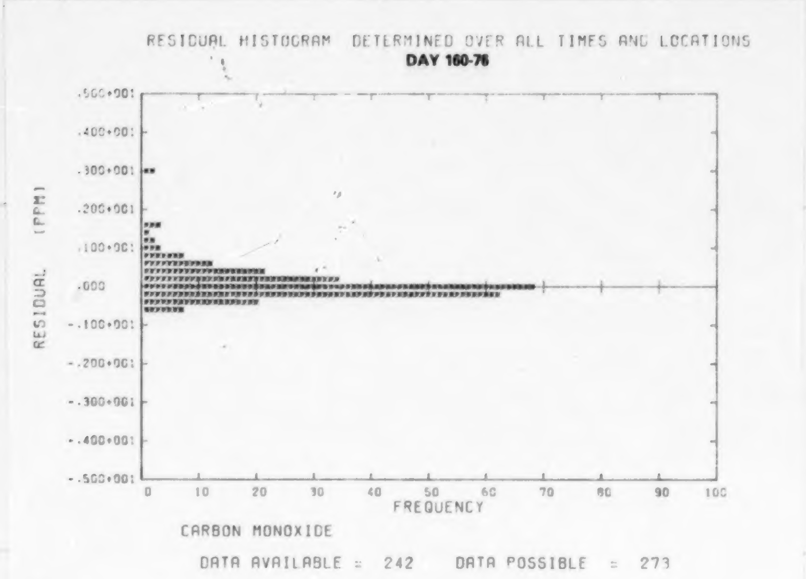

Figure D-16a. Residual histogram for CO from the UAM simulation results for Day 160-76.

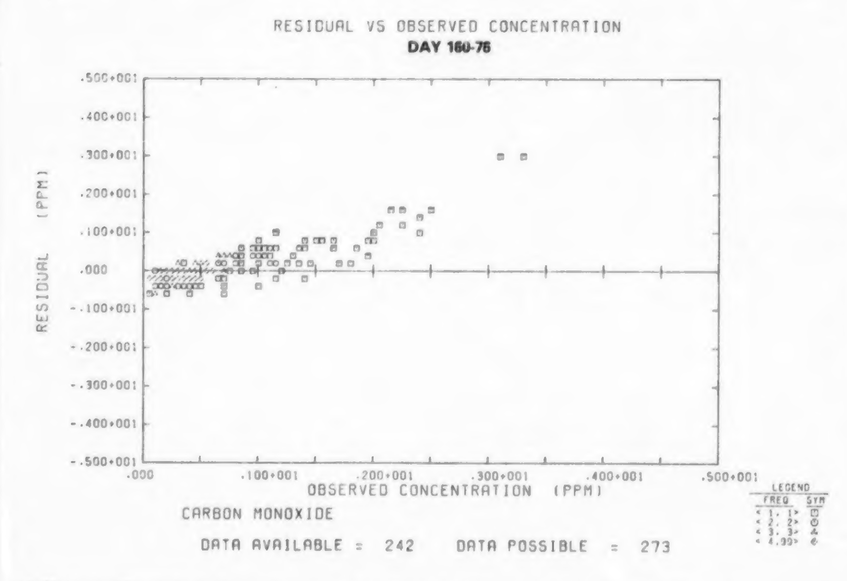

Figure D-16b. Residual vs. observed plot for CO from the UAM simulation results for Day 160-76.

BEGIN FIRST LINE OF TEXT HERE
CENTER OF PAGE
TOP OF IMAGE AREA
DROPPED HEAD: BEGIN SECTIONS HERE
9-1/8"
BEGIN LAST LINE OF TEXT
3/8"
PAGE NUMBER
BOTTOM OF IMAGE AREA: OUTSIDE DIMENSION FOR TABLES AND ILLUSTRATIONS
EPA Form 2350-4 (4-80)
(PREVIOUSLY CIN. EPA FORM 287)
TYPING GUIDE SHEET

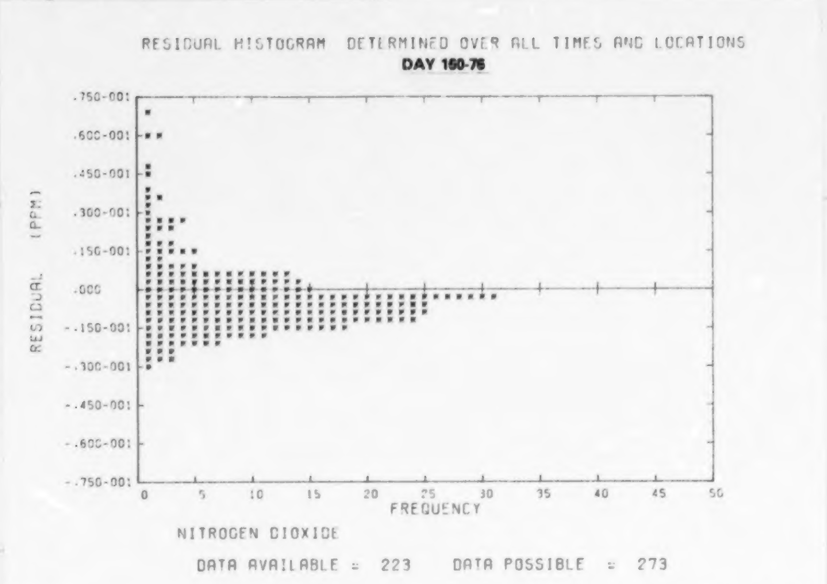

Figure D-17a. Residual histogram for NO_2 from the UAM simulation results for Day 160-76.

9-1/8"

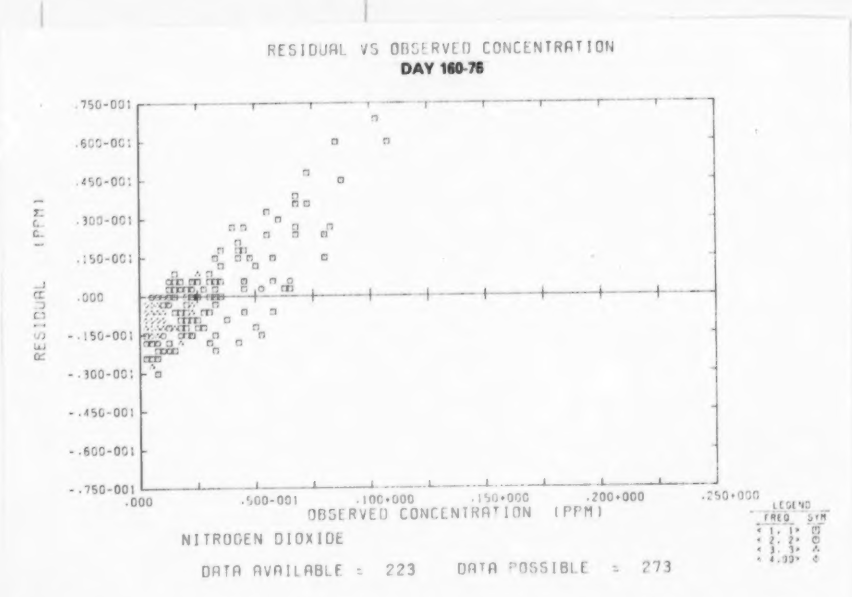

Figure D-17b. Residual vs. observed plot for NO_2 from the UAM simulation results for Day 160-76.

BEGIN LAST LINE OF TEXT
BOTTOM OF IMAGE AREA, OUTSIDE DIMENSION FOR TABLES AND ILLUSTRATIONS
3/8"

PAGE NUMBER
EPA Form 2350-4 (4-80)
(PREVIOUSLY CIN. EPA FORM 287)
TYPING GUIDE SHEET

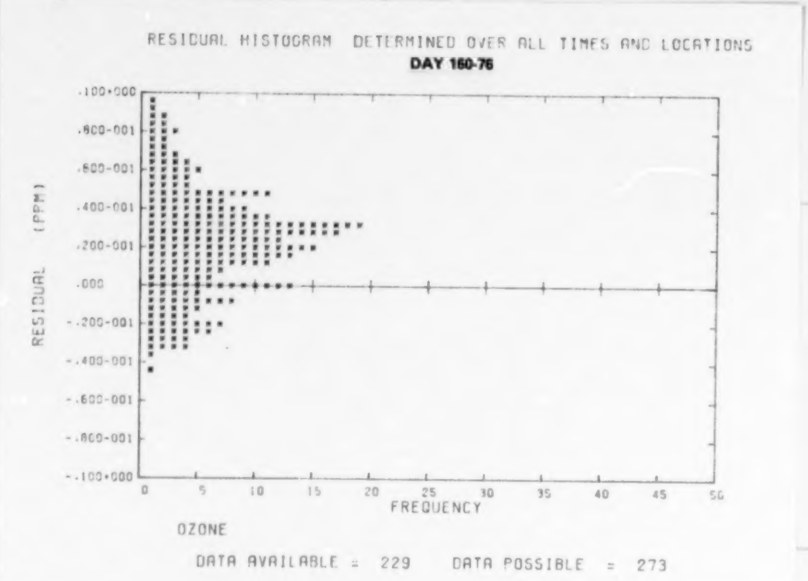

Figure D-18a. Residual histogram for O_3 from the UAM simulation results for Day 160-76.

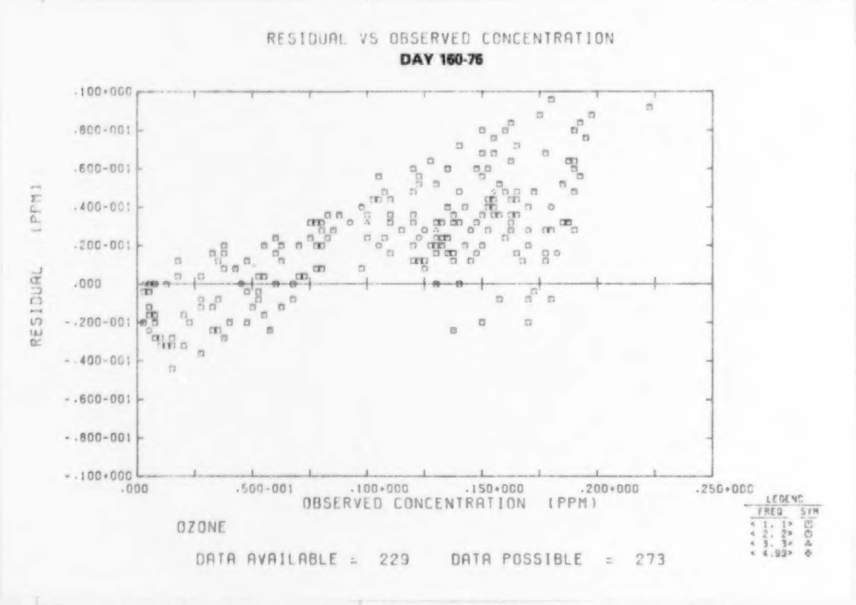

Figure D-18b. Residual vs. observed plot for O_3 from the UAM simulation results for Day 160-76.

BEGIN FIRST LINE OF TEXT HERE
CENTER OF PAGE
TOP OF IMAGE AREA
DROPPED HEAD: BEGIN SECTIONS HERE
9-1/8"
BEGIN LAST LINE OF TEXT
3/8"
BOTTOM OF IMAGE AREA, OUTSIDE DIMENSION FOR TABLES AND ILLUSTRATIONS
PAGE NUMBER
EPA Form 2350-4 (4-80)
(PREVIOUSLY CIN. EPA FORM 287)
TYPING GUIDE SHEET

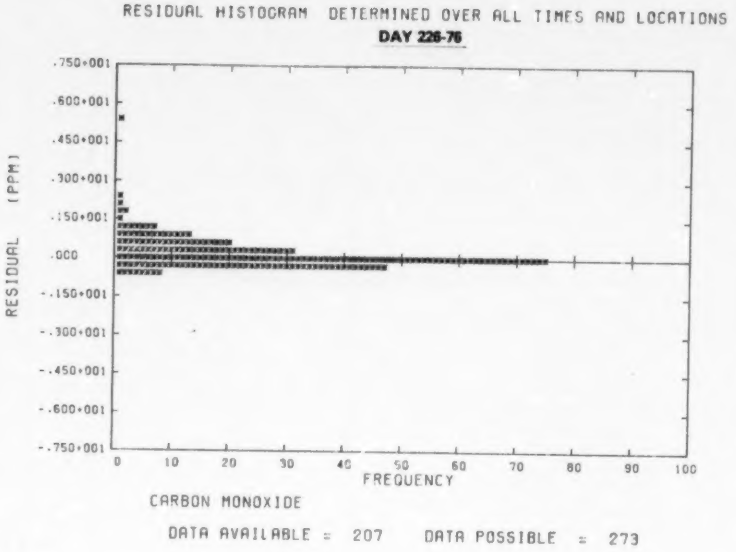

Figure D-19a. Residual histogram for CO from the UAM simulation results for Day 226-76.

9-1/8"

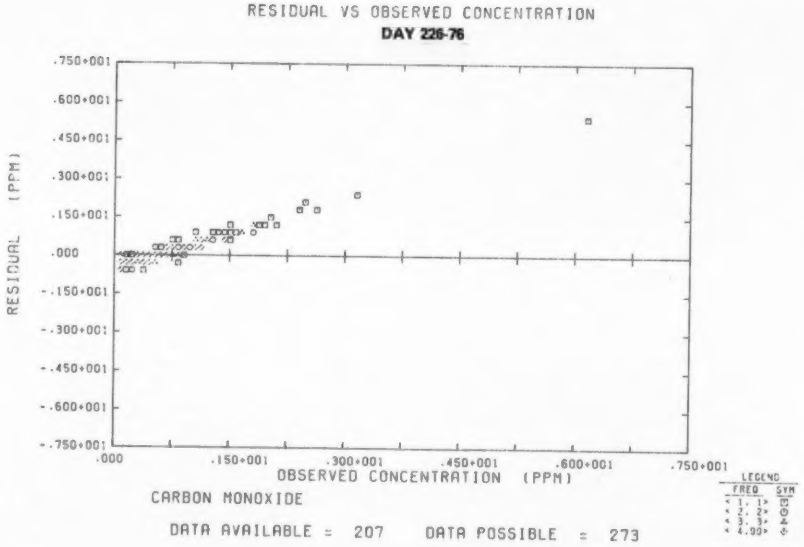

Figure D-19b. Residual vs. observed plot for CO from the UAM simulation results for Day 226-76.

BEGIN LAST LINE OF TEXT
BOTTOM OF IMAGE AREA; OUTSIDE DIMENSION FOR TABLES AND ILLUSTRATIONS
3/8"

PAGE NUMBER
EPA Form 2350-4 (4-80)
(PREVIOUSLY CIN. EPA FORM 287)
TYPING GUIDE SHEET

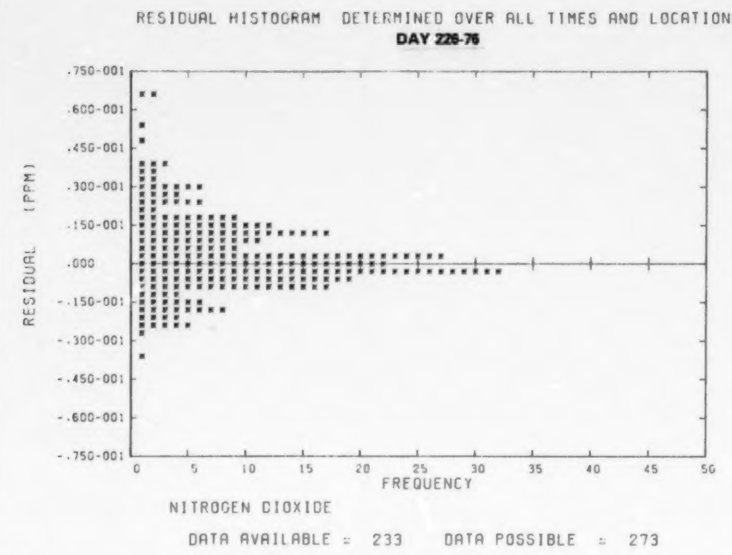

Figure D-20a. Residual histogram for NO_2 from the UAM simulation results for Day 226-76.

9-1/8"

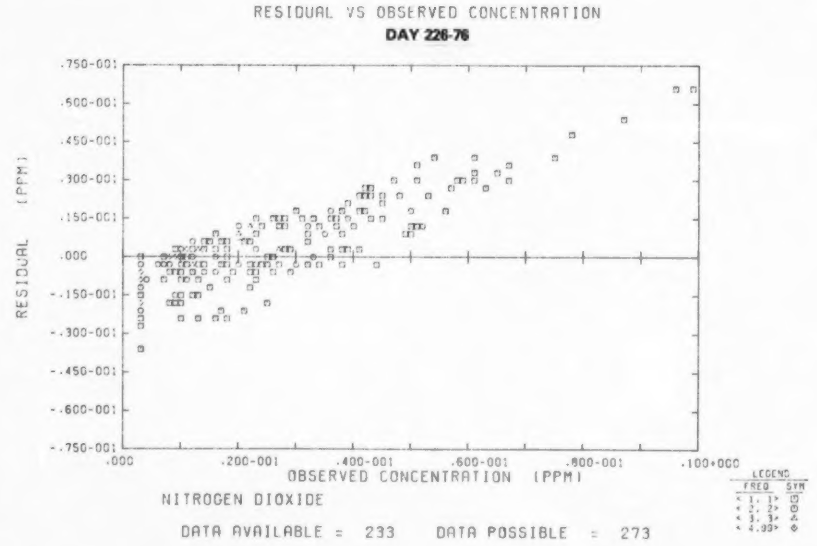

Figure D-20b. Residual vs. observed plot for NO_2 from the UAM simulation results for Day 226-76.

BEGIN LAST LINE OF TEXT
BOTTOM OF IMAGE AREA, OUTSIDE DIMENSION FOR TABLES AND ILLUSTRATIONS
3/8"

PAGE NUMBER
EPA Form 2350-4 (4-80)
(PREVIOUSLY CIN. EPA FORM 287)
U.S. GOVERNMENT PRINTING OFFICE
TYPING GUIDE SHEET

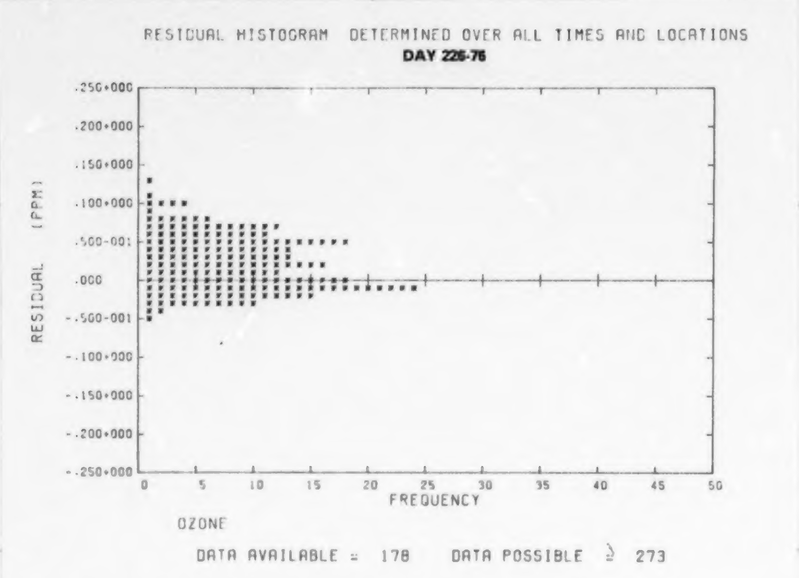

Figure D-21a. Residual histogram for O_3 from the UAM simulation results for Day 226-76.

9-1/8"

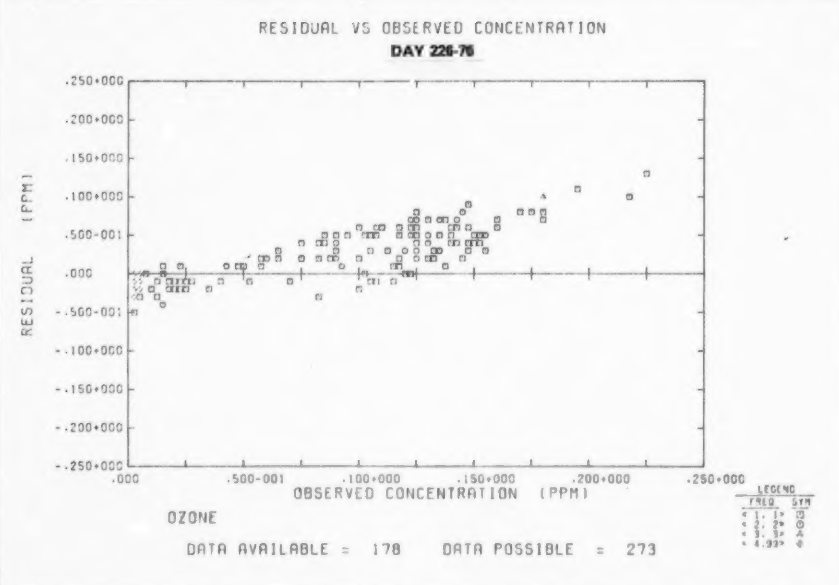

Figure D-21b. Residual vs. observed plot for O_3 from the UAM simulation results for Day 226-76.

BEGIN LAST LINE OF TEXT
BOTTOM OF IMAGE AREA; OUTSIDE DIMENSION FOR TABLES AND ILLUSTRATIONS
3/8"

PAGE NUMBER
EPA Form 2350-4 (4-80)
(PREVIOUSLY CIN. EPA FORM 287)
© U.S. GOVERNMENT PRINTING OFFICE: 1980
TYPING GUIDE SHEET

APPENDIX E

UAM - SUMMARY OF STATISTICAL RESULTS

Three tables are presented in this appendix. Table E-1 summarizes the statistics for the mean quantities on each of the 10 days for the species NO, NO_2, O_3, OLE, NMHC, and CO. Note that the observed OLE (olefin) value was obtained by a temporally and spatially constant splitting factor from NMHC. This factor was based on an analysis of the composite of volatile organic emissions over the entire St. Louis area. The statistical parameters included in this table are (Bencala and Seinfeld, 1979):

(a) mean observed and mean predicted concentration,

(b) mean residual (measures the average bias in the predictions and indicates whether the model predominantly over or underpredicts),

(c) standard deviation (measures the average spread of the residuals, but is insensitive to bias),

(d) mean residual/mean observed (measures the average percentage of over or underprediction), and

(e) error band (measures the percentage of predictions that fall within a 25% band around the observations).

Table E-2 contains a summary of the analysis of trends data for the species NO_2, O_3 and CO. This gives an indication of whether or not the predictions obey the same fundamental relationships as the observations. The parameters contained in this table include:

(a) correlation coefficient (measures the overall degree to which the magnitude of the predictions increases linearly with the magnitude of the observations, but is insensitive to the extent of the increase),

(b) average spatial correlation (average over correlation coefficients for each hour of simulation calculated separately),

(c) average temporal correlation (average over correlation coefficients for each location calculated separately),

(d) slope (the linear least-squares curve fit measure of the average increase in the observations as the predictions increase),

(e) intercept (the linear least-squares curve fit measure of the bias if the slope parameter is very nearly one; otherwise no independent meaning), and

(f) sum of the squared error (a relative measure of the scatter about the linear least-squares fit to the data).

Table E-3 presents data on the concentration maxima for the species NO_2, O_3, and CO for each test day. The parameters listed here are:

(a) peak observed concentration (along with the location and time of occurrence),

(b) peak predicted concentration (at same location as peak observed concentration, along with the time of occurrence),

(c) residual concentration of the peak, and

(d) residual/observed concentration (percentage over or underprediction of the peak).

Note that in all tables a positive residual indicates an underprediction by the model and a negative residual indicates an overprediction.

TABLE E-1. SUMMARY OF MODEL PERFORMANCE STATISTICS FOR MEAN CONCENTRATIONS FROM THE UAM.

Julian date	Species	Mean observed concentration (ppm)	Mean predicted concentration (ppm)	Mean residual (ppm)	Standard deviation (ppm)	Mean Residual / Mean obs. conc. (%)	Error band* (%)
142-75	NO	0.0086	0.0060	0.0025	0.0086	29.1	16.1
	NO_2	0.0134	0.0166	-0.0032	0.0105	-23.9	31.8
	O_3	0.0635	0.0824	-0.0190	0.0322	-29.9	36.9
	OLE	0.0080	0.0047	0.0034	0.0095	42.5	19.6
	NMHC	0.183	0.270	-0.0875	0.220	-47.8	22.3
	CO	0.481	0.519	-0.0379	0.417	-7.9	27.0
178-75	NO	0.0088	0.0065	0.0023	0.0126	26.1	12.6
	NO_2	0.0212	0.0231	-0.0019	0.0145	-9.0	33.9
	O_3	0.0920	0.0841	0.0079	0.0299	8.6	41.9
	OLE	0.0147	0.0059	0.0088	0.0119	59.9	9.3
	NMHC	0.334	0.336	-0.0015	0.276	-0.45	20.2
	CO	0.809	0.719	0.0900	0.571	11.1	31.3
209-75	NO	0.0077	0.0061	0.0016	0.0113	20.8	14.3
	NO_2	0.0149	0.0173	-0.0024	0.0097	-16.1	34.2
	O_3	0.0698	0.0599	0.0099	0.0270	14.2	48.6
	OLE	0.0095	0.0051	0.0044	0.0093	46.3	20.1
	NMHC	0.216	0.246	-0.0301	0.258	-13.9	15.1
	CO	0.486	0.393	0.0927	0.988	19.1	30.9
231-75	NO	0.0084	0.0084	0.00005	0.0104	0.60	16.0
	NO_2	0.0165	0.0183	-0.0018	0.0098	-10.9	30.2
	O_3	0.0518	0.0527	-0.00088	0.0216	-1.7	39.8
	OLE	0.0125	0.00565	0.00683	0.0109	54.6	8.8
	NMHC	0.284	0.287	-0.00384	0.243	-1.4	14.7
	CO	0.437	0.432	0.0049	0.370	1.1	27.8
251-75	NO	0.0198	0.0122	0.00759	0.0300	38.3	15.5
	NO_2	0.0253	0.0254	-0.00013	0.0155	-0.5	32.6
	O_3	0.0507	0.0474	0.00335	0.0201	6.6	45.8
	OLE	0.0193	0.00762	0.0117	0.0183	60.6	10.1
	NMHC	0.438	0.386	0.0517	0.410	11.8	22.8
	CO	0.806	0.590	0.216	0.806	26.8	23.5

BEGIN LAST LINE OF TEXT
BOTTOM OF IMAGE AREA; OUTSIDE DIMENSION FOR TABLES AND ILLUSTRATIONS
3/8"

PAGE NUMBER
EPA Form 2350-4 (4-80)
(PREVIOUSLY CIN. EPA FORM 257)
U.S. GOVERNMENT PRINTING OFFICE: 1980
TYPING GUIDE SHEET

TABLE E-1. (Continued)

SUMMARY OF MODEL PERFORMANCE STATISTICS FOR MEAN CONCENTRATIONS FROM THE UAM.

Julian date	Species	Mean observed concentration (ppm)	Mean predicted concentration (ppm)	Mean residual (ppm)	Standard deviation (ppm)	Mean Residual / Mean obs. conc. (%)	Error band* (%)
159-76	NO	0.0163	0.00751	0.00875	0.0250	53.7	12.3
	NO_2	0.0275	0.0201	0.00739	0.0169	26.9	29.2
	O_3	0.0880	0.104	-0.0163	0.0207	-18.5	60.3
	OLE	0.0182	0.00785	0.0104	0.0180	57.1	11.4
	NMHC	0.414	0.326	0.0878	0.407	21.2	21.7
	CO	0.968	0.615	0.352	2.49	36.4	28.6
160-76	NO	0.00914	0.00723	0.00190	0.0186	20.8	15.7
	NO_2	0.0198	0.0224	-0.00258	0.0152	-13.0	20.2
	O_3	0.107	0.0842	0.0223	0.0282	20.8	46.3
	OLE	0.0130	0.00702	0.00603	0.0120	46.4	14.2
	NMHC	0.297	0.328	-0.0315	0.268	-10.6	22.1
	CO	0.606	0.522	0.0844	0.460	13.9	29.3
195-76	NO	0.00422	0.00318	0.00104	0.00460	24.6	10.5
	NO_2	0.0159	0.0145	0.00138	0.0129	8.7	29.2
	O_3	0.0827	0.0716	0.0111	0.0283	13.4	59.8
	OLE	0.00932	0.00293	0.00639	0.00876	68.6	11.5
	NMHC	0.212	0.200	0.0120	0.202	5.7	25.7
	CO	0.360	0.344	0.0158	0.415	4.4	20.0
226-76	NO	0.00875	0.00489	0.00387	0.0118	44.2	17.7
	NO_2	0.0236	0.0200	0.00362	0.0154	14.0	31.3
	O_3	0.0806	0.0579	0.0227	0.0364	28.2	24.7
	OLE	0.0147	0.00490	0.00979	0.0144	66.6	10.3
	NMHC	0.334	0.247	0.0871	0.320	26.1	26.9
	CO	0.693	0.511	0.182	0.607	26.3	29.5
275-76	NO	0.0364	0.0278	0.00853	0.0421	23.4	17.5
	NO_2	0.0507	0.0457	0.00497	0.0308	9.8	40.8
	O_3	0.0782	0.0801	-0.00192	0.0387	-2.5	36.7
	OLE	0.0304	0.0154	0.0150	0.0200	49.9	11.8
	NMHC	0.691	0.807	-0.116	0.410	-16.8	27.8
	CO	1.74	1.40	0.339	1.29	19.5	28.0

*Percent of predictions within 25% of observations

BEGIN LAST LINE OF TEXT
3/8"
BOTTOM OF IMAGE AREA; OUTSIDE DIMENSION FOR TABLES AND ILLUSTRATIONS

PAGE NUMBER
EPA Form 2350-4 (4-80)
(PREVIOUSLY CIN. EPA FORM 287)
TYPING GUIDE SHEET

TABLE E-2. SUMMARY OF MODEL PERFORMANCE STATISTICS FOR ANALYSIS OF TRENDS DATA FROM THE UAM

Julian date	Species	Correlation coefficient	Average spatial correlation	Average temporal correlation	Slope	Intercept (ppm)	Sum of squared error (ppm^2)
142-75	NO_2	0.598	0.596	0.366	0.530	0.0046	0.0194
	O_3	0.827	0.307	0.868	0.992	-0.0183	0.219
	CO	0.484	0.648	0.321	0.212	0.371	36.1
178-75	NO_2	0.549	0.460	0.463	0.405	0.0119	0.0490
	O_3	0.874	0.447	0.910	0.856	0.0200	0.174
	CO	0.500	0.619	0.287	0.200	0.665	64.7
209-75	NO_2	0.696	0.437	0.692	0.905	-0.00076	0.0180
	O_3	0.750	0.298	0.704	0.520	0.0387	0.212
	CO	0.169	0.417	0.597	0.055	0.464	224.
231-75	NO_2	0.683	0.520	0.490	0.629	0.0050	0.0221
	O_3	0.823	0.460	0.852	0.660	0.0171	0.145
	CO	0.652	0.641	0.696	0.389	0.269	36.4
251-75	NO_2	0.702	0.471	0.633	0.572	0.0108	0.0558
	O_3	0.845	0.413	0.901	0.647	0.0201	0.135
	CO	0.610	0.595	0.543	0.276	0.643	175.

BEGIN LAST LINE OF TEXT
3/8"
BOTTOM OF IMAGE AREA: OUTSIDE DIMENSION FOR TABLES AND ILLUSTRATIONS

PAGE NUMBER
EPA Form 2350-4 (4-80)
(PREVIOUSLY CIN. EPA FORM 287)
TYPING GUIDE SHEET

TABLE E-2. (Continued)

SUMMARY OF MODEL PERFORMANCE STATISTICS FOR ANALYSIS OF TRENDS DATA FROM THE UAM

Julian Date	Species	Correlation coefficient	Average spatial correlation	Average temporal correlation	Slope	Intercept (ppm)	Sum of squared error (ppm^2)
159-76	NO_2	0.0803	0.484	0.724	0.579	0.0159	0.0963
	O_3	0.916	0.388	0.962	0.900	-0.00588	0.0978
	CO	0.254	0.451	0.688	0.0434	0.941	1700.
160-76	NO_2	0.703	0.584	0.547	0.455	0.00962	0.0683
	O_3	0.884	0.382	0.911	0.651	0.0517	0.291
	CO	0.577	0.342	0.446	0.305	0.447	64.3
195-76	NO_2	0.428	0.467	0.100	0.277	0.0119	0.0431
	O_3	0.837	0.045	0.926	0.520	0.0455	0.240
	CO	0.183	0.349	0.318	0.0677	0.337	41.0
226-76	NO_2	0.568	0.492	0.534	0.299	0.0176	0.0692
	O_3	0.839	0.439	0.842	0.484	0.0526	0.394
	CO	0.451	0.572	0.348	0.111	0.637	88.8
275-76	NO_2	0.532	0.646	0.295	0.393	0.0328	0.221
	O_3	0.835	0.263	0.901	0.827	0.0119	0.343
	CO	0.648	0.663	0.498	0.238	1.40	561.

BEGIN LAST LINE OF TEXT
BOTTOM OF IMAGE AREA; OUTSIDE DIMENSION FOR TABLES AND ILLUSTRATIONS
3/8"

PAGE NUMBER
EPA Form 2350-4 (4-80)
(PREVIOUSLY CIN. EPA FORM 287)
TYPING GUIDE SHEET

TABLE E-3. SUMMARY OF MODEL PERFORMANCE STATISTICS FOR CONCENTRATION MAXIMA FROM THE UAM

Julian date	Species	Observed Peak Concentration Value (ppm)	Observed Peak Concentration Location (RAMS site)	Observed Peak Concentration Time (CST)	Predicted Peak Concentration* Value (ppm)	Predicted Peak Concentration* Time (CST)	Residual (ppm)	Residual Obs. conc. (%)
142-75	NO_2	0.0458	102	1300	0.0363	1700	0.0095	20.7
	O_3	0.195	101	1200	0.171	1300	0.0240	12.3
	CO	4.03	121	1700	0.879	1500	3.15	78.2
178-75	NO_2	0.0701	103	0700	0.0431	0900	0.0270	38.5
	O_3	0.202	112	1400	0.160	1500	0.0420	20.8
	CO	4.04	107	0600	1.24	0800	2.80	69.3
209-75	NO_2	0.0501	110	0800	0.0502	0800	-0.0001	-0.2
	O_3	0.209	118	1100	0.114	1100	0.0950	45.5
	CO	14.4	117	1700	0.925	0800	13.5	93.8
231-75	NO_2	0.0574	102	1000	0.0363	1000	0.0211	36.8
	O_3	0.233	121	1400	0.146	1300	0.0870	37.3
	CO	2.96	113	1000	1.02	0700	1.94	65.5
251-75	NO_2	0.120	112	0900	0.0730	1000	0.0470	39.2
	O_3	0.179	121	1200	0.140	1200	0.0390	21.8
	CO	7.80	113	0600	1.43	1100	6.37	81.7

BEGIN FIRST LINE OF TEXT HERE
CENTER OF PAGE
TOP OF IMAGE AREA
DROPPED HEAD; BEGIN SECTIONS HERE
BEGIN LAST LINE OF TEXT
3/8"
PAGE NUMBER
BOTTOM OF IMAGE AREA; OUTSIDE DIMENSION FOR TABLES AND ILLUSTRATIONS
EPA Form 2350-4 (4-80)
(PREVIOUSLY CIN. EPA FORM 287)
TYPING GUIDE SHEET

TABLE E-3. (Continued)

SUMMARY OF MODEL PERFORMANCE STATISTICS FOR CONCENTRATION MAXIMA FROM THE UAM

Julian date	Species	Observed Peak Concentration Value (ppm)	Observed Peak Concentration Location (RAMS site)	Observed Peak Concentration Time (CST)	Predicted Peak Concentration* Value (ppm)	Predicted Peak Concentration* Time (CST)	Residual (ppm)	Residual Obs. conc. (%)
159-76	NO_2	0.149	104	0700	0.0657	0600	0.0833	55.9
	O_3	0.172	114	1400	0.143	1500	0.0290	16.9
	CO	39.4	121	1300	0.658	0500	38.7	98.2
160-76	NO_2	0.106	104	0700	0.0639	0600	0.0421	39.7
	O_3	0.221	115	1600	0.134	1700	0.0870	39.4
	CO	3.27	107	1000	1.64	0500	1.63	49.8
195-76	NO_2	0.0657	102	0600	0.0289	1600	0.0368	56.0
	O_3	0.223	114	1500	0.130	1700	0.0930	41.7
	CO	4.51	115	0600	0.386	1700	4.12	91.4
226-76	NO_2	0.0989	101	0700	0.0371	0500	0.0618	62.5
	O_3	0.225	109	1300	0.115	1400	0.110	48.9
	CO	6.09	105	1500	0.692	0800	5.40	88.7
275-76	NO_2	0.182	101	1000	0.0846	1200	0.0974	53.5
	O_3	0.244	102	1400	0.183	1500	0.0610	25.0
	CO	9.06	112	1700	2.88	0500	6.18	68.2

*at same location as observed peak

BEGIN FIRST LINE OF TEXT HERE
CENTER OF PAGE
TOP OF IMAGE AREA
DROPPED HEAD; BEGIN SECTIONS HERE
BEGIN LAST LINE OF TEXT
3/8"
BOTTOM OF IMAGE AREA; OUTSIDE DIMENSION FOR TABLES AND ILLUSTRATIONS
PAGE NUMBER
EPA Form 2350-4 (4-80)
(PREVIOUSLY CIN. EPA FORM 267)
TYPING GUIDE SHEET